공학박사 학위논문

Periodic Relative Motion for Spacecraft Formation in Elliptic Orbit and Its Application to Formation Reconfiguration

타원 궤도에서의 인공위성 군집비행을 위한 주기적 상대운동과 군집형상 변경에의 적용

2012년 8월

서울대학교 대학원

기계항공공학부

배 종 희

Periodic Relative Motion for Spacecraft Formation in Elliptic Orbit and Its Application to Formation Reconfiguration

타원 궤도에서의 인공위성 군집비행을 위한

주기적 상대운동과 군집형상 변경에의 적용

지도교수 김 유 단

이 논문을 공학박사 학위논문으로 제출함

2012년 7월

서울대학교 대학원

기계항공공학부

배 종 희

배종희의 공학박사 학위논문을 인준함

2012년 7월

위 원 장	박 찬 국	(인)
부위원장	김 유 단	(인)
위 원	김 현 진	(인)
위 원	방 효 충	(인)
위 원	박 찬 덕	(인)

Periodic Relative Motion for Spacecraft Formation in Elliptic Orbit and Its Application to Formation Reconfiguration

A Dissertation

by

JONGHEE BAE

Submitted to the Department of Mechanical and Aerospace Engineering
in partial fulfillment of the requirements for the degree of

DOCTOR OF PHILOSOPHY

in Aerospace Engineering at the

SEOUL NATIONAL UNIVERSITY

July 2012

Approved as to style and content by:

Prof. Changook Park
Mechanical and Aerospace Engineering, Chairman of Committee

Prof. Youdan Kim
Mechanical and Aerospace Engineering, Principal Advisor

Prof. H. Jin Kim
Mechanical and Aerospace Engineering

Prof. Hyochoong Bang
Aerospace Engineering, Korea Advanced Institute of Science and Technology

---

Prof. Chandeok Park
Astronomy, Yonsei University

To my family with love

Abstract

Periodic Relative Motion for Spacecraft Formation in Elliptic Orbit and Its Application to Formation Reconfigurtion

Jonghee Bae

Department of Mechanical and Aerospace Engineering

Seoul National University

Spacecraft formation flying has been widely investigated due to increasing interests in designing clusters around a planet and its applications including rendezvous and maneuver. Multiple spacecraft in formation have many advantages such as cooperative mission execution, reduced cost, flexible configuration, and robustness. Nonlinear relative motion and periodicity condition in elliptic orbits are required to achieve the precise and efficient formation flying and reconfiguration. This dissertation presents periodic relative motion, formation pattern analysis, and spacecraft maneuvers for the formation reconfiguration in elliptic reference orbits.

The major achievement of this study is to present a general periodic condition which guarantees the bounded relative motion of spacecraft formation flying in elliptic orbits. The periodic condition of the circular orbit is easily obtained from the analytic solution of the Hill-Clohessy-Wiltshire equation. For the elliptic orbits, however, the periodic condition is restrictively described in near circular orbits and elliptic orbits at a specific initial position by the Tschauner-Hempel equation due to complex and coupled relative motion dynamics. In this dissertation, the general periodicity condition is derived using

two analytic approaches: the first one based on the state transition matrix, and the second one based on the energy matching condition. Furthermore, the offset condition is investigated to make the leader spacecraft locate at the center of the formation geometry. As a result, the periodic relative motion is developed to remove the secular drift and the offset in the along-track direction. Numerical simulations verify that this periodic condition covers partial periodicity condition of previous studies. The periodic relative motion provides a substantial advantage in the sense that an additional correction is not required with respect to the initial position of the follower spacecraft.

The second accomplishment is to design the formation geometry and to analyze the formation pattern in the elliptic reference orbit. From understanding the natural formation geometry, the spacecraft can remarkably reduce the fuel consumption. The formation design method for circular or nearly circular orbits has been described; however, the formation design and analysis in the elliptic orbits have not been extensively studied due to the nonlinearity and eccentricity. In this dissertation, two formation geometries in the elliptic orbit are designed by considering natural periodic relative motion: radial/along-track plane formation and along-track/cross-track plane formation. The formation patterns including the relative trajectory, velocity, and formation radius are analyzed with respect to the variation of eccentricity. The eccentricity of the reference orbit is a critical factor influencing on the variation of formation radius between two spacecraft in the relative motion.

With the understanding of formation flying in elliptic orbits, the spacecraft maneuver problem for the formation reconfiguration is investigated considering two types of control input: continuous control input and impulsive control input. The formation configuration should be changeable according to the mission requirements and environments during the operation. The follower spacecraft changes the formation radius or the formation geometry with re-

spect to the leader spacecraft, while minimizing the control effort. For the continuous control input, the optimal control problem in the relative motion is solved by the Gauss pseudospectral method, where the initial and final relative positions and velocities are specified. The optimal trajectories between the radial/along-track plane and the along-track/cross-track plane are provided using the minimum energy and minimum fuel cost functions. For the impulsive control input, the Lambert's problem is modified to construct the transfer problem in the relative motion, given two position vectors at the initial and final time and the flight time. In addition, the minimum velocity change for transferring orbits is designed through the grid search.

The results of this research establish that the periodic relative motion is presented at an arbitrary true anomaly in the elliptic reference orbit, the formation geometries are designed and analyzed to reflect the eccentricity of the reference orbit, and the formation reconfiguration is described using two control input types. These results can provide the effective and efficient formation flying in elliptic reference orbits.

Keywords: Spacecraft formation flying, Relative motion dynamics,
Periodicity condition, Formation design and analysis,
Formation reconfiguration, Elliptic orbit

Student Number: 2005–23437

Table of Contents

List of Tables

List of Figures

Chapter 1

Introduction

1.1 Background and Motivation

Many recent studies have focused on spacecraft formation flying because of the growing interest in designing clusters around a planet. Flying multiple spacecraft in a formation has many advantages in terms of flexibility, reliability, financial benefits, and a high image resolution compared to flying a single large spacecraft [1, 2, 3, 4]. For instance, the formation consisting of many satellites can construct a virtual antenna to improve the image resolution by sharing the individual measurements, and then it can provide the Earth mapping and scientific data with high resolution. On the other hand, if a single large satellite has a serious problem such as a hardware/software fault, a given mission cannot be performed. In contrast, even though a failure occurs in one of multiple spacecraft in a formation, the given mission can be completed using the remaining spacecraft.

The autonomous formation flying has been developed for future space missions in many countries. National Aeronautics and Space Administration (NASA) launched the Earth-Observing 1 (EO-1) in 2000, which flew in a formation with Landsat 7 and demonstrated basic technologies of spacecraft

formation flying [5, 6]. NASA provided the StarLight (ST) series for measurements of the Earth's magnetic field, proposed the Terrestrial Planet Finder (TPF) to construct a telescope system for discovering the terrestrial planets such as the Earth [7], and designed the Micro-Arcsecond X-ray Imaging Mission (MAXIM) consisting of 34 spacecraft to obtain the black hole image [8]. Moreover, the Magnetospheric Multiscale (MMS) Mission consisting of four spacecraft was proposed to observe the Earth's magnetosphere and its dynamic iteration with the solar wind by NASA [9]. The Air Force Research Laboratory (AFRL) planned the TechSat 21 program to perform the space-based radar for ground moving target indication and geolocation using several micro-satellites [10, 11]. European Space Agency (ESA) launched the Cluster II mission in 2000 and provided the results on magnetospheric dynamics [12, 13], designed Darwin to search for Earth-like planets [14], and designed the X-ray Evolving Universe Spectroscopy (XEUS) mission consisting of two spacecraft in formation to search for the first giant black hole [15]. In addition, the A-Train is currently performing missions, which is a satellite constellation by international collaboration between NASA and Centre National d'Etudes Spatiales (CNES), consisting of five satellites to build high-resolution three-dimensional images of the Earth's atmosphere and surface [16]. The Laser Interferometer Space Antenna (LISA) was designed to develop a space-based gravitational wave detector at low frequency, which is a joint project between NASA and ESA [17]. PROBA-3 by ESA and PRISMA by the Swedish Space Corporation employ a pair of two satellites to test the technologies of spacecraft formation flying [18, 19].

The dynamic motion of the spacecraft in formation is described by the relative motion between two spacecraft. The Hill-Clohessy-Wiltshire (HCW) equation is widely used to express the relative motion near Keplerian orbits in the Local Vertical Local Horizontal (LVLH) frame [20, 21]. To use this equa-

tion, it is assumed that the reference orbit is circular, the Earth is spherically symmetric, and the relative distance between two spacecraft is much smaller than the distance between the spacecraft and center of the Earth. The HCW equation includes linear constant coefficients, which makes it simple to design a controller to keep a formation or transfer to another orbit. However, these assumptions are not valid when the leader spacecraft has an elliptic reference orbit. To deal with this limitation, the effect of eccentricity of the reference orbit should be considered in the relative dynamics. The Tschauner-Hempel (TH) equation describes the relative dynamics in an elliptic orbit, which considers a true anomaly instead of time as an independent free variable [22]. Also, the differential orbital elements are used to express the relative motion between two satellites [23, 24, 25, 26].

The periodic relative motion of the spacecraft reduces the fuel consumption by satisfying a periodicity condition for formation flying. With the understanding of natural relative motion between spacecraft, the periodic condition eliminates the secular drift of the relative motion and relieves an additional control input to adjust the orbit. In the circular reference orbit, the periodic condition can be determined from the analytic solution of the HCW equation. Six initial conditions in the analytic solution define the relative motion of a follower spacecraft with respect to the leader spacecraft in the LVLH frame, and therefore the term contributing to the secular drift can be selected to be zero. This resulting condition is the periodic condition in a circular orbit [27]. The periodic condition in a circular orbit, however, cannot guarantee the periodic relative motion in the elliptic reference orbit. To deal with this problem, the periodic condition in the elliptic orbit has been developed. The perturbation method was used to obtain the bounded relative motion considering the eccentricity of the reference orbit as a perturbed term in the analytic solution of the HCW equation [28]. The periodic condition at a specific true

anomaly such as perigee and apogee was also presented using the state transition matrix [29]. These results only guarantee the bounded relative motion in near circular reference orbits and elliptic orbits staring at perigee and apogee. Therefore, the general periodic condition is required to remove the secular drift at an arbitrary true anomaly in the elliptic reference orbit as well as in the circular reference orbit.

The spacecraft formation flying requires long time spans of the orbit and less fuel consumption to maintain the desired formation. For this reason, the formation design and analysis become an important research area. In a circular reference orbit, many studies have been investigated to design the formation, and the design procedure of several formation geometries is presented [30]. For the elliptic reference orbit, the formation design method has been developed as the science-based missions; however, the formation design and analysis for the elliptic reference orbit have not been sufficiently studied yet, because the relative dynamics in the elliptic reference orbit are more complicated than that in the circular reference orbit. As a result, analytic investigation on the formation pattern and design in the elliptic orbit is required.

During the spacecraft operation, the formation reconfiguration may be needed to change the formation radius or geometry according to the mission requirements. For the formation reconfiguration, the follower spacecraft should change the orbit with respect to the leader spacecraft, while minimizing the control effort. Lots of works on the maneuver problem have been solved in an inertial frame using the impulsive control input as well as the continuous control input, which include as the Hohmann transfer consisting of the two-impulse maneuver in the circular orbit [23, 31]. The formation reconfiguration problem, however, is different from the traditional maneuver problem, because the formation of multiple spacecraft is expressed by the relative motion with respect to the leader spacecraft, not a planet. Therefore, the traditional

spacecraft maneuver problem should be modified to design the transfer orbit trajectory of the follower spacecraft, where two relative position vectors and the flight time in the local frame are specified.

In this dissertation, a general periodic condition and formation pattern analysis are presented in an elliptic reference orbit. In addition, the maneuver problem is solved to change the formation radius or formation type in the relative motion. The main challenges addressed in this dissertation are as follows:

- Investigate the general periodicity condition to make the relative motion between two spacecraft periodic at an arbitrary position in the elliptic reference orbit
- Design two formation geometries and analyze the formation patterns with respect to the eccentricity and the true anomaly of the reference orbit: radial/along-track plane formation and along-track/cross-track plane formation
- Solve the maneuver problem for the given initial and final conditions and the flight time in the local frame using two control input types: continuous control input and impulsive control input

1.2 Literature Survey

The topics related to this dissertation are *spacecraft relative motion dynamics*, *periodic condition*, *formation design and analysis*, and *maneuver problem*. The previous works are described below.

Spacecraft relative motion dynamics

The HCW equation is widely used to describe the relative motion and to solve

rendezvous and docking problems of satellite systems [20, 21, 27, 31, 32], which is a simple model based on the linearized dynamics of the relative motion in circular reference orbits. In this equation, it is assumed that the differential gravity field is linear without any external perturbation, and the relative distance between two spacecraft is negligible compared with the distance between the spacecraft and center of the Earth. The HCW equation is time-invariant, which is a primary merit, and therefore the application of control is straightforward. However, the HCW equation has a limitation on expressing the relative motion in Keplerian elliptic orbits due to the underlying assumptions regarding nonlinearity and eccentricity, and thereby the formation relative motion deviates from the analytic solution of the HCW equation.

The nonlinearity problem of the HCW equation has been treated by considering higher-order terms [33, 34, 35, 36], and the eccentricity problem has been dealt with by using time or a true anomaly as a free variable. Vaddi et al. considered the effects of the nonlinearity as well as the eccentricity of the relative motion dynamics in an elliptical orbit and corrected the initial conditions of the HCW equation [28]. Through the TH equation [22], which uses a true anomaly of the reference orbit as a free variable, Carter obtained the relative dynamics of the spacecraft formation in the elliptic orbit and derived the analytic solution [37]. As a result, the relative motion with respect to the true anomaly is commonly used to design a formation and control scheme for the spacecraft formation flying [29, 37, 38, 39, 40, 41, 42, 43, 44].

The relative motion between two satellites can also be described using differential orbital elements [45, 46]. Garrison et al. obtained analytical expressions of the relative motion in eccentric orbits using a geometric approach [47], while Schaub studied the relative orbit geometry of the spacecraft formation for a circular reference orbit as well as an elliptic reference orbit [24]. Jiang et al. presented the relative orbit geometry in unperturbed eccentric or-

bits using the first-order relative position equations with the same semi-major axes of two satellites [26].

Periodic condition

Using relative motion dynamics, many researchers have studied the initial conditions for the periodic relative motion of the spacecraft formation flying. The periodic condition can keep the bounded formation with little fuel consumption. To obtain the periodicity condition, the secular drift term in the relative motion should be eliminated. In the circular reference orbit, the initial conditions are simply chosen to remove the secular drift term from the analytic solution of the HCW equation [27, 30].

In an elliptic reference orbit, much work has focused on the development of the periodic relative motion. By correcting the analytic solution of the HCW equation, Vaddi et al. obtained the periodic condition in the elliptic orbit using the perturbation method [28], and Bond presented a stable solution which does not have no error growth with the assumption that the reference orbit is near circular [48]. Vadali et al. and Schaub and Alfriend described the initial conditions considering J_2 perturbation [49, 50]. For the periodic relative motion, the state transition matrix has been also studied extensively [29, 42, 43, 44, 51, 52]. Melton presented a time-explicit solution for the elliptical orbit by expanding the state transition matrix up to the second-order in terms of eccentricity [43], and Broucke presented the state transition matrix which propagates the relative motion for the rendezvous problem [44]. In Refs. [29, 51], the state transition matrix was used to obtain a solution for the linearized relative motion based on the TH equation in eccentric orbits. Inalhan et al. described the periodic conditions at perigee and apogee, and the optimization problem was solved to compute the initial conditions at other positions with those specific periodic conditions and the mission objectives as constraints [29]. Gim and Alfriend described the state transition matrix using a geometric

method [52].

On the other hand, the energy matching condition was used to find the initial condition of the periodic relative motion, too. The specific energy of an elliptic orbit is related to the semi-major axis, and the orbital period of a spacecraft is also dependent on the semi-major axis [31]; if two spacecraft have identical semi-major axes, then they have same orbital energy and period. To maintain the bounded relative motion, the spacecraft in a formation have equal orbital period, which means that their semi-major axes should be identical. This is the energy matching condition for the relative motion dynamics. Baoyin et al. described the relative motion of the spacecraft formation flying and the periodic conditions considering the same orbital period using orbital elements [46]. Based on the energy matching condition, Gurfil dealt with a bounded motion problem and presented the initial conditions [53]. Xign et al. corrected the initial condition of the HCW equation using the energy matching condition and described the periodic relative motion [54].

In addition to the above studies, Sengupta et al. presented the periodic relative motion by dealing with the second-order nonlinearities of the TH equations in eccentric orbits [55], and Sengupta and Vadali studied the effects of the eccentricity and the conditions for the bounded relative motion [56]. They also presented the relationship between the initial conditions and the differential orbit elements. Jiang et al. presented the periodic condition using the reference orbital element approach in the elliptical orbit without any perturbation [57]. Sabatini et al. described the natural periodic relative motion using the numerical and analytical approaches, and found a special inclination having minimum drift relative trajectories [58]. Bando and Ichikawa considered the periodic orbits in near circular orbits for the formation flying and the reconfiguration problem [59].

Formation design and analysis

The problem of the spacecraft formation design has intensively studied considering various space missions. Generally, the formation flying requires long time spans of the orbit and less fuel consumption to maintain the desired formation. As a result, formation design and analysis become a critical issue when dealing with these requirements. Typical desired formation geometries are in-track separation and projected circular formation in the circular reference orbit [60]; for example, the A-Train was designed to have in-track separation. Sabol et al. presented a design method using the analytic solution of the HCW equation and proposed four special formations: in-plane, in-track, circular, and projected circular formation [30]. This method presented a simple analytical procedure for the formation design; however, it only provided the spacecraft formation geometry for the circular reference orbit, not for the general elliptical reference orbit.

The formation design in elliptic orbits has been extensively studied since Carpenter et al. proposed the spacecraft formation flying missions for low Earth orbit (LEO) and highly elliptical orbit (HEO), such as the Molniya satellite formation which has a long observation time [9, 61]. In Refs. [62, 63], the orbit initialization method was presented for a tetrahedron geometry, and Zhang and Sun presented a set of closed-form solutions using the linearized relative motion to design a formation in eccentric orbits [64]. Wang et al. presented the initial mean orbital elements for the natural satellite formation under the first-order geopotential perturbation [65]. Lane and Axelrad illustrated a formation design using the differential orbital elements of unperturbed eccentric orbits [66]. Palmer and Halsall presented a natural formation design based on an analytic model in near circular orbits considering the Earth's oblateness [67]. Xu et al. presented the passive and periodic formations at the critical inclination to minimize the control efforts under J_2 perturbation [68].

Maneuver problem

The maneuver problem from one orbit to another has been under development, since the problem determining the orbit trajectory is usually investigated using observation data. The goals of the traditional maneuver problem are to change the orbit size or shape of a single spacecraft with respect to a planet considering mission requirements, and to minimize the control effort during the maneuver. For the spacecraft formation, on the other hand, the formation can be reconfigured by increasing or decreasing the formation radius and/or changing the formation geometry through the maneuver in the relative motion with respect to the leader spacecraft. This transfer between two orbits can be generally performed by continuous control input or impulsive control input.

Using the continuous control input, the optimal control problem has been studied to find the optimal transfer trajectory where two position vectors and velocity vectors at the initial and final time are specified. The optimal control problem is solved by two approaches: indirect method and direct method. The indirect method provides a solution of the optimal control problem, which satisfies the first-order necessary conditions for the optimality according to the calculus of variations and Pontryagin's minimum principle [69, 70]. The primary advantage of the indirect method is a high accurate solution satisfying the first-order optimality condition. In contrast, the indirect method has small radius of convergence, and therefore good initial guess of unknown boundary condition and state/costate variables is required. On the other hand, the optimal control problem can be easily solved by the direct method, which includes the collocation method and nonlinear programming problem [70]. The main advantage of the direct method is larger radius of convergence than that of the indirect method, and thus good initial guess of boundary condition and state/costate variables is not required. However, the optimality conditions are not considered, and therefore the solution of the direct method is less accurate

than that of the indirect method. Lawden presented the primer vector theory for the trajectory optimization [71], Prussing and Chiu used the primer vector theory for the optimal rendezvous problem using multi-impulse [72], and Jezewski and Stoolz described the trajectory for minimum-fuel consumptions with the constant thrust using the primer vector theory [73]. Based on the HCW equation, Billik obtained the optimal rendezvous maneuvers using a differential game approach [74], and Guelman and Aleshin studied the optimal bounded low-thrust rendezvous problem [75]. In addition, the optimal low-thrust rendezvous was presented based on six orbital elements in Refs. [76, 77], and Schaub et al. presented a feedback control law to keep the formation of satellites using mean orbit elements [78]. The optimal rendezvous problem in the elliptic orbit based on the TH equation was presented in Refs. [37, 38, 40, 41, 79, 80, 81, 82]. Zanon and Campbell presented the optimal low-thrust maneuver for the minimum time or fuel problem, and the optimal planner for spacecraft formation flying based on the TH equation [83]. Palmer obtained the solution of the optimal maneuver problem for the spacecraft formation flying [84].

Much work on the trajectory optimization has been developed using the direct method [85, 86, 87, 88, 89, 90]. The optimal guidance algorithm of the spacecraft formation was described and applied to the MMS Mission and LISA in Ref. [91]. The optimization problem of low-thrust reconfiguration maneuver was studied for the spacecraft formation flying via the direct method in Ref. [92]. Gong et al. presented a method for the formation configuration in the eccentric orbit using the pseudospectral method [93], and Huntington and Rao studied the optimal reconfiguration problem of the spacecraft formation using the Gauss pseudospectral method [94]. Moreover, Wu et al. described the optimal trajectory minimizing the fuel for the reconfiguration of spacecraft formation using the Legendre pseudospectral method [95].

The traditional maneuver problem of the spacecraft orbit transfer has been solved by two-impulsive control inputs. The Hohmann transfer is well known as two-burn minimum fuel transfer in the circular coplanar orbits [23, 31, 96]. For the general two-impulse maneuver problem between two fixed position vectors with the specified flight time, the transfer orbit can be determined by solving the Lambert's problem [31, 97, 98], and therefore the required velocity vectors of the resulting transfer orbit can be calculated at the initial and final time. Many researchers utilized the Lambert's problem to obtain the transfer trajectory between two orbits with respect to a planet [99, 100, 101, 102, 103, 104]. Won considered minimum-fuel and minimum-time orbit transfer problem in two coplanar elliptic orbits [100]. Prussing considered the minimum-fuel impulsive spacecraft trajectory through the multiple-revolution [101], and Shen and Tsiotras studied the optimal fixed-time, two-impulse rendezvous problem between two satellites in the coplanar circular orbit using multiple-revolution Lambert's problem [102, 103]. Thomas and Surka concerned the rendezvous problem between two satellites in nonplanar eccentric orbits through the Lambert's problem [104], and Jiang et al. presented the two-point boundary value problem which was solved by the Lambert's problem for the formation of satellites [105].

For the spacecraft formation, in addition to the above works, Tillerson et al. presented the optimal trajectory using the linear programming (LP) [106, 107], and Richards et al. used the Mixed-Integer Linear Programming (MILP) for the trajectory planning subject to the collision avoidance [108]. In Ref. [109], the spacecraft planning problem was formulated as minimum time or fuel problem, and the reconfiguration of the spacecraft formation was studied using the generating function where the initial and final position vectors and the flight time are specified in Ref. [110]. Vaddi et al. studied the formation reconfiguration problem using the impulsive control based on Gauss's varia-

tional equation [111]. Ketema considered the optimal transfer problem using two impulsive control inputs considering the relative motion of the spacecraft formation [112].

1.3 Contribution

In this dissertation, several contributions are made especially for the periodic relative motion and maneuver problem for spacecraft formation flying in the elliptic reference orbit. The major contributions are summarized as follows:

• **Periodic relative motion in elliptic reference orbits** (Chapter 3): The general periodicity condition is derived to guarantee the bounded relative motion at an arbitrary position in elliptic orbits. In previous works, the initial condition of the periodic relative motion in elliptic orbits was obtained by correcting the analytic solution of the HCW equation through the perturbation method. Moreover, the periodic conditions at specific positions such as perigee and apogee were described using a state transition matrix, and these conditions were considered as constraints in the optimization problem to determine the periodic condition at an arbitrary position. Therefore, it is necessary to analytically obtain the general periodic condition in the elliptic reference orbit so as to understand the complicated relative motion and to maintain the bounded relative motion. In this study, the general periodicity condition in the elliptic orbit is investigated using two approaches: state transition matrix approach and energy matching condition approach. In the state transition matrix approach, a true anomaly is taken as a free variable, and the analytic general periodicity condition is presented at an arbitrary initial position in the elliptic orbit. After that, the relationship between the general initial condition of the state transition matrix approach and that of the energy matching condition approach is established. As a result, the periodic relative

motion with zero secular drift is derived using the resulting periodic condition. Numerical simulation verifies that the periodic condition covers each partial periodic condition of the previous studies. Consequently, the provided periodic condition in the elliptic reference orbit can lead the periodic relative motion at an arbitrary position as well as at specific positions including perigee and apogee without any extra computation such as the perturbation method or the optimization method.

• **Formation pattern analysis and design** (Chapter 4):
The formation geometry in elliptic orbits is designed and its pattern is analyzed with respect to the eccentricity of the reference orbit. For the circular as well as nearly circular orbits, the relative motion of the spacecraft formation can be easily established in the radial/along-track plane. However, for the elliptic reference orbits, it is difficult to analyze and design the relative motion due to the nonlinearity and eccentricity. To perform various formation missions, the relative motion between spacecraft should be studied more rigorously, which will lead to understand the spacecraft formation in the elliptic reference orbit. In this study, two formation types are designed to achieve various formation missions: the radial/along-track plane formation and along-track/cross-track plane formation. Furthermore, the designed formations are analyzed; the variation of the relative distance between two spacecraft is presented according to the eccentricity of the reference orbit in all formation types. These results provide the tendency of the formation radius as a function of eccentricity of the reference orbit, and therefore the obtained results can provide the constraints and guideline to design the spacecraft formation mission between two spacecraft in the elliptic orbits.

- **Maneuver problem in relative motion using continuous and impulsive control input** (Chapter 5):

Transfer trajectories considering the energy and fuel efficiencies are designed to perform the formation reconfiguration. Maneuver problem between two orbits is required to change the formation geometry with respect to the leader spacecraft. Considering the type of thruster, different maneuver problem is defined. For the continuous thrust, a general optimal control problem is treated, and for the impulsive thrust, the Lambert's problem is considered. Note that the traditional maneuver problem is solved in an inertial frame with respect to a planet; however, in this study, it is required to obtain the transfer trajectory with respect to the leader spacecraft in the LVLH frame. For the continuous control input, the optimal control problem is solved based on nonlinear programming problem considering two cost functions, the minimum energy and the minimum fuel, where two relative position and velocity vectors are specified in the formation design procedure. For the impulsive control input, the classical Lambert's problem is modified to solve the maneuver problem in the relative dynamics between two spacecraft in the LVLH frame. Furthermore, the transfer orbit and the velocity change, ΔV, are obtained for the specified initial and final position vectors, and the minimum ΔV is presented through the grid search for the impulsive control input.

1.4 Dissertation Outline

This dissertation focuses on the periodic relative motion and the maneuver problem for the spacecraft formation flying in an elliptic reference orbit. This dissertation is organized as follows.

Chapter 2 describes the celestial mechanics and the relative motion dynamics. To express the motion of spacecraft in an orbit, three types of reference frames are introduced. Six orbital elements are described to present

the two-body orbit, which are widely used to illustrate the orbit of spacecraft. Moreover, the relative motion between two spacecraft is expressed for the spacecraft formation flying. For a circular orbit, the HCW equation and its analytic solution are described, and for an elliptic orbit, the TH equation and its analytic solution are presented.

Chapter 3 presents the general periodic condition via two approaches: state transition matrix and energy matching condition approaches. The state transition matrix can express the state propagation of the given initial conditions, and the energy matching condition can present the energy and period of the reference orbit of spacecraft. The analytic periodic solution is presented using the resulting periodic condition. Numerical simulation is performed to verify and compare the general periodic condition with the results of previous works.

Chapter 4 analyzes the formation pattern and discusses the initialization for the spacecraft formation. To design and analyze the formation, two formation types are considered: radial/along-track plane formation and along-track/cross-track plane formation. The change of the formation patterns in two formation geometries are studied with respect to the eccentricity and true anomaly of the reference orbit. Moreover, the initial conditions consisting of the relative position and velocity vectors are derived for the two formation types. Numerical simulation is performed to illustrate the formation patterns, and the variation of the formation radius is analyzed with respect to the eccentricity of the leader spacecraft. In addition, the angle difference between two follower spacecraft is presented according to the formation radius and the eccentricity of the reference orbit.

Chapter 5 describes the maneuver problem for the formation reconfiguration using the continuous and impulsive control inputs. For the continuous control input, the optimal control problem is selected using the nonlinear programming, and two cost functions are considered: (i) minimum energy, and

(ii) minimum fuel, during the maneuver. For the impulsive control input, the classic Lambert's problem is modified to solve the transfer problem of the relative motion dynamics between two spacecraft in the LVLH frame.

Chapter 6 provides the numerical simulation results to verify the effectiveness of the maneuver for the spacecraft formation. For the numerical simulation, changing the formation radius and geometry in two formation types is considered. The transfer trajectories during the maneuver are shown for the continuous control input and impulsive control input proposed in Chapter 5. For the impulsive control input, the grid search is used to find a set of the initial and final position vectors having the minimum velocity change, and then corresponding transfer orbit is presented.

Chapter 7 summarizes the concluding remarks of this dissertation, and provides recommendations for further works.

Chapter 2

Celestial Mechanics and Relative Motion Dynamics

2.1 Introduction

Spacecraft formation flying can be described using the equation of motion in an inertial reference frame, the differential orbital elements, and the relative dynamics of orbit motion based on the rotating frame. Moreover, the nonlinear equation of motion is linearized with assumptions such as the HCW equation for circular reference orbits and the TH equation for elliptic reference orbit. These equations have been used to solve the rendezvous and docking problem, and they are also applied to the design of spacecraft formation and maneuver problem.

Three types of reference frames are illustrated to present the motion of a spacecraft in an orbit around the Earth in Section 2.2. In addition, the six orbital elements are expressed in Section 2.3, which describe a spacecraft orbit instead of the position and velocity vectors with respect to the Earth in Cartesian coordinate system. In Section 2.4, the nonlinear relative dynamics are presented by the two-body problem. Moreover, the HCW equation and

the analytic solution are described in Section 2.4.1, and the TH equation and its analytic solution presented by the true anomaly as a free variable are expressed in Section 2.4.2.

2.2 Reference Frame

2.2.1 Earth Centered Inertial Frame

The Earth Centered Inertial (ECI) frame is a non-rotating reference frame as shown in Fig. 2.1, where the Newton's laws are valid. The origin of the frame is located at the center of the mass of the Earth and the axes are pointing in fixed directions with respect to the stars. The $X-Y$ plane coincides with the Earth's equatorial plane, the X-axis is taken to point from the center of the mass of the Earth to the direction of vernal equinox, the Z-axis is taken normal to the $X-Y$ plane in the direction of the north pole, and the Y-axis

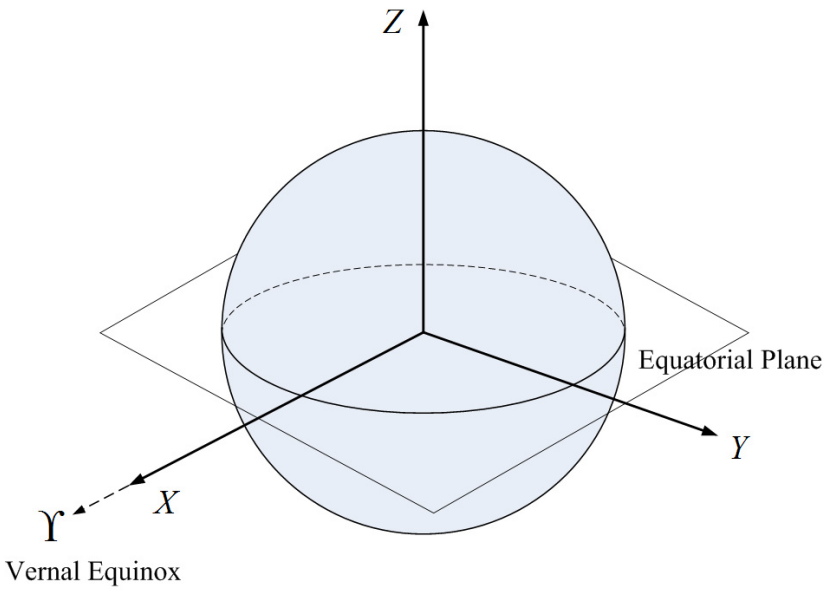

Figure 2.1: Earth Centered Inertial (ECI) frame

is chosen to complete a right-handed coordinate system.

2.2.2 Earth Centered Earth Fixed Frame

The Earth Centered Earth Fixed (ECEF) frame has the origin located at the center of the Earth, and the $X_E - Y_E$ plane coincides with the Earth's equatorial plane as shown in Fig. 2.2. The X_E-axis points toward the intersection between the Greenwich meridian and equator, which is 0° longitude and 0° latitude, the Z_E-axis points through the north pole, and the Y_E-axis points in the direction of 90°E longitude. The X_E-, Y_E-, and Z_E-axes rotate relative to the ECI frame with a constant angular velocity, $\omega_E = 7.2921 \times 10^{-5}\, rad/s$ due to the daily rotation of the Earth, thus the ECEF frame is not an inertial reference frame.

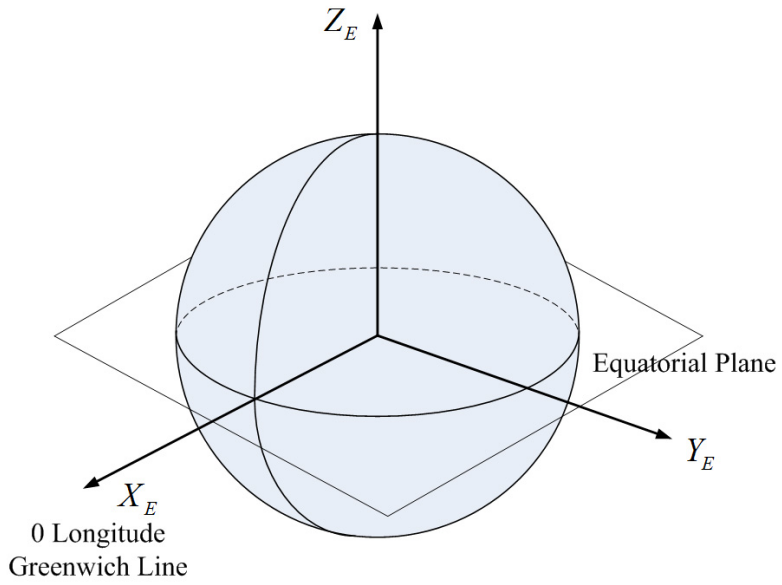

Figure 2.2: Earth Centered Earth Fixed (ECEF) frame

2.2.3 Local Vertical Local Horizontal Frame

The Local-Vertical-Local-Horizontal (LVLH) frame is widely used to describe the relative motion, as shown in Fig. 2.3. The LVLH frame is attached to a spacecraft and orbit-fixed with an origin at the center of the spacecraft, so the LVLH frame rotates with angular velocity. The x-axis points in the radial direction of the spacecraft radius vector $\vec{R}$, the y-axis points in the along-track direction, and the z-axis is perpendicular to the orbital plane and points in the direction of the angular momentum vector. Note that the y-axis does not coincide with the velocity vector; y-axis is align with the velocity vector for a circular orbit and for an elliptic orbit at perigee and apogee.

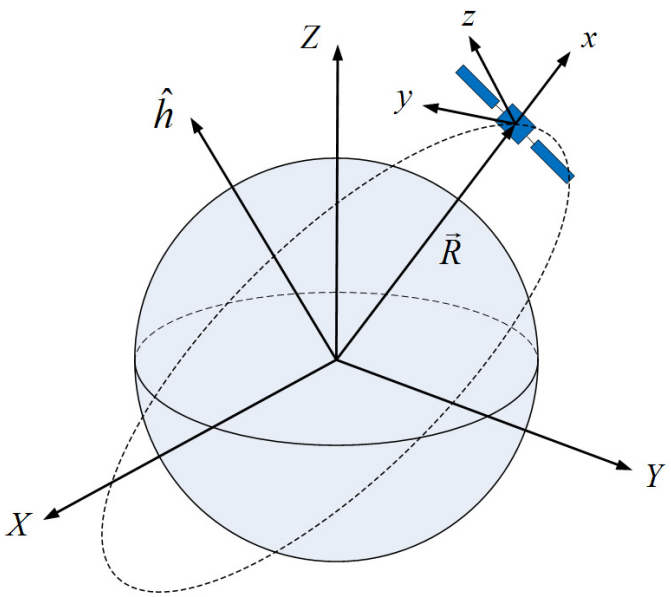

Figure 2.3: Local Vertical Local Horizontal (LVLH) frame

2.3 Orbital Elements

To describe an orbit of a given spacecraft, six parameters are required. For instance, three elements of position and three elements of velocity can present the orbit of a spacecraft. However, these six parameters are difficult to illustrate an orbit, and thus six parameters as Keplerian orbital elements are commonly used to show an orbit of a spacecraft.

Six orbital elements can present the two-body orbit and the initial conditions for solving the equations of motion, as initial position and velocity vectors can provide a solution of the differential equations of motion. Figure 2.4 shows the classical orbital elements $\{a, e, i, \Omega, \omega, \nu\}$; a is semi-major axis, e is eccentricity, i is inclination, Ω is longitude of the ascending node, ω is argument of perigee, and ν is true anomaly. Two constant values, a and e,

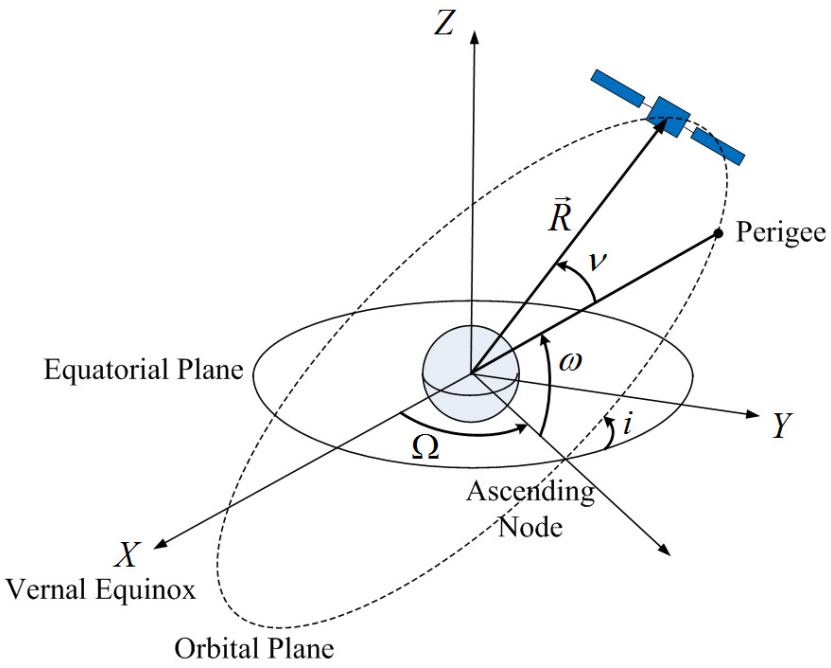

Figure 2.4: Orbital elements

determine the size and shape of an orbit; a describes half the distance across the major axis of an orbit, and e defines the shape of an orbit. i defines the tilt of the orbital plane with respect to the equatorial plane ($0^\circ \leq i \leq 180^\circ$), Ω is the angle between the vernal equinox direction (X) and the ascending node in the equatorial plane ($0^\circ \leq \Omega \leq 360^\circ$), which defines the location where a spacecraft crosses from the Southern Hemisphere into the Northern Hemisphere, ω is the angle from the ascending node to perigee ($0^\circ \leq \omega \leq 360^\circ$), and ν presents the current position of a spacecraft relative to the perigee ($0^\circ \leq \nu \leq 360^\circ$).

Three parameters, i, Ω, and ω, can describe the orbit plane orientation as (3-1-3) Euler angles, and then the following direction cosine matrix can be obtained as

$$C = C(i, \Omega, \theta) = \begin{bmatrix} \cos\Omega\cos\theta - \sin\Omega\sin\theta\cos i & \sin\Omega\cos\theta + \cos\Omega\sin\theta\cos i & \sin\theta\sin i \\ -\cos\Omega\sin\theta - \sin\Omega\cos\theta\cos i & -\sin\Omega\sin\theta + \cos\Omega\cos\theta\cos i & \cos\theta\sin i \\ \sin\Omega\sin i & -\cos\Omega\sin i & \cos i \end{bmatrix} \tag{2.1}$$

where $\theta = \omega + \nu$. With Eq. (2.1), the inertial position vector $\vec{R}$ can be expressed as

$$\vec{R} = R \begin{bmatrix} \cos\Omega\cos\theta - \sin\Omega\sin\theta\cos i \\ \sin\Omega\cos\theta + \cos\Omega\sin\theta\cos i \\ \sin\theta\sin i \end{bmatrix} \tag{2.2}$$

where R is the distance between a spacecraft and the Earth. Therefore, orbital elements can directly illustrate the current inertial position vector.

2.4 Relative Motion Dynamics

In this section, the relative motion between the leader and follower spacecraft is expressed for the spacecraft formation flying.

First, let us describe the two-body problem. Two bodies exist with mass m_1 and m_2 moving in space. The motion can be described with respect to an inertial frame which has basis unit vectors $\{\mathbf{i}_x, \mathbf{i}_y, \mathbf{i}_z\}$, when the only forces are gravitational attraction. The position and velocity of m_i in the inertial frame can be defined by

$$\mathbf{r}_i = x_i\mathbf{i}_x + y_i\mathbf{i}_y + z_i\mathbf{i}_z \tag{2.3}$$

$$\mathbf{v}_i = \frac{dx_i}{dt}\mathbf{i}_x + \frac{dy_i}{dt}\mathbf{i}_y + \frac{dz_i}{dt}\mathbf{i}_z \tag{2.4}$$

The distance between two bodies is obtained as

$$r_{12} = ||\mathbf{r}_1 - \mathbf{r}_2|| \tag{2.5}$$

The force of attraction for m_1 and m_2 can be expressed according to Newton's second law as

$$m_1\frac{d^2\mathbf{r}_1}{dt^2} = G\frac{m_1m_2}{r_{12}^3}(\mathbf{r}_2 - \mathbf{r}_1) \tag{2.6}$$

$$m_2\frac{d^2\mathbf{r}_2}{dt^2} = G\frac{m_1m_2}{r_{21}^3}(\mathbf{r}_1 - \mathbf{r}_2) \tag{2.7}$$

where G is the universal gravity constant. Equations (2.6) and (2.7) yield

$$m_1\frac{d^2\mathbf{r}_1}{dt^2} + m_2\frac{d^2\mathbf{r}_2}{dt^2} = 0 \tag{2.8}$$

The gravitational coefficient μ is defined as

$$\mu = G(m_1 + m_2) \tag{2.9}$$

For the spacecraft in the Earth's orbit, because the mass m_2 of the spacecraft can be negligible compared to the mass m_1 of the Earth ($m_1 \gg m_2$), μ can be approximated as

$$\mu = Gm_1 \tag{2.10}$$

From Eqs. (2.6) and (2.7), the equation of motion of m_2 relative to m_1 can be expressed as follows:

$$\ddot{\mathbf{r}} = -\frac{\mu}{r^3}\mathbf{r} \tag{2.11}$$

where $\mathbf{r} = \mathbf{r}_2 - \mathbf{r}_1$. Equation (2.11) is known as the two-body problem. The gravitational potential energy function can be obtained as

$$V(\mathbf{r}) = -\frac{\mu}{r} \tag{2.12}$$

Next, the relative motion between the leader and follower spacecraft is considered for the spacecraft formation flying as shown in Fig. 2.5. In Fig. 2.5, $\boldsymbol{R} \in \Re^3$ is the position vector of the leader spacecraft, $\boldsymbol{R}_f \in \Re^3$ is the position vector of the follower spacecraft, and $\boldsymbol{\rho} \in \Re^3$ is the relative position vector of the follower spacecraft with respect to the leader spacecraft; $\boldsymbol{R}_f$ is given as

$$\boldsymbol{R}_f = \boldsymbol{R} + \boldsymbol{\rho} \tag{2.13}$$

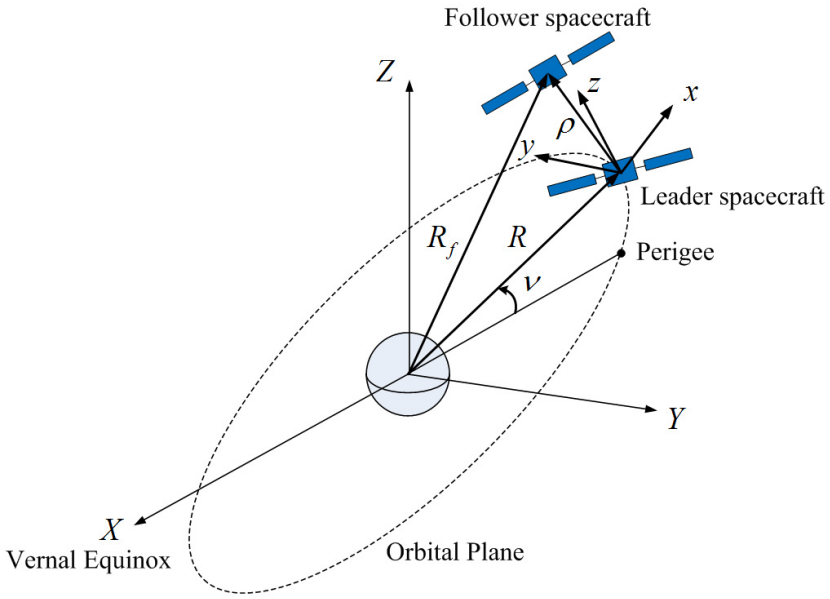

Figure 2.5: Relative motion between leader and follower Spacecraft

If the Earth is assumed to be a uniformly distributed sphere, the leader and follower spacecraft have a gravitational potential function V and V_f from Eq. (2.12) as follows:

$$V = -\frac{\mu}{R} \tag{2.14}$$

$$V_f = -\frac{\mu}{R_f} \tag{2.15}$$

where $R = ||\boldsymbol{R}||$ is the distance between the leader spacecraft and the Earth, and $R_f = ||\boldsymbol{R}_f||$ is the distance between the follower spacecraft and the Earth. The equations of motion between the Earth and leader spacecraft and between the Earth and follower spacecraft in the ECI frame, respectively, are given by

$$\ddot{\boldsymbol{R}} = -\frac{\mu}{R^3}\boldsymbol{R} \tag{2.16}$$

$$\ddot{\boldsymbol{R}}_f = -\frac{\mu}{R_f^3}\boldsymbol{R}_f \tag{2.17}$$

The relative position vector in ECI frame, I, can be expressed as

$$[\boldsymbol{\rho}]_I = \boldsymbol{R}_f - \boldsymbol{R} \tag{2.18}$$

The relative acceleration is given by

$$[\ddot{\boldsymbol{\rho}}]_I = -\frac{\mu}{R_f^3}\boldsymbol{R}_f + \frac{\mu}{R^3}\boldsymbol{R} \tag{2.19}$$

To present the relative motion between the leader and follower spacecraft in rotating LVLH frame, L, the relative motion in the ECI frame is expressed in terms of the LVLH frame using following transport theorem [113].

$$[\ddot{\boldsymbol{\rho}}]_I = \ddot{\boldsymbol{\rho}} + 2\omega \times \dot{\boldsymbol{\rho}} + \dot{\omega} \times \dot{\boldsymbol{\rho}} + \omega \times (\omega \times \boldsymbol{\rho}) \tag{2.20}$$

where $\boldsymbol{\rho} = [\boldsymbol{\rho}]_L$ and $\omega = [\omega_x \quad \omega_y \quad \omega_z]^T \in \Re^3$ is the angular velocity. If only external forces act on a central gravitational field, then $\omega_x = \omega_y = 0$ and $\omega_z = \dot{\theta} = \dot{\nu}$, as the argument of perigee is constant, where θ is the latitude angle of the leader spacecraft, $\dot{\theta}$ is the orbital angular velocity, and ν is the

true anomaly of the leader spacecraft. In the LVLH frame, $\boldsymbol{R} \equiv [R \quad 0 \quad 0]^T$ and $\boldsymbol{\rho} \equiv [x \quad y \quad z]^T$, and then $\boldsymbol{R}_f$ is defined as follows:

$$\boldsymbol{R}_f = [R + x \quad y \quad z]^T \tag{2.21}$$

Substituting Eqs. (2.19) and (2.21) into Eq. (2.20), the nonlinear relative dynamics can be represented as follows:

$$\begin{aligned}
\ddot{x} &= 2\dot{\theta}\dot{y} + \ddot{\theta}y + \dot{\theta}^2 x - \frac{\mu(R+x)}{\{(R+x)^2 + y^2 + z^2\}^{3/2}} + \frac{\mu}{R^2} \\
\ddot{y} &= -2\dot{\theta}\dot{x} - \ddot{\theta}x + \dot{\theta}^2 y - \frac{\mu y}{\{(R+x)^2 + y^2 + z^2\}^{3/2}} \\
\ddot{z} &= -\frac{\mu z}{\{(R+x)^2 + y^2 + z^2\}^{3/2}}
\end{aligned} \tag{2.22}$$

In the orbital mechanics, the radius and angular velocity of the leader spacecraft are defined as [113]

$$R = \frac{a(1-e^2)}{1 + e\cos\nu} \tag{2.23}$$

$$\dot{\theta} = \frac{n(1 + e\cos\nu)^2}{(1-e^2)^{3/2}} \tag{2.24}$$

where a is the semi-major axis, e is the eccentricity, and $n = \sqrt{\frac{\mu}{a^3}}$ is the natural frequency of the leader spacecraft.

2.4.1 Hill-Clohessy-Wiltshire Equation

If the leader spacecraft has a circular reference orbit, then $e = 0$, and R and $\dot{\theta}$ in Eq. (2.22) are constant; $R = a$, $\dot{\theta} = n$, and $\ddot{\theta} = 0$. In addition, it is assumed that the follower spacecraft is very close to the leader spacecraft ($||\boldsymbol{\rho}|| \ll ||\boldsymbol{R}||$). Then, Eq. (2.22) can be rewritten as follows:

$$\begin{aligned}
\ddot{x} &= 2n\dot{y} + 3n^2 x \\
\ddot{y} &= -2n\dot{x} \\
\ddot{z} &= -n^2 z
\end{aligned} \tag{2.25}$$

Equation (2.25) is the Hill-Clohessy-Wiltshire (HCW) equation [20, 21]. Note that the relative motion in the circular reference orbit has decoupled in-plane motion ($x - y$) from the cross-track motion (z); the in-plane motion can be modeled as a coupled harmonic oscillator, and out-of-plane motion can be modeled as a harmonic oscillator.

The analytic solution of the HCW equation is given by [27]

$$x(t) = \frac{\dot{x}_0}{n}\sin nt - \left(3x_0 + \frac{2\dot{y}_0}{n}\right)\cos nt + 4x_0 + \frac{2\dot{y}_0}{n} \tag{2.26}$$

$$y(t) = \frac{2\dot{x}_0}{n}\cos nt + \left(6x_0 + \frac{4\dot{y}_0}{n}\right)\sin nt - (6nx_0 + 3\dot{y}_0)\,t - \frac{2\dot{x}_0}{n} + y_0 \tag{2.27}$$

$$z(t) = \frac{\dot{z}_0}{n}\sin nt + z_0\cos nt \tag{2.28}$$

where the subscript '0' is used to denote initial conditions at $t = 0$.

2.4.2 Tschauner-Hempel Equation

If the leader spacecraft has an elliptic reference orbit, the HCW equation cannot describe the relative motion because of the eccentricity of the reference orbit. To analyze the nonlinear relative motion equations in the elliptic reference orbit, Eq. (2.22) can be rewritten using the true anomaly ν as an independent variable, considering that ν of the reference orbit monotonically increases and describes the angular velocity with the radius presenting the orbital motion. The following transformation is considered:

$$\begin{aligned} \dot{(\cdot)} &= (\cdot)'\dot{\theta} \\ \ddot{(\cdot)} &= (\cdot)''\dot{\theta}^2 + \dot{\theta}\dot{\theta}'(\cdot)' \end{aligned} \tag{2.29}$$

where $(\cdot)'$ and $(\cdot)''$ denote the first and second derivatives with respect to ν, and

$$\dot{\theta} = \dot{\nu} = \frac{\sqrt{\mu p}}{R^2} = \sqrt{\frac{\mu}{p^3}}(1 + e\cos\nu)^2 \tag{2.30}$$

Using Eq. (2.29) with the assumption that $||\boldsymbol{\rho}|| \ll ||\boldsymbol{R}||$, the relative motion equation can be expressed as

$$\begin{aligned} x'' &= \frac{2e\sin\nu}{1+e\cos\nu}x' + 2y' + \frac{3+e\cos\nu}{1+e\cos\nu}x - \frac{2e\sin\nu}{1+e\cos\nu}y \\ y'' &= -2x' + \frac{2e\sin\nu}{1+e\cos\nu}y' + \frac{2e\sin\nu}{1+e\cos\nu}x + \frac{e\sin\nu}{1+e\cos\nu}y \\ z'' &= \frac{2e\sin\nu}{1+e\cos\nu}z' - \frac{1}{1+e\cos\nu}z \end{aligned} \tag{2.31}$$

Note that the radial and along-track components are coupled, but the cross-track component is decoupled from in-plane motion.

The analytical solution of the relative motion in an elliptic orbit is expressed as [29, 37]

$$\begin{aligned} x(\nu) &= c_1 e\sin\nu + c_2 e\left(2eH(\nu)\sin\nu - \frac{\cos\nu}{(1+e\cos\nu)^2}\right) - c_3\cos\nu \\ y(\nu) &= \left(c_1 + 2c_2 eH(\nu)\right)(1+e\cos\nu) \\ &\quad + c_3\left(1+\frac{1}{1+e\cos\nu}\right)\sin\nu + \frac{c_4}{1+e\cos\nu} \\ z(\nu) &= \frac{1}{1+e\cos\nu}\left(c_5\sin\nu + c_6\cos\nu\right) \end{aligned} \tag{2.32}$$

where $c_i,\ i = 1, \cdots, 6$ are integration constants, and $H(\nu)$ is an integration function with the expression of

$$H(\nu) = \int_{\nu_0}^{\nu} \frac{\cos\nu}{(1+e\cos\nu)^3} d\nu \tag{2.33}$$

The relative velocity can be obtained by

$$\begin{aligned} x'(\nu) &= c_1 e\cos\nu + c_2 e\left(2eH(\nu)\cos\nu + \frac{2e\sin\nu\cos\nu}{(1+e\cos\nu)^3} + \frac{\sin\nu(1-e\cos\nu)}{(1+e\cos\nu)^3}\right) \\ &\quad + c_3\sin\nu \\ y'(\nu) &= -c_1 e\sin\nu + 2c_2 e\left\{\frac{\cos\nu}{(1+e\cos\nu)^2} - e\sin\nu H(\nu)\right\} \\ &\quad + c_3\left\{\frac{(2+e\cos\nu)\cos\nu}{1+e\cos\nu} + \frac{e\sin^2\nu}{(1+e\cos\nu)^2}\right\} + \frac{c_4 e\sin\nu}{(1+e\cos\nu)^2} \\ z'(\nu) &= \frac{1}{(1+e\cos\nu)^2}\left\{c_5(1+e\cos\nu) - c_6\sin\nu\right\} \end{aligned} \tag{2.34}$$

2.5 Concluding Remarks

In this chapter, the relative motion dynamics are presented for the spacecraft formation flying. In Section 2.2, the ECI, ECEF, and LVLH frames are illustrated to describe the relative motion between two spacecraft. In addition, the orbital elements are described to express the motion of a spacecraft around the Earth, and they provide the position and velocity vectors of a spacecraft in Section 2.3. From the two-body problem, the relative motion dynamics between two spacecraft are expressed in Section 2.4, and the HCW equation is presented for the circular reference orbit. Moreover, the TH equation is presented to consider the eccentricity of the reference orbit. The analytics solutions of the HCW equation and the TH equation are also presented. Through these relative motion dynamics and analytic solutions, the periodic relative motion and formation geometry will be derived for the spacecraft formation.

Chapter 3

General Periodicity Condition

3.1 Introduction

For the spacecraft formation flying, all spacecraft in a formation have an identical period. When the leader spacecraft has a circular reference orbit, the HCW equation can describe the relative motion of the follower spacecraft as expressed in Eq. (2.25). As shown in the analytic solution of the HCW equation, $y(t)$ in Eq. (2.27) contains a secular term which grows large as time goes by. To avoid the secular drift in $y(t)$, the periodic condition can be obtained as

$$\dot{y}_0 = -2nx_0 \tag{3.1}$$

With Eq. (3.1), the analytic solutions in Eqs. (2.26)–(2.28) are expressed as follows:

$$\begin{aligned} x(t) &= \frac{\dot{x}_0}{n}\sin nt + x_0 \cos nt \\ y(t) &= \frac{2\dot{x}_0}{n}\cos nt - 2x_0 \sin nt - \frac{2\dot{x}_0}{n} + y_0 \\ z(t) &= \frac{\dot{z}_0}{n}\sin nt + z_0 \cos nt \end{aligned} \tag{3.2}$$

These resulting analytic solutions are used to analyze and design the spacecraft formation in circular reference orbits [30]. However, the HCW equation

and analytic solution in Eq. (3.2) cannot present the relative motion in elliptic reference orbits, since the HCW equation and analytic solution do not contain the eccentricity effect of the reference orbit. To make the spacecraft maintain a periodic relative motion in Keplerian elliptic orbits, a general periodicity condition for the elliptic reference orbit is required. In this chapter, the periodic condition is derived by investigating an analytic solution given in Eq. (2.32). To obtain the periodic condition, a state transition matrix and an energy matching condition approaches are used; the state transition matrix can express the state propagation of the given initial conditions, and the energy matching condition can describe the periods of Kelperian orbits. Then, the two resulting conditions are compared to each other.

The state transition matrix approach for the periodic relative motion is discussed and the general periodicity condition is derived in Section 3.2. Moreover, the periodic condition is obtained by the energy matching condition in Section 3.3. In Section 3.4, the analytic periodic solution in the elliptic reference orbit is described through the resulting periodicity condition. In Section 3.5, numerical simulations are performed to verify the periodicity condition, and the results with the periodic condition are compared with the results using the solution of the HCW equation and using the condition of previous studies.

3.2 State Transition Matrix Approach

The general periodic condition is derived using a state transition matrix with the analytic solution of the relative motion in an elliptic reference orbit.

Theorem 1 *The general periodicity condition, Eq. (3.3), from the state transition matrix approach makes the relative motion of two spacecraft have a bounded periodic motion in an arbitrary elliptical reference orbit.*

$$\begin{aligned}(2+e\cos\nu_0)x(\nu_0) - e\sin\nu_0 y(\nu_0) \\ + e\sin\nu_0 x'(\nu_0) + (1+e\cos\nu_0)y'(\nu_0) = 0\end{aligned} \tag{3.3}$$

Proof: Let us define the state vector $X(\nu) \in \Re^{6\times 1}$ and the integration constant vector $C \in \Re^{6\times 1}$ as

$$X(\nu) = \begin{bmatrix} x(\nu) & x'(\nu) & y(\nu) & y'(\nu) & z(\nu) & z'(\nu) \end{bmatrix}^T \tag{3.4}$$

$$C = \begin{bmatrix} c_1 & c_2 & c_3 & c_4 & c_5 & c_6 \end{bmatrix}^T \tag{3.5}$$

With the state and integration constant vectors, Eqs. (2.32) and (2.34) can be written as

$$X(\nu) = \Phi(\nu)C \tag{3.6}$$

where $\Phi(\nu) \in \Re^{6\times 6}$ is a fundamental matrix solution as given by

$$\Phi(\nu) = \begin{bmatrix} p_{11} & p_{12} & p_{13} & p_{14} & 0 & 0 \\ p_{21} & p_{22} & p_{23} & p_{24} & 0 & 0 \\ p_{31} & p_{32} & p_{33} & p_{34} & 0 & 0 \\ p_{41} & p_{42} & p_{43} & p_{44} & 0 & 0 \\ 0 & 0 & 0 & 0 & p_{55} & p_{56} \\ 0 & 0 & 0 & 0 & p_{65} & p_{66} \end{bmatrix} \tag{3.7}$$

with the corresponding values of the matrix elements:

$$
\begin{aligned}
p_{11} &= e\sin\nu \\
p_{12} &= e\left(2eH(\nu)\sin\nu - \frac{\cos\nu}{(1+e\cos\nu)^2}\right) \\
p_{13} &= -\cos\nu \\
p_{14} &= 0 \\
p_{21} &= e\cos\nu \\
p_{22} &= e\left(2eH(\nu)\cos\nu + \frac{\sin\nu}{(1+e\cos\nu)^2}\right) \\
p_{24} &= 0 \\
p_{13} &= -\cos\nu \\
p_{31} &= 1+e\cos\nu \\
p_{32} &= 2e(1+e\cos\nu)H(\nu), \\
p_{33} &= \frac{2+e\cos\nu}{1+e\cos\nu}\sin\nu \\
p_{34} &= \frac{1}{1+e\cos\nu} \\
p_{41} &= -e\sin\nu \\
p_{42} &= 2e\left(\frac{\cos\nu}{(1+e\cos\nu)^2} - eH(\nu)\sin\nu\right) \\
p_{43} &= \cos\nu + \frac{e+\cos\nu}{(1+e\cos\nu)^2} \\
p_{44} &= \frac{e\sin\nu}{(1+e\cos\nu)^2} \\
p_{55} &= \frac{\sin\nu}{1+e\cos\nu} \\
p_{56} &= \frac{\cos\nu}{1+e\cos\nu} \\
p_{65} &= \frac{e+\cos\nu}{(1+e\cos\nu)^2} \\
p_{66} &= \frac{-\sin\nu}{(1+e\cos\nu)^2}
\end{aligned}
$$

Using Eq. (3.6), the initial state vector at $\nu = \nu_0$ can be expressed as follows:

$$X(\nu_0) = \Phi(\nu_0)C \tag{3.8}$$

where $X(\nu_0) = [x(\nu_0)\ x'(\nu_0)\ y(\nu_0)\ y'(\nu_0)\ z(\nu_0)\ z'(\nu_0)]^T$. Because the fundamental matrix is invertible, the integration constant vector C in Eq. (3.8) can be obtained as

$$C = \Phi^{-1}(\nu_0)X(\nu_0) \tag{3.9}$$

Substituting Eq. (3.9) into Eq. (3.6) gives

$$\begin{aligned} X(\nu) &= \Phi(\nu)\Phi^{-1}(\nu_0)X(\nu_0) \\ &= T(\nu, \nu_0)X(\nu_0) \end{aligned} \tag{3.10}$$

In this equation, the matrix $T(\nu, \nu_0) = \Phi(\nu)\Phi^{-1}(\nu_0)$ is a state transition matrix. Using $H(\nu_0) = 0$ in Eq. (3.7), the inverse of $\Phi(\nu_0)$ can be obtained as

$$\Phi^{-1}(\nu_0) = \begin{bmatrix} q_{11} & q_{12} & q_{13} & q_{14} & 0 & 0 \\ q_{21} & q_{22} & q_{23} & q_{24} & 0 & 0 \\ q_{31} & q_{32} & q_{33} & q_{34} & 0 & 0 \\ q_{41} & q_{42} & q_{43} & q_{44} & 0 & 0 \\ 0 & 0 & 0 & 0 & q_{55} & q_{56} \\ 0 & 0 & 0 & 0 & q_{65} & q_{66} \end{bmatrix} \tag{3.11}$$

with the corresponding values of the matrix elements:

$$
\begin{aligned}
q_{11} &= \frac{\sin\nu_0}{e} \\
q_{12} &= \frac{\cos\nu_0}{e} \\
q_{13} &= 0 \\
q_{14} &= 0 \\
q_{21} &= \frac{(2+e\cos\nu_0)(1+e\cos\nu_0)^2}{e^2} \\
q_{22} &= \frac{\sin\nu_0(1+e\cos\nu_0)^2}{e}, \\
q_{23} &= -\frac{\sin\nu_0(1+e\cos\nu_0)^2}{e} \\
q_{24} &= \frac{(1+e\cos\nu_0)^3}{e^2} \\
q_{31} &= -\frac{2(1+e\cos\nu_0)}{e} \\
q_{32} &= 0 \\
q_{33} &= \sin\nu_0 \\
q_{34} &= -\frac{1+e\cos\nu_0}{e} \\
q_{41} &= \frac{\sin\nu_0(3+e\cos\nu_0)(1+e\cos\nu_0)}{e} \\
q_{42} &= -\frac{\cos\nu_0(1+e\cos\nu_0)^2}{e} \\
q_{43} &= 1-2\sin^2\nu_0+e\cos^3\nu_0 \\
q_{44} &= \frac{\sin\nu_0(2+e\cos\nu_0)(1+e\cos\nu_0)}{e} \\
q_{55} &= \sin\nu_0 \\
q_{56} &= \cos\nu_0(1+e\cos\nu_0) \\
q_{65} &= e+\cos\nu_0 \\
q_{66} &= -\sin\nu_0(1+e\cos\nu_0)
\end{aligned}
$$

Substituting Eqs. (3.7) and (3.11) into the definition of the state transition matrix, we have

$$T(\nu,\nu_0)=\Phi(\nu)\Phi^{-1}(\nu_0)=\begin{bmatrix} T_{11} & T_{12} & T_{13} & T_{14} & 0 & 0 \\ T_{21} & T_{22} & T_{23} & T_{24} & 0 & 0 \\ T_{31} & T_{32} & T_{33} & T_{34} & 0 & 0 \\ T_{41} & T_{42} & T_{43} & T_{44} & 0 & 0 \\ 0 & 0 & 0 & 0 & T_{55} & T_{56} \\ 0 & 0 & 0 & 0 & T_{65} & T_{66} \end{bmatrix} \tag{3.12}$$

with the corresponding values of the matrix elements:

$$\begin{aligned}
T_{11} &= p_{11}q_{11}+p_{12}q_{21}+p_{13}q_{31} \\
T_{12} &= p_{11}q_{12}+p_{12}q_{22}+p_{13}q_{32} \\
T_{13} &= p_{12}q_{23}+p_{13}q_{34} \\
T_{14} &= p_{12}q_{24}+p_{13}q_{34} \\
T_{21} &= p_{21}q_{11}+p_{22}q_{21}+p_{23}q_{31} \\
T_{22} &= p_{21}q_{12}+p_{22}q_{22}+p_{23}q_{32} \\
T_{23} &= p_{22}q_{23}+p_{23}q_{33} \\
T_{24} &= p_{22}q_{24}+p_{23}q_{34} \\
T_{31} &= p_{31}q_{11}+p_{32}q_{21}+p_{33}q_{31}+p_{34}q_{41} \\
T_{32} &= p_{31}q_{12}+p_{32}q_{22}+p_{33}q_{32}+p_{34}q_{42} \\
T_{33} &= p_{32}q_{23}+p_{33}q_{33}+p_{34}q_{43} \\
T_{34} &= p_{32}q_{24}+p_{33}q_{34}+p_{34}q_{44} \\
T_{41} &= p_{41}q_{11}+p_{42}q_{21}+p_{43}q_{31}+p_{44}q_{41} \\
T_{42} &= p_{41}q_{12}+p_{42}q_{22}+p_{43}q_{32}+p_{44}q_{42} \\
T_{43} &= p_{42}q_{23}+p_{43}q_{33}+p_{44}q_{43}
\end{aligned}$$

$$T_{44} = p_{42}q_{24} + p_{43}q_{34} + p_{44}q_{44}$$

$$T_{55} = p_{55}q_{55} + p_{56}q_{65}$$

$$T_{56} = p_{55}q_{56} + p_{56}q_{66}$$

$$T_{65} = p_{65}q_{55} + p_{66}q_{65}$$

$$T_{66} = p_{65}q_{56} + p_{66}q_{66}$$

At this point, to deal with the periodic relative motion, a state transition matrix mapping between $\nu = \nu_0$ and $\nu = 2\pi + \nu_0$ is considered. Using Eq. (3.12), the state transition matrix $T(2\pi + \nu_0, \nu_0)$ is given by

$$T(2\pi + \nu_0, \nu_0) = \begin{bmatrix} \bar{T}_{11} & \bar{T}_{12} & \bar{T}_{13} & \bar{T}_{14} & 0 & 0 \\ \bar{T}_{21} & \bar{T}_{22} & \bar{T}_{23} & \bar{T}_{24} & 0 & 0 \\ \bar{T}_{31} & \bar{T}_{32} & \bar{T}_{33} & \bar{T}_{34} & 0 & 0 \\ \bar{T}_{41} & \bar{T}_{42} & \bar{T}_{43} & \bar{T}_{44} & 0 & 0 \\ 0 & 0 & 0 & 0 & \bar{T}_{55} & \bar{T}_{56} \\ 0 & 0 & 0 & 0 & \bar{T}_{65} & \bar{T}_{66} \end{bmatrix} \tag{3.13}$$

with the corresponding values of the matrix elements:

$$\bar{T}_{11} = 1 + 2H(2\pi + \nu_0)\sin\nu_0(2 + e\cos\nu_0)(1 + e\cos\nu_0)^2$$

$$\bar{T}_{12} = 2eH(2\pi + \nu_0)\sin^2\nu_0(1 + e\cos\nu_0)^2$$

$$\bar{T}_{13} = -2eH(2\pi + \nu_0)\sin^2\nu_0(1 + e\cos\nu_0)^2$$

$$\bar{T}_{14} = 2H(2\pi + \nu_0)\sin\nu_0(1 + e\cos\nu_0)^3$$

$$\bar{T}_{21} = 2H(2\pi + \nu_0)\cos\nu_0(2 + e\cos\nu_0)(1 + e\cos\nu_0)^2$$

$$\bar{T}_{22} = 1 + 2eH(2\pi + \nu_0)\sin\nu_0\cos\nu_0(1 + e\cos\nu_0)^2$$

$$\bar{T}_{23} = -2eH(2\pi + \nu_0)\sin\nu_0\cos\nu_0(1 + e\cos\nu_0)^2$$

$$\bar{T}_{24} = 2H(2\pi + \nu_0)\cos\nu_0(1 + e\cos\nu_0)^3$$

$$\bar{T}_{31} = \frac{2H(2\pi+\nu_0)}{e}(2+e\cos\nu_0)(1+e\cos\nu_0)^3$$

$$\bar{T}_{32} = 2H(2\pi+\nu_0)\sin\nu_0(1+e\cos\nu_0)^3$$

$$\bar{T}_{33} = 1-2H(2\pi+\nu_0)\sin\nu_0(1+e\cos\nu_0)^3$$

$$\bar{T}_{34} = \frac{2H(2\pi+\nu_0)}{e}(1+e\cos\nu_0)^4$$

$$\bar{T}_{41} = -2H(2\pi+\nu_0)\sin\nu_0(2+e\cos\nu_0)(1+e\cos\nu_0)^2$$

$$\bar{T}_{42} = -2eH(2\pi+\nu_0)\sin^2\nu_0(1+e\cos\nu_0)^2$$

$$\bar{T}_{43} = 2eH(2\pi+\nu_0)\sin^2\nu_0(1+e\cos\nu_0)^2$$

$$\bar{T}_{44} = 1-2H(2\pi+\nu_0)\sin\nu_0(1+e\cos\nu_0)^3$$

$$\bar{T}_{55} = 1$$

$$\bar{T}_{56} = 0$$

$$\bar{T}_{65} = 0$$

$$\bar{T}_{66} = 1$$

To ensure that the relative motion is closed periodic motion, the following condition should be satisfied by Eq. (3.13):

$$\begin{aligned} x(2\pi+\nu_0) = &\left\{1+2H(2\pi+\nu_0)\sin\nu_0(2+e\cos\nu_0)(1+e\cos\nu_0)^2\right\}x(\nu_0) \\ &+\left\{2eH(2\pi+\nu_0)\sin^2\nu_0(1+e\cos\nu_0)^2\right\}x'(\nu_0) \\ &+\left\{-2eH(2\pi+\nu_0)\sin^2\nu_0(1+e\cos\nu_0)^2\right\}y(\nu_0) \\ &+\left\{2H(2\pi+\nu_0)\sin\nu_0(1+e\cos\nu_0)^3\right\}y'(\nu_0) \end{aligned} \tag{3.14}$$

$$\begin{aligned} x'(2\pi+\nu_0) = &\left\{2H(2\pi+\nu_0)\cos\nu_0(2+e\cos\nu_0)(1+e\cos\nu_0)^2\right\}x(\nu_0) \\ &+\left\{1+2eH(2\pi+\nu_0)\sin\nu_0\cos\nu_0(1+e\cos\nu_0)^2\right\}x'(\nu_0) \\ &+\left\{-2eH(2\pi+\nu_0)\sin\nu_0\cos\nu_0(1+e\cos\nu_0)^2\right\}y(\nu_0) \\ &+\left\{2H(2\pi+\nu_0)\cos\nu_0(1+e\cos\nu_0)^3\right\}y'(\nu_0) \end{aligned} \tag{3.15}$$

$$
\begin{aligned}
y(2\pi+\nu_0) = &\left\{\frac{2H(2\pi+\nu_0)}{e}(2+e\cos\nu_0)(1+e\cos\nu_0)^3\right\}x(\nu_0) \\
&+\left\{2H(2\pi+\nu_0)\sin\nu_0(1+e\cos\nu_0)^3\right\}x'(\nu_0) \\
&+\left\{1-2H(2\pi+\nu_0)\sin\nu_0(1+e\cos\nu_0)^3\right\}y(\nu_0) \\
&+\left\{\frac{2H(2\pi+\nu_0)}{e}(1+e\cos\nu_0)^4\right\}y'(\nu_0) \qquad (3.16)
\end{aligned}
$$

$$
\begin{aligned}
y'(2\pi+\nu_0) = &\left\{-2H(2\pi+\nu_0)\sin\nu_0(2+e\cos\nu_0)(1+e\cos\nu_0)^2\right\}x(\nu_0) \\
&+\left\{-2eH(2\pi+\nu_0)\sin^2\nu_0(1+e\cos\nu_0)^2\right\}x'(\nu_0) \\
&+\left\{2eH(2\pi+\nu_0)\sin^2\nu_0(1+e\cos\nu_0)^2\right\}y(\nu_0) \\
&+\left\{1-2H(2\pi+\nu_0)\sin\nu_0(1+e\cos\nu_0)^3\right\}y'(\nu_0) \qquad (3.17)
\end{aligned}
$$

$$z(2\pi+\nu_0) = z(\nu_0) \qquad (3.18)$$

$$z'(2\pi+\nu_0) = z'(\nu_0) \qquad (3.19)$$

Because $H(\nu)$ in Eqs. (3.14)–(3.19) is nonzero and increased with respect to the eccentricity of the reference orbit as shown in Fig. 3.1, the general periodicity condition is derived to satisfy $X(2\pi+\nu_0) = X(\nu_0)$ as follows:

$$
\begin{aligned}
&(2+e\cos\nu_0)x(\nu_0) - e\sin\nu_0 y(\nu_0) \\
&\quad + e\sin\nu_0 x'(\nu_0) + (1+e\cos\nu_0)y'(\nu_0) = 0 \qquad (3.20)
\end{aligned}
$$

Consequently, with the general periodicity condition in Eq. (3.3), $X(2\pi+\nu_0) = X(\nu_0)$ is satisfied which means that the relative motion between spacecraft is periodic in elliptic reference orbits. □

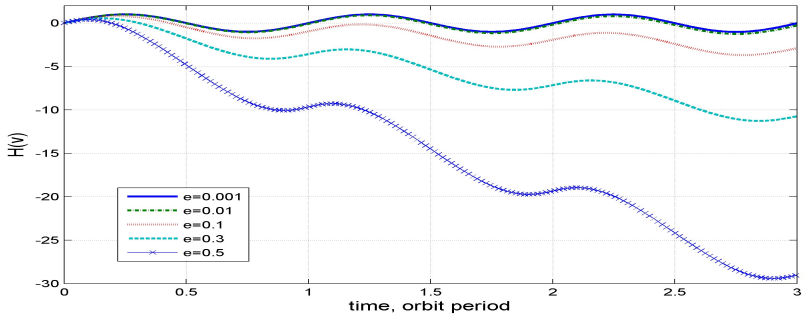

Figure 3.1: $H(\nu)$ with respect to eccentricity

Specifically, previous works show special cases of the general periodicity condition, Eq. (3.3). When the reference orbit is circular ($e = 0$), the periodicity condition is obtained as

$$y'(\nu_0) = -2x(\nu_0) \tag{3.21}$$

Equation (3.21) is identical to the initial condition of the HCW equations in the true anomaly domain [27, 30, 31]. In addition, when the eccentric reference orbit starts at the perigee ($e \neq 0$ and $\nu_0 = 0$), the periodicity condition is presented as

$$y'(\nu_0) = -\frac{2+e}{1+e}x(\nu_0) \tag{3.22}$$

Also, the periodicity condition in the eccentric reference orbit starting at the apogee ($e \neq 0$ and $\nu_0 = \pi$) is given by

$$y'(\nu_0) = -\frac{2-e}{1-e}x(\nu_0) \tag{3.23}$$

Equations (3.22) and (3.23) are equal to the initial conditions in an earlier study in Ref. [29].

3.3 Energy Matching Condition Approach

In this section, the periodicity condition is derived using an energy matching condition for the periodic relative motion in arbitrary elliptic orbits. Then, the resulting condition is compared with the result from the state transition matrix approach described in previous section.

The energy matching condition describes the periods of Keplerian elliptical orbits [113]. The period of the spacecraft in the Earth's orbit is defined by

$$p = 2\pi\sqrt{\frac{a^3}{\mu}} \tag{3.24}$$

Note that two satellites satisfy the energy matching condition when their semi-major axes are equal.

From the dot product of Eq. (2.11) with the velocity vector $\mathbf{v}$, the law of conservation of energy can be obtained as follows:

$$\frac{1}{2}\mathbf{v}\cdot\mathbf{v} - \frac{\mu}{r} = \varepsilon = \text{constant} \tag{3.25}$$

According to the eccentricity and orbital energy of the spacecraft orbit, an orbital motion can be classified as

$$\begin{array}{lll} \text{circle:} & e = 0, & \varepsilon < 0 \\ \text{ellipse:} & 0 < e < 1, & \varepsilon < 0 \\ \text{parabola:} & e = 0, & \varepsilon = 0 \\ \text{hyperbola:} & e > 0, & \varepsilon > 0 \end{array} \tag{3.26}$$

In addition, for the elliptic reference orbit, the total specific energy is defined as follows:

$$\varepsilon = -\frac{\mu}{2a} \tag{3.27}$$

From Eqs. (3.25) and (3.27), the total specific energy of the leader spacecraft comprising the kinematic and potential energies is written as

$$\varepsilon_l = \frac{1}{2}\boldsymbol{v}\cdot\boldsymbol{v} - \frac{\mu}{R} = -\frac{\mu}{2a} \tag{3.28}$$

where $\boldsymbol{v} \in \Re^3$ is velocity vector and a is semi-major axis of the leader spacecraft. The total specific energy of the follower spacecraft is expressed as

$$\varepsilon_f = \frac{1}{2}\boldsymbol{v}_f \cdot \boldsymbol{v}_f - \frac{\mu}{R_f} = -\frac{\mu}{2a_f} \tag{3.29}$$

where $\boldsymbol{v}_f \in \Re^3$ is velocity vector and a_f is the semi-major axis of the follower spacecraft. The energy difference between the leader and follower spacecraft can be written as

$$\Delta\varepsilon = \varepsilon_f - \varepsilon_l = \frac{\mu}{2a} - \frac{\mu}{2a_f} \tag{3.30}$$

Substituting Eqs. (3.28) and (3.29) into Eq. (3.30) yields

$$\Delta\varepsilon = \frac{1}{2}\boldsymbol{v}_f \cdot \boldsymbol{v}_f - \frac{\mu}{R_f} - \left(\frac{1}{2}\boldsymbol{v} \cdot \boldsymbol{v} - \frac{\mu}{R}\right) \tag{3.31}$$

To guarantee one-to-one relative motion, the energy matching condition can be expressed as follows:

$$\Delta\varepsilon = 0 \tag{3.32}$$

Note that Eqs. (3.30) and (3.32) show that the semi-major axes of the leader and follower spacecraft are equal, and then two spacecraft have same period. Consequently, a specific condition for the periodic relative motion can be obtained using Eqs. (3.31) and (3.32).

The velocities of the leader and follower spacecraft in the LVLH frame are defined as

$$\begin{aligned} \boldsymbol{v} &= \left[\dot{\boldsymbol{R}}\right]_L + \omega \times \boldsymbol{R} \\ &= \begin{bmatrix} \dot{R} \\ 0 \\ 0 \end{bmatrix} + \begin{bmatrix} 0 \\ 0 \\ \dot{\theta} \end{bmatrix} \times \begin{bmatrix} R \\ 0 \\ 0 \end{bmatrix} = \begin{bmatrix} \dot{R} \\ R\dot{\theta} \\ 0 \end{bmatrix} \end{aligned} \tag{3.33}$$

$$
\begin{aligned}
\boldsymbol{v}_f &= \left[\dot{\boldsymbol{R}}_f\right]_L + \omega \times \boldsymbol{R}_f \\
&= \begin{bmatrix} \dot{R}+\dot{x} \\ \dot{y} \\ \dot{z} \end{bmatrix} + \begin{bmatrix} 0 \\ 0 \\ \dot{\theta} \end{bmatrix} \times \begin{bmatrix} R+x \\ y \\ z \end{bmatrix} = \begin{bmatrix} \dot{R}+\dot{x}-y\dot{\theta} \\ \dot{y}+(R+x)\dot{\theta} \\ \dot{z} \end{bmatrix}
\end{aligned} \tag{3.34}
$$

Substitution of Eqs. (3.33) and (3.34) into Eq. (3.31) gives

$$
\begin{aligned}
\Delta\varepsilon =& \frac{1}{2}\left\{(\dot{R}+\dot{x}-y\dot{\theta})^2 + (\dot{y}+(R+x)\dot{\theta})^2 + \dot{z}^2 - \dot{R}^2 - R^2\dot{\theta}^2\right\} \\
&+ \left\{\frac{\mu}{R} - \frac{\mu}{\sqrt{(R+x)^2+y^2+z^2}}\right\}
\end{aligned} \tag{3.35}
$$

Equation (3.35) can be expressed using the Taylor series expansion around the leader's relative motion as

$$
\begin{aligned}
\Delta\varepsilon =& \frac{1}{2}\left\{(\dot{x}-y\dot{\theta})^2 + (\dot{y}+x\dot{\theta})^2 + \dot{z}^2\right\} + (\dot{R}\dot{x} - \dot{R}y\dot{\theta} + Rx\dot{\theta}^2 + R\dot{y}\dot{\theta}) \\
&+ \frac{\mu}{R^3}\left\{Rx - x^2 + \frac{1}{2}y^2 + \frac{1}{2}z^2 + \cdots\right\}
\end{aligned} \tag{3.36}
$$

In addition, Eq. (3.36) can be written in the true anomaly domain using Eq. (2.29) as follows:

$$
\begin{aligned}
\Delta\varepsilon =& \frac{1}{2}\dot{\nu}^2\left\{(x'-y)^2 + (y'+x)^2 + z'^2\right\} \\
&+ \dot{\nu}^2\left(\frac{e\sin\nu}{1+e\cos\nu}R(x'-y) + R(x+y')\right) \\
&+ \frac{\dot{\nu}^2}{1+e\cos\nu}\left\{Rx - x^2 + \frac{1}{2}y^2 + \frac{1}{2}z^2 + \cdots\right\}
\end{aligned} \tag{3.37}
$$

The initial condition at $\nu = \nu_0$ for the periodic relative motion can be described by Eq. (3.37) as

$$
\begin{aligned}
\Delta\varepsilon =& \frac{1}{2}{\dot{\nu}_0}^2\left\{(x'(\nu_0)-y(\nu_0))^2 + (y'(\nu_0)+x(\nu_0))^2 + z'(\nu_0)^2\right\} \\
&+ {\dot{\nu}_0}^2\left(\frac{e\sin\nu_0}{1+e\cos\nu_0}R(x'(\nu_0)-y(\nu_0)) + R(x(\nu_0)+y'(\nu_0))\right) \\
&+ \frac{{\dot{\nu}_0}^2}{1+e\cos\nu_0}\left\{Rx(\nu_0) - x(\nu_0)^2 + \frac{1}{2}y(\nu_0)^2 + \frac{1}{2}z(\nu_0)^2 + \cdots\right\}
\end{aligned} \tag{3.38}
$$

With the same assumption of the TH equation ($||\boldsymbol{\rho}|| \ll ||\boldsymbol{R}||$), the initial condition for the periodic relative motions which satisfies the energy matching condition in Eq. (3.32) is obtained as

$$\begin{aligned}\frac{e\sin\nu_0}{1+e\cos\nu_0}\big(x'(\nu_0)-y(\nu_0)\big)\\ +\big(x(\nu_0)+y'(\nu_0)\big)+\frac{1}{1+e\cos\nu_0}x(\nu_0)=0\end{aligned} \tag{3.39}$$

Consequently, Eq. (3.39) can be rewritten as follows:

$$\begin{aligned}(2+e\cos\nu_0)x(\nu_0)-e\sin\nu_0 y(\nu_0)\\ +e\sin\nu_0 x'(\nu_0)+(1+e\cos\nu_0)y'(\nu_0)=0\end{aligned} \tag{3.40}$$

Equation (3.40) is identical to Eq. (3.3), the general periodicity condition derived via the state transition matrix approach. As a result, it can be stated that the general periodicity condition guarantees the bounded periodic relative motion in arbitrary elliptical orbits.

Remark 1 *The periodicity condition in Eq. (3.40) through the energy matching condition approach is equivalent to the periodicity condition in Eq. (3.3) derived through the state transition matrix approach, which means that the resulting periodicity condition provides the bounded periodic relative motion between spacecraft in elliptic orbits.*

3.4 Analytic Periodic Solution

With the general periodicity condition, Eq. (3.3), the analytic periodic solution of the relative motion in elliptical orbits can be expressed from Eq. (2.32), as follows:

$$\begin{aligned}x(\nu)&=c_1 e\sin\nu-c_3\cos\nu\\ y(\nu)&=c_1(1+e\cos\nu)+c_3\left(\frac{2+e\cos\nu}{1+e\cos\nu}\right)\sin\nu+\frac{c_4}{1+e\cos\nu}\\ z(\nu)&=\frac{1}{1+e\cos\nu}(c_5\sin\nu+c_6\cos\nu)\end{aligned} \tag{3.41}$$

The relative velocity can be written as follows:

$$
\begin{aligned}
x'(\nu) &= c_1 e\cos\nu + c_3\sin\nu \\
y'(\nu) &= -c_1 e\sin\nu + c_3\left\{\frac{(2+e\cos\nu)\cos\nu}{1+e\cos\nu} + \frac{e\sin^2\nu}{(1+e\cos\nu)^2}\right\} \\
&\quad + \frac{c_4 e\sin\nu}{(1+e\cos\nu)^2} \\
z'(\nu) &= \frac{1}{(1+e\cos\nu)^2}\left\{c_5(1+e\cos\nu) - c_6\sin\nu\right\}
\end{aligned}
\tag{3.42}
$$

Using Eq. (3.9) with Eqs. (3.3) and (3.11), the coefficients can be obtained via

$$
\begin{aligned}
c_1 &= \frac{\sin\nu_0}{e}x(\nu_0) + \frac{\cos\nu_0}{e}x'(\nu_0) \\
c_2 &= 0 \\
c_3 &= -\cos\nu_0 x(\nu_0) + \sin\nu_0 x'(\nu_0) \\
c_4 &= \frac{\sin\nu_0(1+e\cos\nu_0)}{e}x(\nu_0) - \frac{(1+e\cos\nu_0)(e+\cos\nu_0)}{e}x'(\nu_0) \\
&\quad + \cos\nu_0(e+\cos\nu_0)y(\nu_0) + \frac{\sin\nu_0(1+e\cos\nu_0)}{e}y'(\nu_0) \\
c_5 &= \sin\nu_0 z(\nu_0) + \cos\nu_0(1+e\cos\nu_0)z'(\nu_0) \\
c_6 &= (e+\cos\nu_0)z(\nu_0) - \sin\nu_0(1+e\cos\nu_0)z'(\nu_0)
\end{aligned}
\tag{3.43}
$$

3.5 Numerical Simulation

Numerical simulations are performed to verify the periodicity condition presented in Section 3.2. For the numerical simulation, the elliptic orbit of the leader spacecraft is considered, and orbital elements of the leader spacecraft are summarized in Table 3.1. All simulations are performed by integrating the complete nonlinear model of Eq. (2.22).

The numerical simulation results with the general periodic condition are shown and compared to those with the initial conditions of the HCW equation and of the perturbation method of previous studies. For the numerical

Table 3.1: Orbital elements of leader spacecraft

Parameter	Value
$a \quad (m)$	6.8781×10^6
$i \quad (deg)$	66.01
$\Omega \quad (deg)$	277
$\omega \quad (deg)$	45

simulation, the radial/along-track $(x - y)$ plane formation and the along-track/cross-track $(y - z)$ plane formation are considered.

3.5.1 Radial/Along-Track Plane Formation

In this simulation, the eccentricity of the reference orbit is considered as $e = 0.001$, and initial conditions are selected at the perigee ($\nu_0 = 0$). The initial conditions of three cases are summarized in Tables 3.2. The numerical simulation results with the initial condition of the HCW equation are shown in Fig. 3.2. As shown in Fig. 3.2, the initial position of the follower spacecraft at $t = t_0$ is marked by a circle, and the position of the leader spacecraft is indicated by a star. Figure 3.2 shows the formation trajectory, the in-plane motion, and the out-of-plane motion of the follower spacecraft in the LVLH frame. Clearly, the given initial condition of the HCW equation cannot guarantee the bounded relative motion in the elliptic reference orbit. Figure 3.3 shows the formation trajectory with the corrected initial condition from the perturbation method. As shown in Fig. 3.3, the secular drift of the relative motion is much smaller than that in Fig. 3.2; however, it can be seen that the secular drift remains in the radial/along-track motion. The numerical simulation results with the general periodicity conditions are shown in Fig. 3.4. As shown in the results, the follower spacecraft goes around the leader space-

craft, and the formation trajectory with the proposed initial conditions has the periodic in-plane and out-plane motion. Compared with Figs. 3.2 and 3.3, the secular drift in Fig. 3.4 is significantly reduced by the general periodicity condition.

Table 3.2: Initial conditions for radial/along-track plane formation

	HCW solution	Corrected solution	Proposed Solution
position (m)	$[-5000, 0, 0]$	$[-5000, 0, 0]$	$[-5000, 0, 0]$
velocity (m/s)	$[0, 11.0440, 0, 0]$	$[0, 11.0640, 0]$	$[0, 11.0685, 0]$

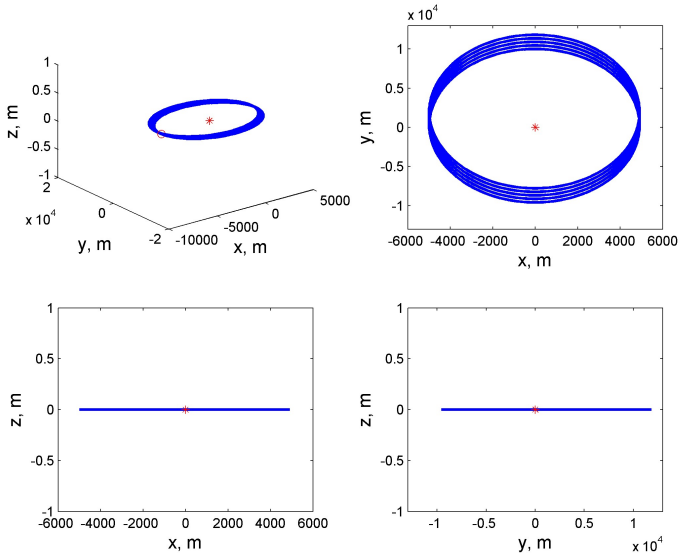

Figure 3.2: Radial/along-track plane formation with the HCW solution

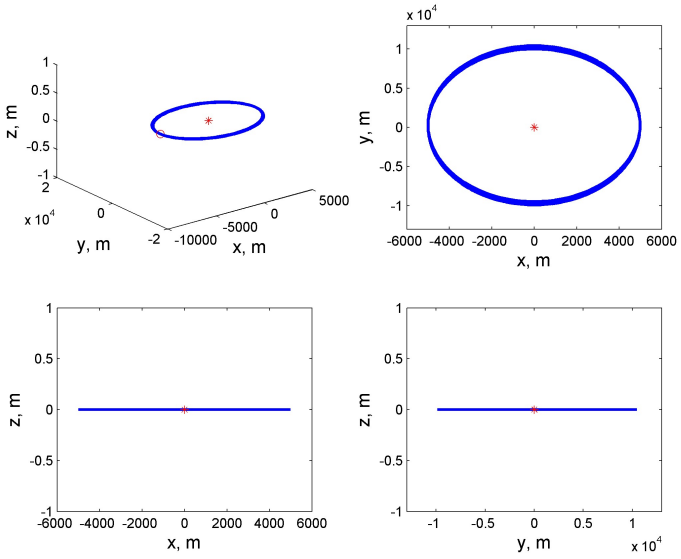

Figure 3.3: Radial/along-track plane formation with the corrected solution

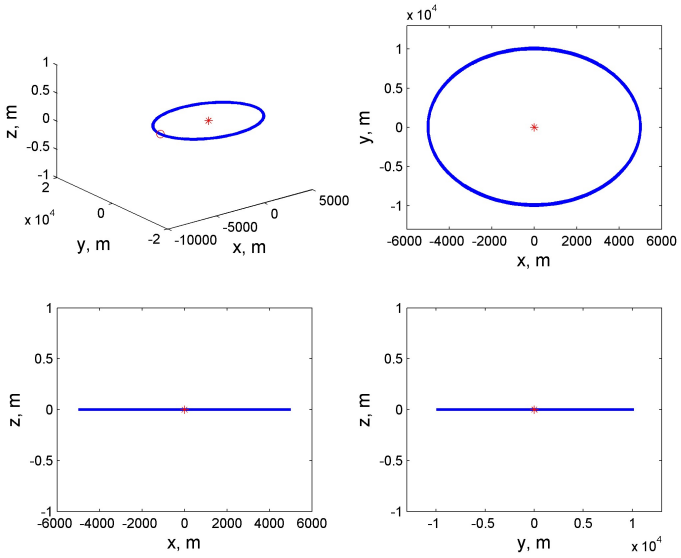

Figure 3.4: Radial/along-track plane formation with the proposed solution

3.5.2 Along-Track/Cross-Track Plane Formation

In this simulation, the eccentricity of the reference orbit is considered as $e = 0.05$, and initial conditions are selected at the perigee ($\nu_0 = 0$). The obtained initial conditions of three cases are summarized in Tables 3.3. The numerical simulation results with the initial condition of the HCW equation for the along-track/cross-track plane formation are shown in Fig. 3.5. Similar to Fig. 3.2, the follower spacecraft with the initial condition of the HCW equation does not have a bounded trajectory in the elliptic orbit. Figure 3.6 shows the trajectory of follower spacecraft with the corrected initial conditions from the perturbation method. As shown in Fig. 3.6, the secular drift of the relative motion is significantly reduced compared with that in Fig. 3.5. The numerical simulation results with the general periodicity conditions are shown in Fig. 3.7. As shown in Fig. 3.7, the formation trajectory with the general periodic condition has periodic in-plane and out-plane motion, and the secular drift is remarkably reduced compared with Figs. 3.5 and 3.6. Consequently, the general periodicity condition guarantees the bounded periodic relative motion in elliptic reference orbits.

Table 3.3: Initial conditions for along-track/cross-track plane formation

	HCW solution	Corrected solution	Proposed solution
position (m)	$[25, 0, 50]$	$[25, 0, 50]$	$[25, 0, 50]$
velocity (m/s)	$[0, -0.0441, 0]$	$[0, -0.04770, 0]$	$[0. - 0.047662, 0]$

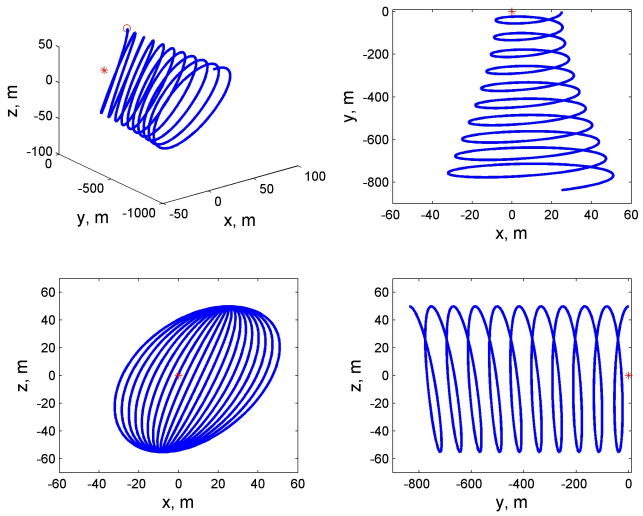

Figure 3.5: Along-track/cross-track plane formation with the HCW solution

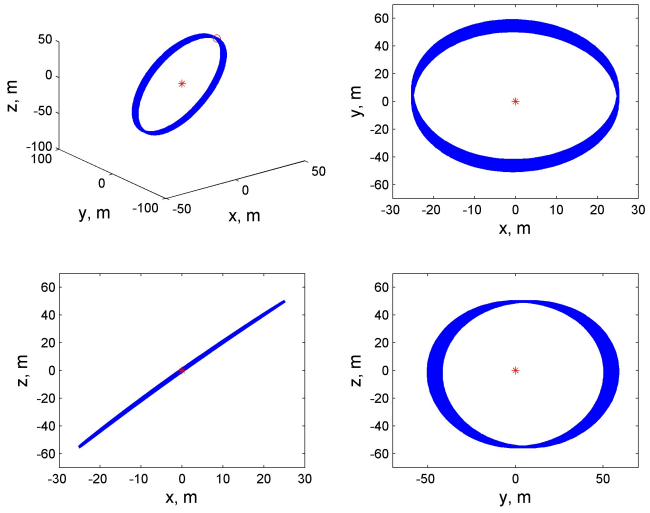

Figure 3.6: Along-track/cross-track plane formation with the corrected solution

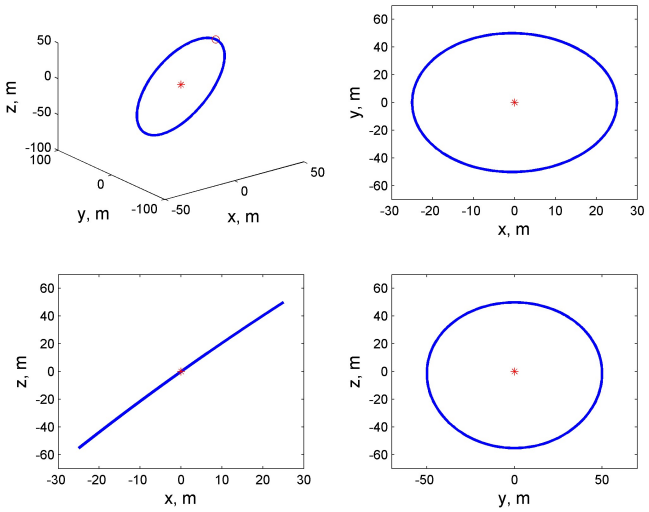

Figure 3.7: Along-track/cross-track plane formation with the proposed solution

3.6 Concluding Remarks

In this chapter, the general periodicity condition is derived via two approaches. One approach is based on the state transition matrix in Section 3.2. Using the property of the state transition matrix, the periodicity condition is obtained to provide a bounded periodic analytic solution of the relative motion. Another approach is presented by the energy matching condition in Section 3.3. The energy matching condition is related to the semi-major axis and period of the spacecraft, and therefore the condition to keep the periodic relative motion is expressed. The resulting condition is compared with the periodic condition from the state transition matrix, and these two results are concluded to be identical.

Furthermore, the resulting periodic condition satisfies the condition of zero secular drift in the HCW equation for the circular reference orbit, and the periodic conditions at the perigee and apogee in the elliptic reference orbit are identical to the the previous studies. Finally, the analytic periodic solution is expressed with the periodicity condition, and this solution will be used to design the spacecraft formation in next chapter.

Numerical simulation is performed to verify the presented periodic condition. With the initial conditions of the HCW equation in Ref. [30], the numerical simulation results show that the follower spacecraft does not keep the periodic relative motion with respect to the leader spacecraft. In contrast, the simulation results with the general periodicity condition proposed in this dissertation show that the follower spacecraft maintains the periodic relative motion in the elliptic reference orbit.

Chapter 4

Formation Pattern Analysis and Design

4.1 Introduction

For the spacecraft formation flying, the relative motion between spacecraft is generally described in the local frame instead of the inertial frame, and then the formation pattern is analyzed in the local frame. In the circular reference orbit, the relative motion can be easily illustrated, and initial conditions for the HCW equation can be selected according to desired formation type. As shown in Eq. (3.2), the radial/along-track motion and the cross-track motion are separated, and the radial/along-track motion forms an ellipse of a fixed eccentricity in the local frame. It means that the major axis in the along-track direction is always twice the minor axis in the radial direction. In order to choose the initial conditions, Sabol et al. presented the satellite formation flying design for a circular orbit, and they considered four formation types: in-plane formation, in-track formation, circular formation, and projected circular formation [30]. However, this formation flying design cannot be directly applied to an elliptic orbit, since the described initial conditions from HCW

equation do not contain the eccentricity information of the reference orbit.

For the elliptic reference orbit, from the analytic periodic solution as expressed in Eq. (3.41), it is expected that the relative motion in elliptical orbits will not be a circle or an ellipse in any plane of the local frame due to the eccentricity of the reference orbit. Because the motion of the follower spacecraft is influenced by the eccentricity of the leader spacecraft, the relative motion becomes complicated, and the analysis of the formation in the elliptic orbits has not been completely investigated yet. In this dissertation, the spacecraft formation in arbitrary elliptic orbits is analyzed; specifically, the radial/along-track ($x-y$) plane and the along-track/cross-track ($y-z$) plane formations are considered. According to formation type, corresponding initial conditions are introduced for spacecraft formation flying in the elliptic reference orbit. Also, the variation between the maximum and minimum formation radius and the eccentricity of the relative motion are discussed according to the reference eccentricity in all designed formation types. The obtained results will provide constraints on the formation design process in general elliptic orbits.

The periodic relative motion is represented in Section 4.2, which has zero secular drift and zero offset in the along-track direction. Using this periodic solution, two formation geometries are designed, and each formation is analyzed according to the eccentricity and the true anomaly of the reference orbit; the radial/along-track plane formation is discussed in Section 4.3, and the along-track/cross-track plane formation is analyzed in Section 4.4. The numerical simulation results of the two formation types are illustrated in Section 4.5. Through the simulation results, the formation patterns of each formation are analyzed in Sections 4.5.1 and 4.5.2, respectively. Moreover, two follower spacecraft are considered to increase the number of spacecraft in formation, and then the angle difference between two followers is shown in Section 4.5.3. In Section 4.5.4, the simulation results are summarized and analyzed.

4.2 Periodic Relative Motion

To simplify the expression, Eq. (3.41) can be rewritten as follows:

$$\begin{aligned} x(\nu) &= a_1(1+e\cos\nu)\sin\nu - a_3(1+e\cos\nu)\cos\nu \\ y(\nu) &= a_1(2+e\cos\nu)\cos\nu + a_3(2+e\cos\nu)\sin\nu + \frac{a_1}{e} + a_4 \\ z(\nu) &= a_5\sin\nu + a_6\cos\nu \end{aligned} \tag{4.1}$$

where

$$\begin{aligned} a_1 &= \frac{c_1 e}{1+e\cos\nu}, \qquad a_3 = \frac{c_3}{1+e\cos\nu}, \qquad a_4 = \frac{c_4}{1+e\cos\nu} \\ a_5 &= \frac{c_5}{1+e\cos\nu}, \qquad a_6 = \frac{c_6}{1+e\cos\nu} \end{aligned} \tag{4.2}$$

Equation (4.1) can also be expressed as

$$\begin{aligned} x(\nu) &= \xi_1\sin(\nu+\psi_1)(1+e\cos\nu) \\ y(\nu) &= \xi_1\cos(\nu+\psi_1)(2+e\cos\nu) + \frac{a_1}{e} + a_4 \\ z(\nu) &= \xi_2\sin(\nu+\psi_2) \end{aligned} \tag{4.3}$$

where

$$\xi_1 = \sqrt{a_1^2 + a_3^2}, \qquad \sin(\psi_1) = \frac{-a_3}{\xi_1}, \qquad \cos(\psi_1) = \frac{a_1}{\xi_1} \tag{4.4}$$

$$\xi_2 = \sqrt{a_5^2 + a_6^2}, \qquad \sin(\psi_2) = \frac{a_6}{\xi_2}, \qquad \cos(\psi_2) = \frac{a_5}{\xi_2} \tag{4.5}$$

In Eq. (4.3), the last two terms in the along-track component are the offset in the radial/along-track plane. To remove this offset term, which means that the center of relative motion locates at the position of leader spacecraft, the following initial condition can be chosen.

$$\frac{a_1}{e} + a_4 = 0 \tag{4.6}$$

Substituting Eq. (4.2) into Eq. (4.6), the initial condition $y(\nu_0)$ is obtained as follows:

$$y(\nu_0) = \frac{2+e\cos\nu_0}{1+e\cos\nu_0}x'(\nu_0) \tag{4.7}$$

Equation (4.7) is the general condition for the zero offset in the along-track direction.

Remark 2 *The zero offset condition in Eq. (4.7) makes the position of the leader spacecraft locate at the geometry center of the relative motion in elliptic reference orbits.*

With Eq. (4.7), Eq. (4.3) can be written as

$$\begin{aligned} x(\nu) &= \xi_1 \sin(\nu + \psi_1)(1 + e\cos\nu) \\ y(\nu) &= \xi_1 \cos(\nu + \psi_1)(2 + e\cos\nu) \\ z(\nu) &= \xi_2 \sin(\nu + \psi_2) \end{aligned} \tag{4.8}$$

Equation (4.8) can be rewritten to simplify the expression as follows:

$$\begin{aligned} x(\nu) &= D_1 \sin(\nu + \psi_1) \\ y(\nu) &= \gamma D_1 \cos(\nu + \psi_1) \\ z(\nu) &= \gamma_0 D_2 \sin(\nu + \psi_2) \end{aligned} \tag{4.9}$$

where

$$D_1 = \xi_1(1 + e\cos\nu) \tag{4.10}$$

$$D_2 = \xi_2(1 + e\cos\nu) \tag{4.11}$$

$$\gamma = \frac{2 + e\cos\nu}{1 + e\cos\nu} \tag{4.12}$$

$$\gamma_0 = \frac{1}{1 + e\cos\nu} \tag{4.13}$$

Equation (4.9) presents the periodic relative motion with the zero secular drift and offset. Using Eqs. (3.3) and (4.7), the coefficients in Eq. (3.43) can be simplified as follows:

$$
\begin{aligned}
c_1 &= \frac{\sin\nu_0}{e}x(\nu_0) + \frac{\cos\nu_0}{e}x'(\nu_0) \\
c_3 &= -\cos\nu_0 x(\nu_0) + \sin\nu_0 x'(\nu_0) \\
c_4 &= -\frac{\sin\nu_0}{e}x(\nu_0) - \frac{\cos\nu_0}{e}x'(\nu_0) \\
c_5 &= \sin\nu_0 z(\nu_0) + \cos\nu_0(1+e\cos\nu_0)z'(\nu_0) \\
c_6 &= (e+\cos\nu_0)z(\nu_0) - \sin\nu_0(1+e\cos\nu_0)z'(\nu_0)
\end{aligned}
\tag{4.14}
$$

In general, the relative motions in the radial/along-track plane and the along-track/cross-track plane are not a circle or an ellipse with a constant level of eccentricity, due to the eccentricity of the reference orbit e and the time-varying true anomaly ν, as shown in Eq. (4.9). Consequently, it is necessary to analyze these formation motions with respect to the eccentricity and the true anomaly of the reference orbit in the local frame. Using Eq. (4.9), the radial/along-track plane formation and along-track/cross-track plane formation are investigated in the consideration of the eccentricity and the true anomaly in the following sections.

4.3 Radial/Along-Track Plane Formation

To understand the radial/along-track plane formation, let us consider the radial/along-track plane formation with the following equation from Eq. (4.9).

$$
\frac{x^2(\nu)}{D_1^2} + \frac{y^2(\nu)}{\gamma^2 D_1^2} = 1 \tag{4.15}
$$

In the circular reference orbit ($e = 0$), γ equals 2 in Eq. (4.12), and then the radial/along-track motion of the follower spacecraft is an ellipse with constant eccentricity of $e_f = \sqrt{3}/2$, where e_f denotes the eccentricity of the follower spacecraft in the LVLH frame.

In the elliptic reference orbit, however, $\gamma \geq 1$ is not constant and changes with respect to ν as shown in Eq. (4.12). Thus, the relative motion of the

follower spacecraft in the radial/along-track plane is an ellipse which has semi-major axis γD_1 and semi-minor axis D_1. In addition, the eccentricity of the follower spacecraft in the radial/along-track plane formation varies as

$$e_f = \sqrt{1 - \left(\frac{D_1}{\gamma D_1}\right)^2} = \sqrt{1 - \frac{1}{\gamma^2}} = \frac{\sqrt{3 + 2e\cos\nu}}{2 + e\cos\nu} \tag{4.16}$$

This indicates that the major axis in the along-track direction is γ times the minor axis in the radial direction. Figure 4.1 shows the eccentricity change of the follower spacecraft according to the true anomaly in the local frame. As shown in Fig. 4.1, when the leader spacecraft has a small eccentricity, $e = 0.001$ and $e = 0.01$, e_f has a value near $\sqrt{3}/2$. However, the variation of e_f increases as e becomes large, and e_f has maximum value at $\nu = \pi$, and has minimum value at $\nu = 0,\ 2\pi$. From Eq. (4.16), the eccentricity of the follower spacecraft in the local frame has the following boundary.

$$\frac{\sqrt{3 + 2e}}{2 + e} \leq e_f \leq \frac{\sqrt{3 - 2e}}{2 - e} \tag{4.17}$$

In addition, the ratio between the minimum and maximum eccentricities of the follower spacecraft can be obtained as

$$\Delta(e) = \frac{\text{minimum } e_f}{\text{maximum } e_f} = \frac{(2 - e)\sqrt{3 + 2e}}{(2 + e)\sqrt{3 - 2e}} \tag{4.18}$$

It should be noted that the ratio $\Delta(e)$ in Eq. (4.18) only depends on e, which is the eccentricity of the leader spacecraft. Table 4.1 summarizes the eccentricity of the follower spacecraft in the local frame according to e. The difference between the minimum and the maximum eccentricities of the follower spacecraft becomes large as e increases, as shown in Table 4.1. It means that the variation between the maximum and the minimum formation radii grows, as the reference eccentricity increases. Using the analytic results as shown in Fig. 4.1 and Table 4.1 as a constraint, the designer can select an eccentricity of the reference orbit, and formation radius between two spacecraft with respect to requirements of the space mission.

Remark 3 *The radial/along-track plane formation has a varying eccentricity in the local frame, e_f, and the variation of e_f becomes large as e is increased. Therefore, the follower spacecraft cannot maintain a constant relative distance with respect to the leader spacecraft in elliptic orbits.*

In the radial/along-track plane formation, the follower spacecraft cannot maintain a constant distance from the leader spacecraft as explained above. However, the initial conditions can be selected to make the relative distance between two spacecraft keep constant value at specific true anomaly. For example, if a mission is required to keep constant distance r_d at perigee ($\nu = 0$) in the radial/along-track plane, the following constraint can be considered.

$$x^2(0) + y^2(0) = r_d^2 \tag{4.19}$$

$$z(0) = 0, \qquad z'(0) = 0 \tag{4.20}$$

When $\nu = 0$, Eq. (4.15) can be expressed as

$$x^2(0) + \frac{y^2(0)}{\gamma^2(0)} = D_1^2(0) \tag{4.21}$$

where

$$\gamma(0) = \frac{2+e}{1+e}, \qquad D_1^2(0) = x(\nu_0)^2 + x'(\nu_0)^2 \tag{4.22}$$

Thus, the initial conditions at $\nu_0 = 0$ can be selected as follows:

$$x(\nu_0) = 0, \quad y(\nu_0) = r_d, \quad z(\nu_0) = 0 \tag{4.23}$$

$$x'(\nu_0) = \frac{1+e}{2+e} r_d, \quad y'(\nu_0) = 0, \quad z'(\nu_0) = 0 \tag{4.24}$$

With these initial conditions, the coefficients in Eq. (4.14) are defined, and the analytic solutions for the radial/along-track plane formation can be obtained.

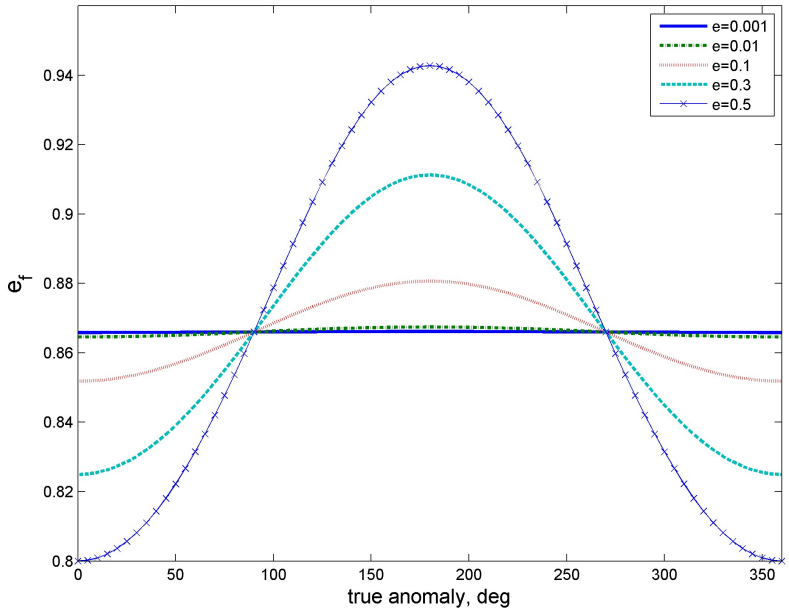

Figure 4.1: The eccentricity of follower satellite in the radial/along-track motion

Table 4.1: The eccentricity ratio of the radial/along-track motion

e	0	0.001	0.01	0.1	0.3	0.5
Minimum e_f	0.8660	0.8659	0.8646	0.8518	0.8249	0.8000
Maximum e_f	0.8660	0.8662	0.8675	0.8807	0.9113	0.9428
$\Delta(e)$	1	0.9997	0.9967	0.9672	0.9052	0.8485

4.4 Along-Track/Cross-Track Plane Formation

Let us consider the along-track/cross-track plane formation with the following equation from Eq. (4.9).

$$y^2(\nu) + z^2(\nu) = \gamma^2 D_1^2 \cos^2(\nu + \psi_1) + \gamma_0^2 D_2^2 \sin^2(\nu + \psi_2) \tag{4.25}$$

As shown in Eq. (4.25), the along-track/cross-track plane formation can be defined by selecting D_1 and D_2 which are related with ξ_1 and ξ_2 as shown in Eqs. (4.10) and (4.11), that is ψ_1 and ψ_2 from Eqs. (4.4) and (4.5). To analyze the along-track/cross-track plane formation, two cases are considered in this study; $D_1^2 = D_2^2$ and $4D_1^2 = D_2^2$. In addition, it will be described how the along-track/cross-track plane formation is changed for these two cases.

4.4.1 Along-Track/Cross-Track Plane Formation under $D_1^2 = D_2^2$

When $D_1^2 = D_2^2$, Eq. (4.25) can be written as

$$\frac{y^2(\nu)}{\gamma^2 D_1^2} + \frac{z^2(\nu)}{\gamma_0^2 D_1^2} = 1 \tag{4.26}$$

In the circular reference orbit ($e = 0$), γ is 2 and γ_0 is 1 as shown in Eqs. (4.12) and (4.13), and then the along-track/cross-track motion is an ellipse with constant eccentricity of $e_f = \sqrt{3}/2$, where e_f is the eccentricity of follower spacecraft in the local frame.

However, in the elliptic reference orbit, $\gamma > 0$ and $\gamma_0 \geq 1$ are not constant and change with respect to ν; the relative motion in the along-track/cross-track plane formation has an ellipse with semi-major axis γD_1 and semi-minor axis $\gamma_0 D_1$. Thus, the eccentricity of the follower spacecraft in the along-track/cross-track motion changes as follows:

$$e_f = \sqrt{1 - \left(\frac{\gamma_0 D_1}{\gamma D_1}\right)^2} = \sqrt{1 - \left(\frac{1}{2 + e\cos\nu}\right)^2}$$
$$= \frac{\sqrt{(3 + e\cos\nu)(1 + e\cos\nu)}}{2 + e\cos\nu} \tag{4.27}$$

Note that the major axis in the along-track direction is $(2 + e\cos\nu)$ times the minor axis in the cross-track direction. Figure 4.2 shows the eccentricity change of the follower according to the true anomaly. As shown in Fig. 4.2, the follower spacecraft has an eccentricity near $\sqrt{3}/2$ when $e = 0.001$ and $e = 0.01$; however, the variation of e_f increases as e becomes large to 0.5. Moreover, the maximum value of e_f is at $\nu = 0, 2\pi$ and the minimum value is at $\nu = \pi$. Thus, the eccentricity of the follower spacecraft in Eq. (4.27) has the following boundary.

$$\frac{\sqrt{(3-e)(1-e)}}{2-e} \leq e_f \leq \frac{\sqrt{(3+e)(1+e)}}{2+e} \tag{4.28}$$

In addition, the ratio between the minimum and maximum eccentricities of the follower spacecraft can be obtained as

$$\Delta(e) = \frac{\text{minimum eccentricity}}{\text{maximum eccentricity}} = \frac{(2+e)\sqrt{(3-e)(1-e)}}{(2-e)\sqrt{(3+e)(1+e)}} \tag{4.29}$$

It should be noted that the ratio $\Delta(e)$ in Eq. (4.29) only depends on e, which is the eccentricity of the leader spacecraft. The difference between the minimum and the maximum eccentricities of the follower spacecraft becomes large as e increases, as shown in Table 4.2. The variation between the maximum and the minimum formation radii is increased when the leader spacecraft has a high eccentricity. Compared with the results in previous section, the variation of the formation radius in the along-track/cross-track plane formation is greater than that of the radial/along-track plane formation as e becomes large. Figure 4.2 and Table 4.2 give the guideline and constraints to design the spacecraft

formation in the along-track/cross-track plane formation, and therefore a reference eccentricity and formation radius can be chosen according to the space missions.

Remark 4 *The along-track/cross-track plane formation has a varying eccentricity in the local frame, and this eccentricity only depends on the eccentricity of the reference orbit. Thus, the relative distance between the leader and follower spacecraft becomes large, as e is increased.*

Similar to the radial/along-track plane formation, the follower spacecraft cannot maintain a constant distance from the leader spacecraft in along-track/cross-track plane formation under $D_1^2 = D_2^2$. Instead, the initial conditions can be selected to make the relative distance between two spacecraft keep constant value at given true anomaly. In order to keep constant distance r_d at perigee ($\nu = 0$) in the along-track/cross-track plane, for example, the following constraint is considered.

$$y^2(0) + z^2(0) = r_d^2 \tag{4.30}$$

If $\nu = 0$, Eq. (4.26) can be written as

$$\frac{y^2(0)}{\gamma^2(0)} + \frac{z^2(0)}{\gamma_0^2(0)} = D_1^2(0) \tag{4.31}$$

where

$$\gamma_0(0) = \frac{1}{1+e}, \qquad \gamma(0) = \frac{2+e}{1+e}, \qquad D_1^2(0) = D_2^2(0) \tag{4.32}$$

Thus, the initial conditions at $\nu_0 = 0$ can be selected as follows:

$$x(\nu_0) = 0, \quad y(\nu_0) = r_d, \quad z(\nu_0) = 0 \tag{4.33}$$

$$x'(\nu_0) = \frac{1+e}{2+e} r_d, \quad y'(\nu_0) = 0, \quad z'(\nu_0) = \frac{1}{2+e} r_d \tag{4.34}$$

With these initial conditions, the coefficients in Eq. (4.14) are obtained, and the analytic solutions for the along-track/cross-track plane formation under $D_1^2 = D_2^2$ can be determined.

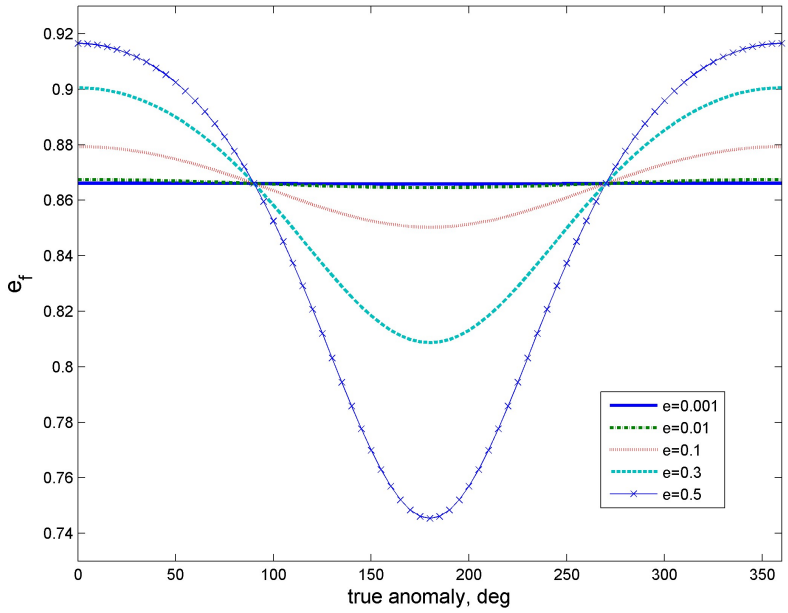

Figure 4.2: The eccentricity of follower satellite in the along-track/cross-track motion ($D_1^2 = D_2^2$)

Table 4.2: The eccentricity ratio of the along-track/cross-track motion ($D_1^2 = D_2^2$)

e	0	0.001	0.01	0.1	0.3	0.5
Minimum e_f	0.8660	0.8659	0.8646	0.8503	0.8087	0.7454
Maximum e_f	0.8660	0.8662	0.8675	0.8793	0.9005	0.9165
$\Delta(e)$	1	0.9997	0.9967	0.9670	0.8980	0.8133

4.4.2 Along-Track/Cross-Track Plane Formation under $4D_1^2 = D_2^2$

Let us consider the along-track/cross-track plane formation under $4D_1^2 = D_2^2$, that is $2\xi_1 = \xi_2$. Equation (4.25) can be written as

$$\frac{y^2(\nu)}{\gamma^2 D_1^2} + \frac{z^2(\nu)}{4\gamma_0^2 D_1^2} = 1 \tag{4.35}$$

In the circular reference orbit ($e = 0$), the along-track/cross-track motion is a circle ($e_f = 0$), which is the projected circular formation in the circular reference orbit [30].

In the elliptic reference orbit, however, γ and γ_0 are not constant and change with respect to ν; as described in Eq. (4.35), the relative motion in the along-track/cross-track plane has varying semi-major axis and semi-minor axis with respect to ν. The eccentricity of the follower spacecraft in the along-track/cross-track motion changes as follows:

$$e_f = \begin{cases} \sqrt{1-\left(\frac{\gamma D_1}{2\gamma_0 D_1}\right)^2} = \sqrt{1-\left(\frac{2+e\cos\nu}{2}\right)^2} = \frac{\sqrt{-e\cos\nu(4+e\cos\nu)}}{2}, & \text{if } \frac{\pi}{2} \le \nu \le \frac{3\pi}{2} \\ \sqrt{1-\left(\frac{2\gamma_0 D_1}{\gamma D_1}\right)^2} = \sqrt{1-\left(\frac{2}{2+e\cos\nu}\right)^2} = \frac{\sqrt{e\cos\nu(4+e\cos\nu)}}{2+e\cos\nu}, & \text{else} \end{cases} \tag{4.36}$$

Note that the major axis in the cross-track direction is $2/(2 + e\cos\nu)$ times the minor axis in the along-track direction when $\frac{\pi}{2} \le \nu \le \frac{3\pi}{2}$; however, the major axis in the along-track direction is $(2 + e\cos\nu)/2$ times the minor axis in the cross-track direction when $0 \le \nu < \frac{\pi}{2}$ and $\frac{3\pi}{2} < \nu \le 2\pi$. It means that the direction of major axis varies with respect to ν. Figure 4.3 shows the eccentricity change of the follower spacecraft in the local frame according to the true anomaly. As shown in Fig. 4.3, the along-track/cross-track plane has similar formation pattern to projected circular formation when eccentricity is small, and it can be seen that e_f has maximum value at $\nu = \pi$ and minimum

value at $\nu = \frac{\pi}{2}, \frac{3\pi}{2}$. The eccentricity of the follower spacecraft in the along-track/cross-track plane has the following boundary.

$$0 \leq e_f \leq \frac{\sqrt{e(4-e)}}{2} \tag{4.37}$$

The maximum eccentricity of the follower spacecraft in the local frame becomes large as e increases, as shown in Table 4.3. It means that the variation between the maximum and the minimum formation radii is extended as the reference eccentricity becomes large.

Remark 5 *In the along-track/cross-track plane formation with condition* $4D_1^2 = D_2^2$*, the eccentricity of the follower spacecraft,* e_f*, in the local frame is dependent on* e*. The variations of both* e_f *and the relative distance between spacecraft are increased as* e *becomes large in elliptic orbits.*

In the along-track/cross-track plane formation under $4D_1^2 = D_2^2$, the follower spacecraft cannot keep the invariant distance from the leader spacecraft such as the projected circular formation for the circular orbit. Instead, the initial conditions can be chosen for constant relative distance between the leader and follower spacecraft at specific true anomaly. In order to maintain constant distance r_d at perigee ($\nu = 0$) in the along-track/cross-track plane, the following constraint is considered.

$$y^2(0) + z^2(0) = r_d^2 \tag{4.38}$$

If $\nu = 0$, Eq. (4.35) can be written as

$$\frac{y^2(0)}{\gamma^2(0)} + \frac{z^2(0)}{4\gamma_0^2(0)} = D_1^2(0) \tag{4.39}$$

where

$$\gamma_0(0) = \frac{1}{1+e}, \qquad \gamma(0) = \frac{2+e}{1+e}, \qquad 4D_1^2(0) = D_2^2(0) \tag{4.40}$$

Thus, the initial conditions at $\nu_0 = 0$ can be selected as follows:

$$x(\nu_0) = 0, \quad y(\nu_0) = r_d, \quad z(\nu_0) = 0 \tag{4.41}$$

$$x'(\nu_0) = \frac{1+e}{2+e} r_d, \quad y'(\nu_0) = 0, \quad z'(\nu_0) = \frac{2}{2+e} r_d \tag{4.42}$$

With these initial conditions, the coefficients in Eq. (4.14) are given, and the analytic solutions for the along-track/cross-track plane formation under $4D_1^2 = D_2^2$ can be obtained.

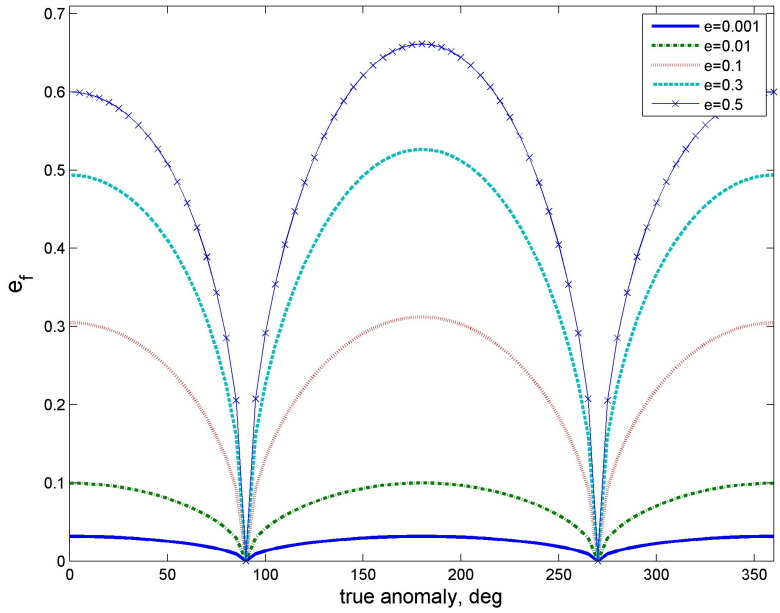

Figure 4.3: The eccentricity of follower satellite in the along-track/cross-track motion ($4D_1^2 = D_2^2$)

Table 4.3: The maximum eccentricity of the along-track/cross-track motion ($4D_1^2 = D_2^2$)

e	0	0.001	0.01	0.1	0.3	0.5
Minimum e_f	0	0	0	0	0	0
Maximum e_f	0	0.0316	0.0999	0.3122	0.5268	0.6614

4.5 Numerical Simulation

Numerical simulations are performed to verify the two formation types as investigated in the previous sections. The numerical simulation results of the radial/along-track plane and the along-track/cross-track plane formations with one follower spacecraft at $\nu_0 = 0$ are shown for several different eccentricities of the reference orbit, $e = 0.001$, 0.01, 0.1, 0.3, and 0.5. Other orbit elements are same as Table 3.1. In order to investigate the relative motion of the multiple spacecraft formation, moreover, the numerical simulation results applying another follower spacecraft are illustrated according to various eccentricities of the reference orbit. Then, these results are analyzed in the viewpoint of the angle difference between two follower spacecraft with respect to the formation radius and the eccentricity.

All numerical simulation results are shown in the LVLH frame instead of the ECI frame to describe the relative motion of the follower spacecraft with respect to the leader spacecraft, since it is difficult to denote the rela-

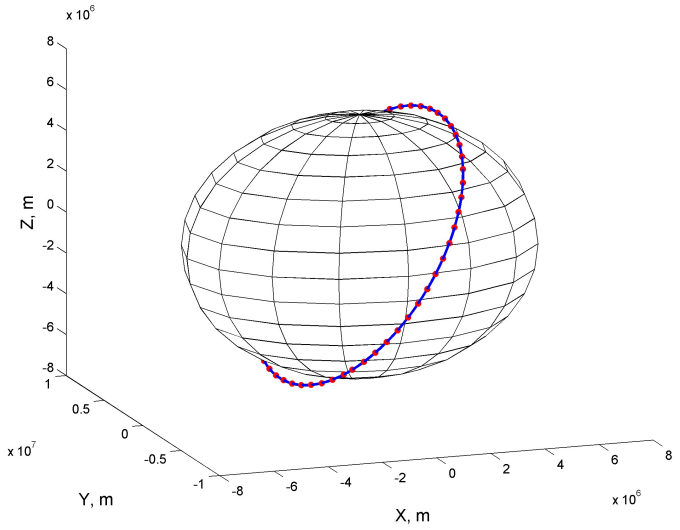

Figure 4.4: Trajectories of leader and follower spacecraft in the ECI frame

tive motion in the inertial frame, as shown in Fig. 4.4. Figure 4.4 illustrates the trajectory of the leader and follower spacecraft for the radial/along-track plane formation in the ECI frame when the eccentricity is 0.01; the solid line denotes the trajectory of the leader spacecraft and the dotted line shows the trajectory of the follower spacecraft. As shown in Fig. 4.4, the trajectories of spacecraft around the Earth can be realized, but the formation pattern of the follower spacecraft is hard to recognize with respect to the leader spacecraft. Therefore, the results are shown in the LVLH frame to investigate and verify the formation pattern of the follower spacecraft with respect to the leader spacecraft.

4.5.1 Radial/Along-Track Plane Formation

Figures 4.5–4.9 show the results for the radial/along-track plane formation. The trajectory, the in-plane motion, and the out-of-plane motion are shown in Fig. 4.5. Figures 4.6, 4.7, and 4.8 illustrate the time history of velocity, the magnitude of velocity, and the radial/along-track motions according to the eccentricity of the reference orbit, respectively. Figure 4.9 shows the history of the formation radius with respect to e. As shown in Fig. 4.5, the in-plane motion is periodic and bounded for all e; however, the eccentricity and the formation radius of the follower spacecraft are changed with respect to the e, as summarized in Table 4.1. In Figs. 4.6 and 4.7, the speed variation of the follower spacecraft becomes extended as the eccentricity of the reference orbit goes from 0.001 to 0.5, and the follower spacecraft has large velocity near perigee ($\nu = 0$). This velocity change can also be shown in Fig. 4.8. In Fig. 4.8, the origin denotes the position of the leader spacecraft, the initial position of the follower spacecraft is marked by a triangle, and the follower spacecraft is marked with the same time interval. Figure 4.8 shows that the follower spacecraft has almost the same speed when the eccentricity is small,

$e = 0.01$; however, the speed increases near the perigee when the eccentricity of the reference orbit is increased. Moreover, as shown in Fig. 4.9, the follower spacecraft has the minimum formation radius at the perigee and apogee. The difference between the maximum and minimum radii increases as the eccentricity of the reference orbit becomes large.

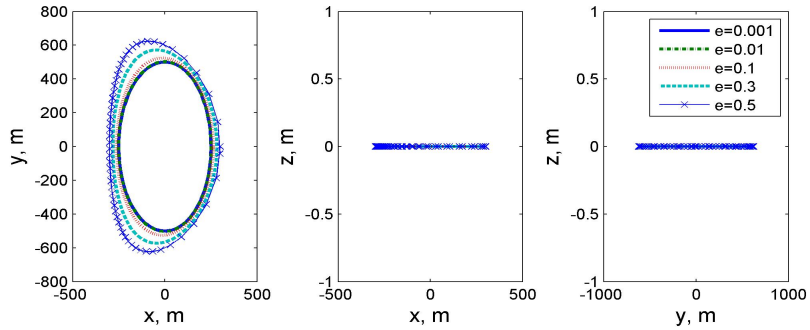

Figure 4.5: In-plane and out-of-plane motion: RAPF

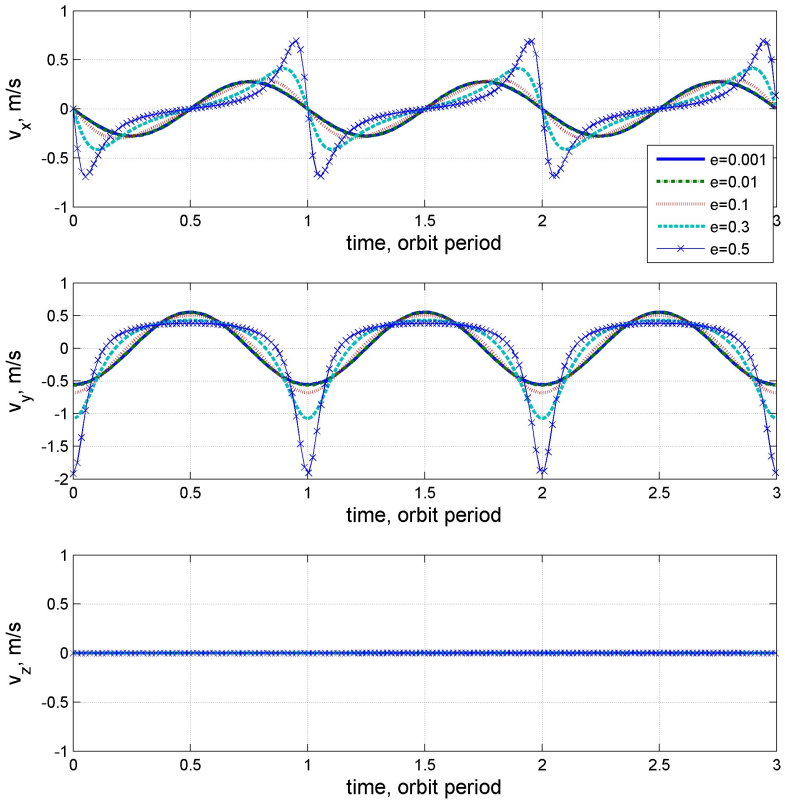

Figure 4.6: Time history of the velocity: RAPF

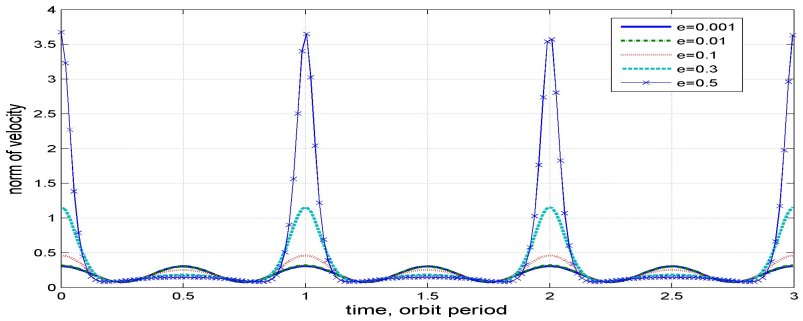

Figure 4.7: Time history of the velocity norm: RAPF

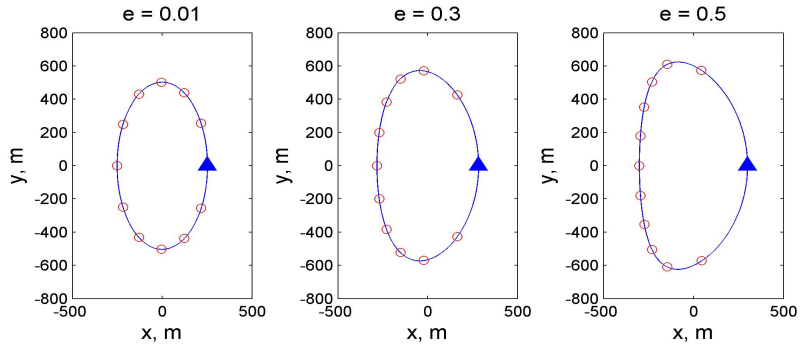

Figure 4.8: Radial/along-track motion: RAPF

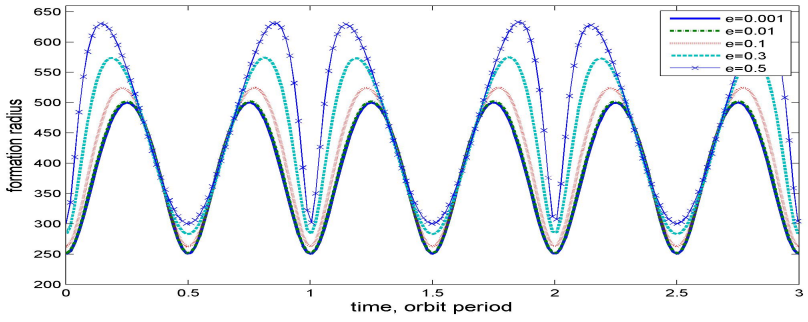

Figure 4.9: Time history of the formation radius: RAPF

4.5.2 Along-Track/Cross-Track Plane Formation

In this simulation, the along-track/cross-track plane formation under $4D_1^2 = D_2^2$ is considered, because the condition $D_1^2 = D_2^2$ provides the similar results of the radial/along-track plane formation. Figures 4.10–4.14 illustrate the results for the along-track/cross-track plane formation according to the different eccentricities under $4D_1^2 = D_2^2$. The trajectory, the in-plane and out-of-plane motions with the proposed initial conditions are shown in Fig. 4.10. Figures 4.11 and 4.12 describe the time history of velocity and the magnitude of velocity according to the eccentricity of reference orbit, respectively, and Fig. 4.13 illustrates the along-track/cross-track motions for the various eccentricities. Fig. 4.14 shows the time history of the formation radius with respect to the reference eccentricity. Figure 4.10 shows that the in-plane and out-of-plane motions are periodic and bounded. Similar to Fig. 4.5, the follower spacecraft has different formation shape with respect to the eccentricity of the leader spacecraft; the eccentricity of the follower spacecraft and the formation radius are extended as e is increased. As shown in Figs. 4.11 and 4.12, the velocity of the follower spacecraft changes as the leader spacecraft has different eccentricities, and the speed increases at the perigee and slows down at the apogee. It is shown in Fig. 4.13, the speed of follower spacecraft is almost equal, when $e = 0.01$; however, the speed is significantly increased near perigee when the the eccentricity of the reference orbit goes to 0.5. In Fig. 4.14, the difference between the maximum and minimum formation radii increases as e increases to 0.5, which was already shown in Table 4.3. As shown in Fig. 4.14, the minimum radius appears at the perigee while the maximum radius shows at the apogee.

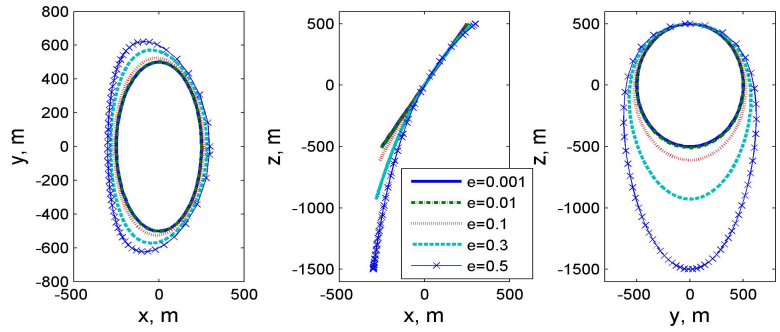

Figure 4.10: In-plane and out-of-plane motion: ACPF

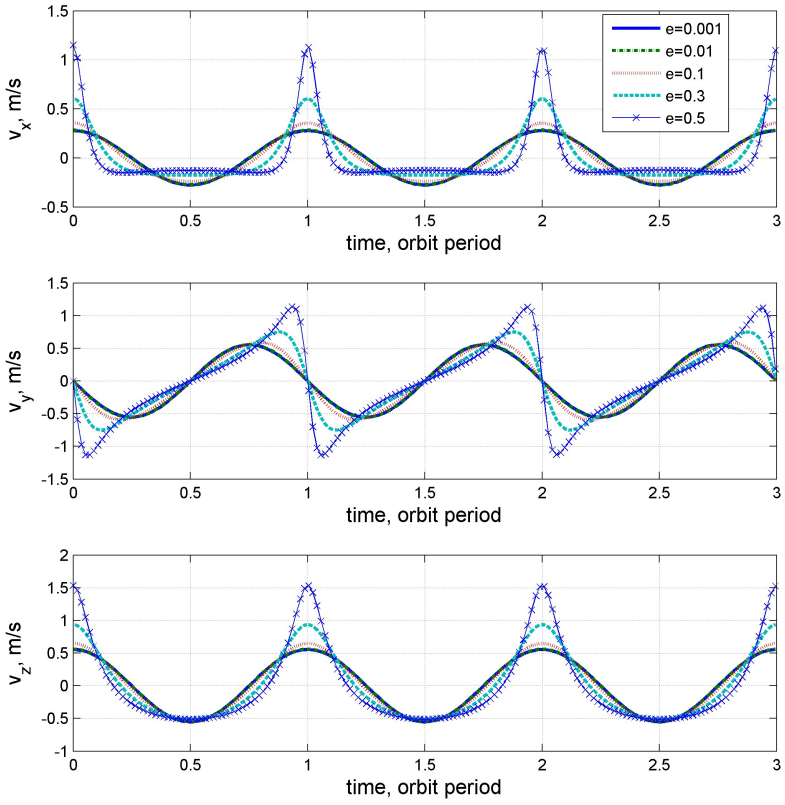

Figure 4.11: Time history of the velocity: ACPF

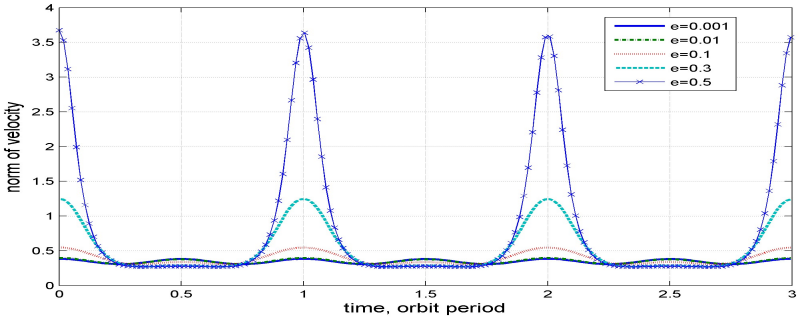

Figure 4.12: Time history of the velocity norm: ACPF

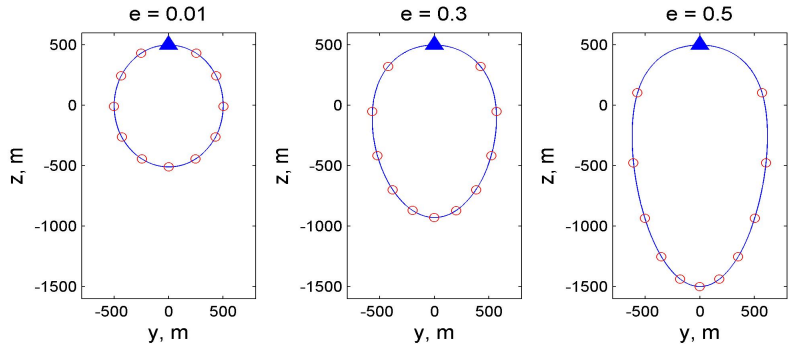

Figure 4.13: Along-track/cross-track motion: ACPF

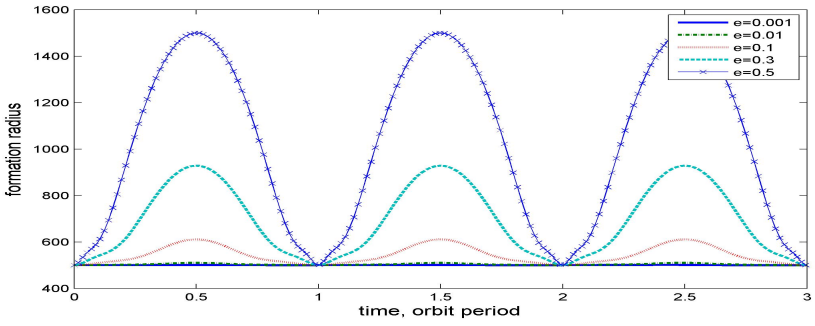

Figure 4.14: Time history of the formation radius: ACPF

4.5.3 Angle Difference between Two Follower Spacecraft

In accordance with the mission requirements, the number of followers can be increased. For the multiple followers, the distance information between follower spacecraft is important to handle the measured data from each spacecraft. From this aspect, numerical simulation is performed using two follower spacecraft, and the angle difference defined in Fig. 4.15 is analyzed according to the change of the formation radius and eccentricity of the reference orbit for the formation type described in previous sections. The initial conditions of the follower 1 and the follower 2 are selected at $\nu_0 = 0°$ and $\nu_0 = 180°$, respectively, in order to make the angle difference between two followers keep 180°.

The simulation results of the radial/along-track plane formation using two follower spacecraft are shown in Figs. 4.16–4.19. Figure 4.16 shows the trajectory of two followers according to various formation radii with the same

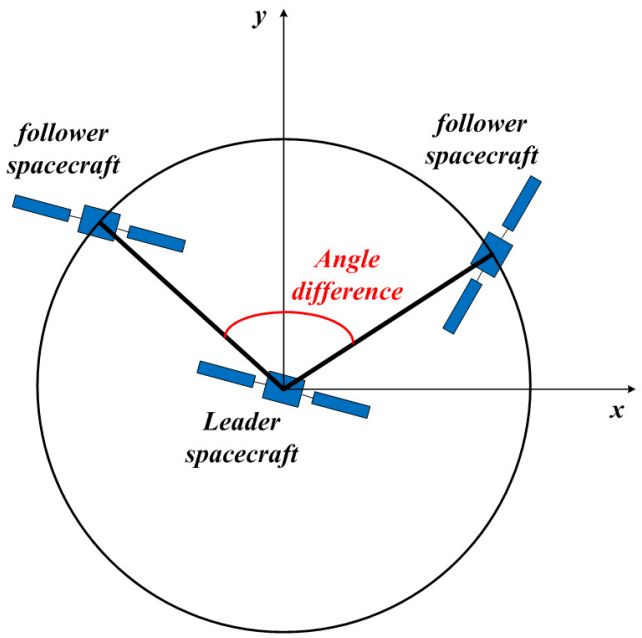

Figure 4.15: Definition of the angle difference

eccentricity of the reference orbit, $e = 0.1$. In Fig. 4.16, the origin denotes the leader spacecraft, the initial position of the follower 1 is marked by a circle, and the initial position of the follower 2 is marked by a triangle. Figure 4.17 shows the time history of the angle difference between the follower 1 and follower 2. As shown in Fig. 4.17, the angle difference between two followers is changed within the range of 165° to 195°, although the initial angle difference is 180°; however, the bound of the angle difference does not change as the formation radius is increased. It means that the angle difference is not influenced by the formation radius.

Figure 4.18 shows the trajectory of two followers according to various reference eccentricities with the desired formation radius $r = 500\,m$; the origin denotes the position of the leader spacecraft, the initial position of the follower 1 is marked by a circle, and the initial position of the follower 2 is marked by a triangle. Figure 4.19 shows the time history of the angle difference between the follower 1 and the follower 2. As compared with Fig. 4.17, Fig. 4.19 shows that the range of the angle difference varies as e is changed; the maximum of the angle difference is extended as the eccentricity increases. When the eccentricity has a small value, two follower spacecraft keep the angle difference near 180°; however, they cannot maintain the constant angle difference as the eccentricity is increased. For example, although the initial angle difference is 180°, the range of the angle difference is between 130° and 230° when $e = 0.5$. This is because the speed of the follower spacecraft is increased near the perigee and decreased near the apogee when the leader spacecraft has a highly elliptical orbit, as shown in Fig. 4.8.

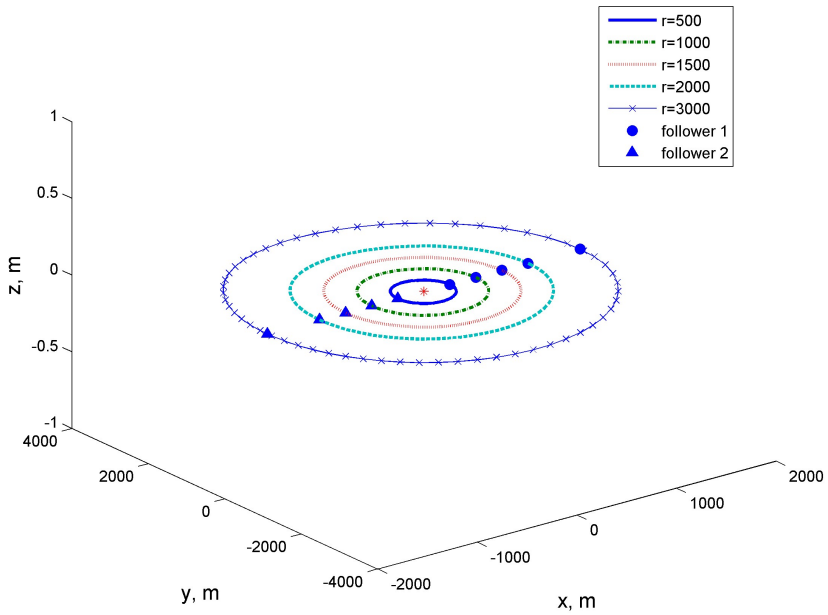

Figure 4.16: Relative trajectory with respect to r: RAPF, $e = 0.1$

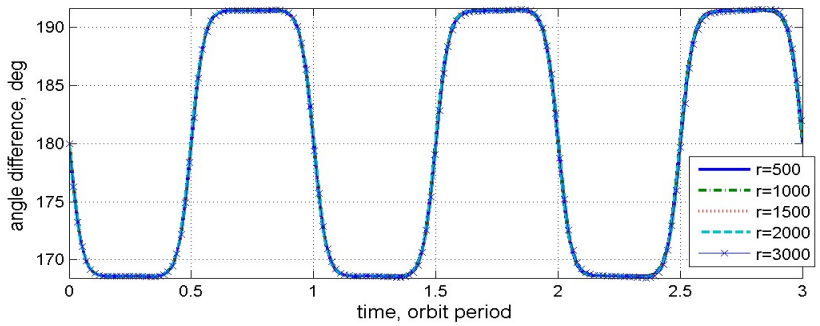

Figure 4.17: Time history of angle difference with respect to r: RAPF, $e = 0.1$

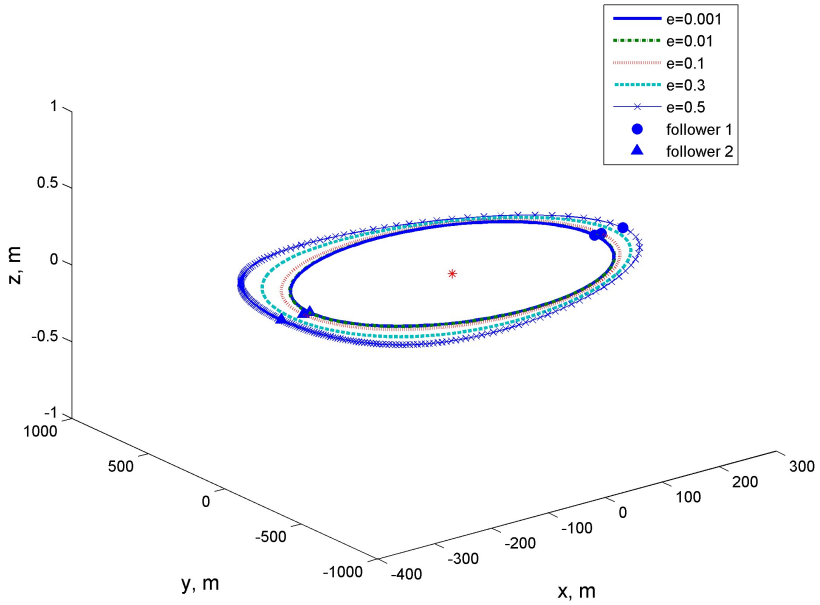

Figure 4.18: Relative trajectory with respect to e: RAPF, $r = 500m$

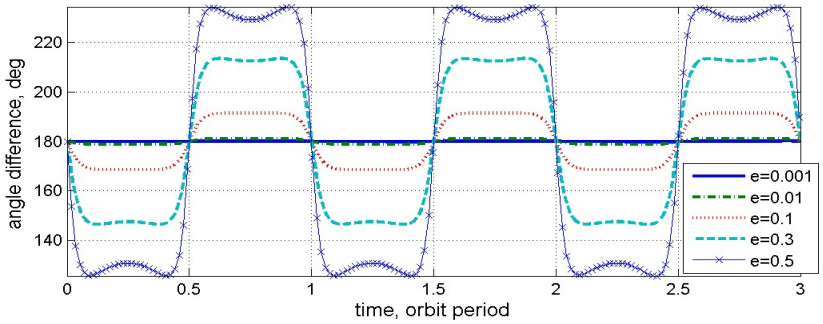

Figure 4.19: Time history of angle difference with respect to e: RAPF, $r = 500m$

The simulation results of the along-track/cross-track plane formation using two follower spacecraft under $4D_1^2 = D_2^2$ are shown in Figs. 4.20–4.23. Figure 4.20 shows the trajectory of two followers according to various formation radii with the eccentricity of the leader spacecraft, $e = 0.1$; the origin denotes the leader spacecraft, the initial position of the follower 1 is marked by a circle, and the initial position of the follower 2 is marked by a triangle. Figure 4.21 shows the time history of the angle difference between the follower 1 and follower 2. As shown in Fig. 4.21, the angle difference varies within the range of 150° to 210°, but the bound of the angle difference does not increase as the formation radius becomes large similar to Fig. 4.17.

Figure 4.22 shows the trajectory of two followers according to various reference eccentricities with the desired formation radius $r = 500\,m$; the origin denotes the leader spacecraft, the initial position of the follower 1 is marked by a circle, and the initial position of the follower 2 is marked by a triangle. Figure 4.23 shows the time history of the angle difference between the follower 1 and 2. As compared with Fig. 4.21, Fig. 4.23 describes that two followers do not keep 180°, and the amplitude of the angle difference is extended as e is increased. Thus, the bound of the angle difference is influenced by the eccentricity of the leader spacecraft.

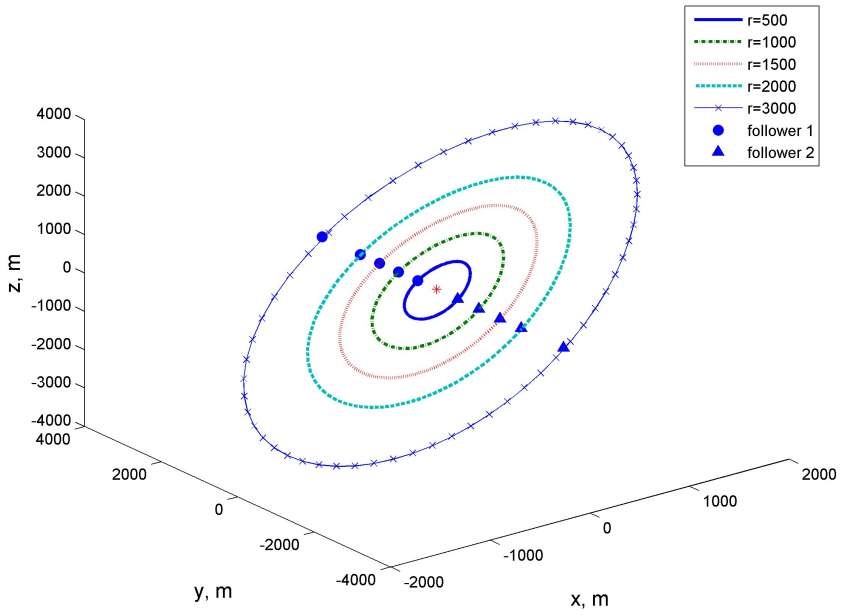

Figure 4.20: Relative trajectory with respect to r: ACPF, $e = 0.1$

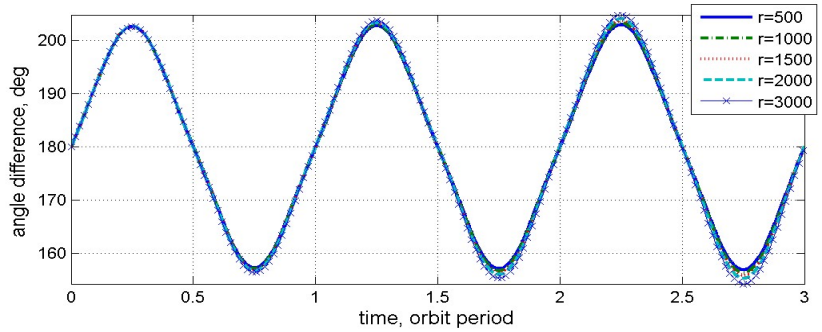

Figure 4.21: Time history of angle difference with respect to r: ACPF, $e = 0.1$

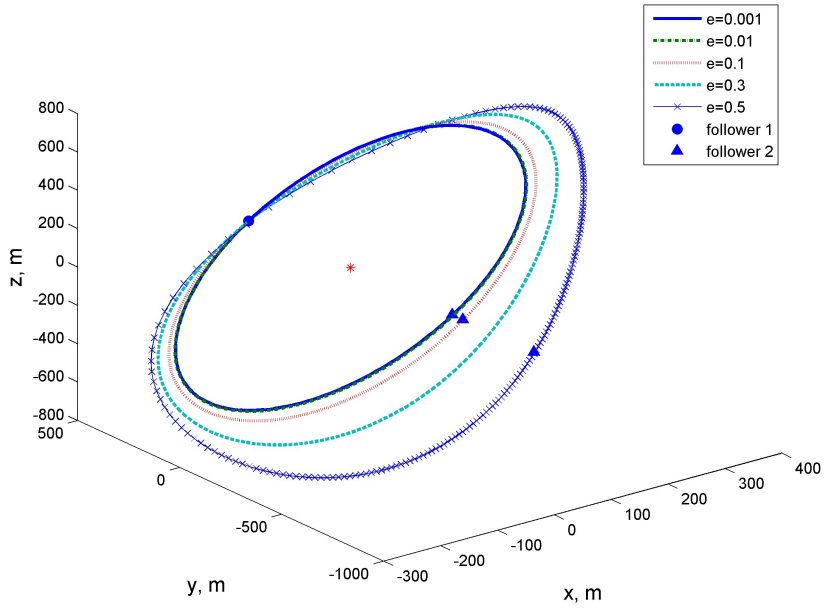

Figure 4.22: Relative trajectory with respect to e: ACPF, $r = 500m$

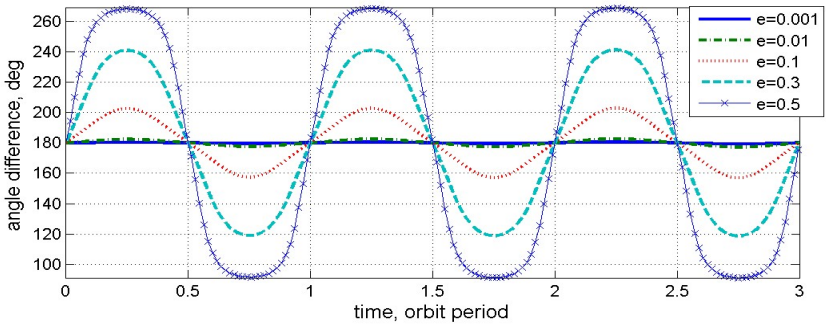

Figure 4.23: Time history of angle difference with respect to e: ACPF, $r = 500m$

4.5.4 Pattern Analysis of the Spacecraft Formation

Tables 4.4 and 4.5 summarize the formation radius according to the eccentricity of the reference orbit as shown in Figs. 4.9 and 4.14. The results show the tendency of the formation radius as a function of different eccentricities. As shown in Tables 4.4 and 4.5, the larger the eccentricity, the larger the maximum formation radius in both formation types, the radial/along-track plane and the along-track/cross-track plane formations. Furthermore, the ratio between the minimum and the maximum formation radii decreases as the eccentricity increases, as explained in Sections 4.3 and 4.4. The variation of the formation radius in the along-track/cross-track plane formation is reduced more significantly than that in the radial/along-track plane formation; the ratio between the minimum and maximum formation radii changes from 99.60 % to 33.32 % in the along-track/cross-track plane formation as shown in Table 4.5, while the range of the ratio is from 49.97 % to 47.18 % in the

Table 4.4: The maximum and minimum formation radius and ratio: RAPF

e	0.001	0.01	0.1	0.3	0.5
Maximum (m)	500.5910	502.8526	525.2467	575.8436	635.8959
Minimum (m)	250.1249	251.2437	261.9047	282.6082	300.0000
Min/Max (%)	49.97	49.96	49.86	49.08	47.18

Table 4.5: The maximum and minimum formation radius and ratio: ACPF

e	0.001	0.01	0.1	0.3	0.5
Maximum (m)	501.2318	510.0911	611.0675	928.4897	1499.8289
Minimum (m)	499.2380	499.8871	499.9788	499.9637	499.8053
Min/Max (%)	99.60	98.00	81.82	53.85	33.32

radial/along-track plane formation as shown in Table 4.4.

Tables 4.6 and 4.7 summarize the angle difference between two follower spacecraft according to the eccentricity of the reference orbit as shown in Figs. 4.19 and 4.23. As shown in Tables 4.6 and 4.7, when the reference eccentricity is small, the angle difference between two followers is near 180°. In contrast, two follower spacecraft cannot keep the constant angle difference as the reference eccentricity is increased, and the variation of the angle difference in the along-track/cross-track plane formation is severer than that in the radial/along-track plane formation. In the radial/along-track plane formation, the variation of the angle difference from 180° is 54.3901° for $e = 0.5$, but 0.1728° for $e = 0.0001$; however, in the along-track/cross-track plane formation, the angle difference has variation of 100.3352° for $e = 0.1$, and of 0.2292° for $e = 0.001$. Through these results, it is noted that the eccentricity of the reference orbit should be selected near zero to keep the same angle difference between two follower spacecraft during the formation mission. Moreover, if the

Table 4.6: The maximum and minimum angle difference: RAPF

e	0.001	0.01	0.1	0.3	0.5
Maximum (deg)	180.1728	181.1705	191.4309	213.5507	234.3901
Minimum (deg)	179.8406	178.8343	168.5721	146.4483	125.6110
Variation (deg)	0.1728	1.1705	11.4309	33.5507	54.3901

Table 4.7: The maximum and minimum angle difference: ACPF

e	0.001	0.01	0.1	0.3	0.5
Maximum (deg)	180.2292	182.2917	202.7676	245.0862	280.3552
Minimum (deg)	179.7708	177.7083	157.2324	114.9138	79.6448
Variation (deg)	0.2292	2.2917	22.7676	65.0862	100.3552

leader spacecraft is in an elliptic orbit, it is necessary to use the information of the angle difference between two followers for the utilization of the measured data from the spacecraft in a formation. On the other hand, when the formation mission requires the elliptical reference orbit and the constant angle difference between two followers, the follower spacecraft requires the orbit control to adjust the position.

The simulation results and analysis of this study provide a guideline when selecting the desired formation pattern in the elliptical reference orbits. In addition, the variations between the minimum and maximum formation radii and the range of the angle difference provide the constraints to be satisfied in the process of the formation design.

4.6 Concluding Remarks

In this chapter, the periodic relative motion and the formation geometry are developed. The periodic relative motion is derived to eliminate the secular drift and the offset in the along-track direction in Section 4.2. Two formation types are considered to analyze the formation pattern and to develop the formation geometry. The radial/along-track plane formation is analyzed with respect to the eccentricity and true anomaly of the reference orbit in Section 4.3. Moreover, the initial condition to maintain the formation in the radial/along-track plane formation is presented. In Section 4.4, the formation pattern analysis of the along-track/cross-track plane formation is presented and the initial condition of the along-track/cross-track plane formation is developed. For the along-track/cross-track plane formation, two cases are studied: $D_1^2 = D_2^2$ and $4D_1^2 = D_2^2$. In Section 4.5, the numerical simulation results are illustrated to analyze the formation pattern of the follower spacecraft according to the eccentricity and true anomaly of the leader spacecraft in two formation geometries. In addition, the angle difference is shown to consider the multiple follower spacecraft.

Through the analysis of the formation pattern, the eccentricity of the follower spacecraft in the local frame is not a constant value, and therefore the relative distance between two spacecraft varies according to e. When the leader spacecraft has a small eccentricity, the formation radius does not change a lot; however, as the eccentricity of the leader spacecraft is increased, the variation of the formation radius becomes significantly large in all formation geometries. These analytic results provide the guideline or constraint to design the formation in the elliptic reference orbit.

Chapter 5

Maneuver for Formation Reconfiguration

5.1 Introduction

In this chapter, the maneuver problem for the spacecraft formation reconfiguration is considered. The maneuver problem between two orbits in the inertial frame has been widely studied [70, 96]. For the spacecraft formation, the maneuver can change the formation radius and configuration between two spacecraft. However, a follower spacecraft from one orbit to another with respect to the leader spacecraft in the LVLH frame, where the initial and final positions, velocities, transfer time, and the orbit elements of the leader spacecraft are specified, has not been sufficiently investigated.

The maneuver problem can be formulated according to the control input type: continuous control input and impulsive control input. For the continuous control input case, the optimization theory can be applied, where the position and velocity vectors at the initial and final time are specified. The trajectory optimization using the continuous control input can be classified into two categories: indirect method and direct method [69, 70, 114]. In the

indirect method, the optimal trajectory is obtained by deriving and solving the first-order necessary conditions for the optimality via the calculus of variations and Pontryagin's minimum principle. This method has advantages that accurate solution is obtained by satisfying the first-order optimality conditions; however, the appropriate initial guess of the state/costate values for the unknown boundary conditions is required to obtain the converged solution. In the direct method, on the other hand, the continuous optimization problem can be solved by direct applying a nonlinear programming. The state and control variables are updated to minimize the cost function, while the boundary conditions and several constraints are satisfied. The advantage of the direct method lies in the larger radii of convergence than that of the indirect method, and therefore the convergence is not sensitive to the initial guess of the state trajectory and input history. In contrast, the direct method provides less accurate solution than the indirect method. In this study, the optimal trajectory is obtained by using the nonlinear programming and collocation method.

For the impulsive control input case, the transfer orbit between two orbits can be determined by the specified position vectors at the initial and final time [96]. The maneuver usually leads to change of the orbital plane, and therefore several orbital elements are varied; (i) in the coplanar maneuver, semi-major axis a, eccentricity e, and augment of perigee ω change, (ii) in the non-coplanar maneuver, inclination i and longitude of ascending node Ω change, and (iii) in the combined maneuver, all orbital elements change. The Hohmann transfer is known as a global optimum two-impulsive transfer between circular coplanar orbits, and a transfer orbit is an ellipse cotangential to the circles at its apses [31, 96]. The most general transfer uses two nontangential burns, which can apply to any orbit type. This transfer problem in the two-body problem can be usually solved by the Lambert's problem [31]. Lambert's problem provides the transfer orbit between fixed two position vectors with given transfer time.

Various methods dealing with the Lambert's problem have been discussed by many researchers [99, 100, 101, 102, 103, 104].

The maneuver problem for the spacecraft formation is described in Section 5.2. In Section 5.3, the transfer problem using the continuous control input is solved by the optimal control theory with the Gauss pseudospectral method. The maneuver problem in the relative motion using the impulsive control input is treated and discussed by modifying the classical Lambert's problem in Section 5.4.

5.2 Maneuver for Spacecraft Formation

One objective of the maneuver for the spacecraft formation is to change the formation configuration between the leader and follower spacecraft in the LVLH frame, as shown in Fig. 5.1. To do this, minimization of the control fuel during the maneuver is important, since the remaining fuel is critical for life of the spacecraft. Therefore, in this study, to transfer from given position and velocity vectors on the initial configuration to desired position and velocity vectors on the final configuration, two types of control input are considered: continuous control input and impulsive control input. Table 5.1 summarizes the characteristics of two control inputs [115, 116, 117, 118].

For the continuous control input, the trajectory optimization problem for the formation reconfiguration is formulated by the parameter optimization,

Table 5.1: Characteristics of thruster

	Impulsive control input	Continuous control input
Propulsion	Chemical thruster	Ion thruster
I_{sp} (s)	$100 - 500$	$\sim 5,000$
Force (N)	$0.1 - 10^3$	$10^{-3} - 10$

given two position and velocity vectors at the initial and final time. Generally, the parameter optimization methods are categorized according to the variables to be parameterized and the method to satisfy dynamic equation. The most common method is control parameterization technique [119]; the only control history is expressed as a finite parameter representation, and the differential dynamic equations are solved by numerical integration. Another type is state and control parameterization technique [85]; the state and control variables are parameterized, and the differential dynamic equations are changed to algebraic constraints so that the numerical integration can be satisfied at each node. Pseudospectral or orthogonal collocation method is widely used in this technique [120]. In a pseudospectral method, the state and control variables are approximated using a finite basis of global interpolating polynomials at a set of discretization nodes, and the differentiation of state in dynamic equation is approximated by the derivative of interpolating polynomial, which is

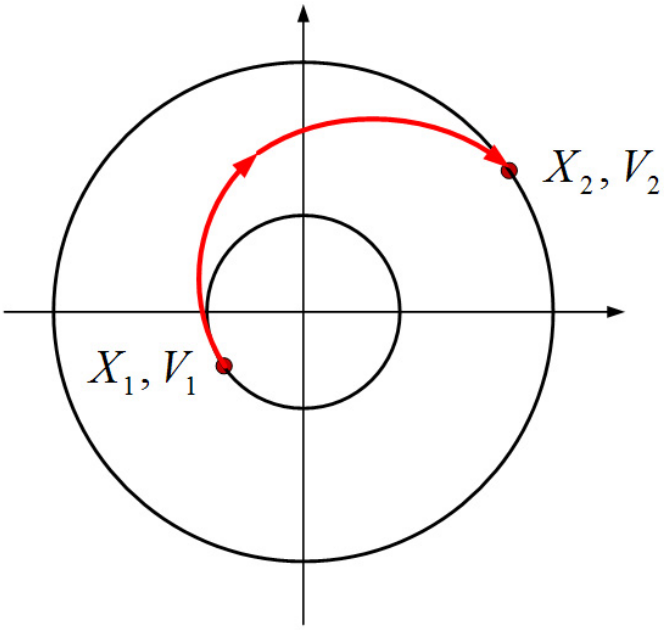

Figure 5.1: Geometry of maneuver

converted to constraints at the collocation nodes. In addition, the collocation points are selected to be roots of an orthogonal polynomial. The primary advantage of the pseudospectral method is fast convergence rate, and therefore various problems have been solved using the pseudospectral method [94, 121, 122, 123, 124].

For the impulsive control input, the transfer orbit between two orbits can be generally defined by the Lambert's problem, where two position vectors are known at the initial and final time [97, 98]. The classical Lambert's problem deals with the transfer problem of a single spacecraft in the inertial frame. In this study, the classical Lambert's problem is modified to change the formation radius or formation geometry between the leader and follower spacecraft in the LVLH frame using two-impulses. By solving the two-point boundary value problem in the relative motion, the formation reconfiguration and orbit transfer of the spacecraft formation can be obtained. The desired transfer orbit can be characterized by the initial position and final position of the follower spacecraft in the LVLH frame. In this study, the periodic analytic solutions are used to find the initial and final positions of the follower spacecraft. Although the leader spacecraft moves on elliptic reference orbits, which is Keplerian motion, the relative motion including the relative position and velocity vectors does not have the characteristics of Keplerian motion. However, the follower spacecraft with respect to the Earth is also Keplerian motion, because the follower spacecraft maintaining a desired formation type moves on the Earth's orbit, too. As a result, the maneuver problem of the follower spacecraft in the relative motion can be solved by utilizing the classical Lambert's problem. The difference between this approach and the classical Lambert's problem lies on the point of transfer time. In the classical Lambert's problem, the transfer orbit is determined using the flight time which can be selected for the one single spacecraft in the orbit. On the other hand, in the relative motion of

the spacecraft formation, it is assumed that the relative distance between the leader and follower spacecraft is very small, and then the transfer orbit of the follower spacecraft is obtained using the transfer time depending on the flight time of the leader spacecraft [105, 112]. By dealing with this maneuver problem, the transfer orbit and the velocity vector for the maneuver between two orbits can be obtained, and thereby the total required ΔV can be computed.

5.3 Continuous Control Input

5.3.1 Dynamic Model

In Chapter 2, the relative motion is presented without the external force acting on the spacecraft. Sometimes, the spacecraft uses the control forces to maintain the desired position or transfer the orbit. The equation of relative motion can be written considering the external forces as follows:

$$\begin{aligned}
\ddot{x} &= 2\dot{\theta}\dot{y} + \ddot{\theta}y + \dot{\theta}^2 x - \frac{\mu(R+x)}{\{(R+x)^2+y^2+z^2\}^{3/2}} + \frac{\mu}{R^2} + u_x \\
\ddot{y} &= -2\dot{\theta}\dot{x} - \ddot{\theta}x + \dot{\theta}^2 y - \frac{\mu y}{\{(R+x)^2+y^2+z^2\}^{3/2}} + u_y \\
\ddot{z} &= -\frac{\mu z}{\{(R+x)^2+y^2+z^2\}^{3/2}} + u_z
\end{aligned} \tag{5.1}$$

where u_x, u_y, and u_z are the control inputs in radial, along-track, and cross-track direction, respectively. Equation (5.1) can be rewritten in the true-anomaly domain as

$$\begin{aligned}
x'' &= \frac{2e\sin\nu}{1+e\cos\nu}x' + 2y' + \frac{3+e\cos\nu}{1+e\cos\nu}x - \frac{2e\sin\nu}{1+e\cos\nu}y + \frac{(1-e^2)^3}{n^2(1+e\cos\nu)^4}u_x \\
y'' &= -2x' + \frac{2e\sin\nu}{1+e\cos\nu}y' + \frac{2e\sin\nu}{1+e\cos\nu}x + \frac{e\sin\nu}{1+e\cos\nu}y + \frac{(1-e^2)^3}{n^2(1+e\cos\nu)^4}u_y \\
z'' &= \frac{2e\sin\nu}{1+e\cos\nu}z' - \frac{1}{1+e\cos\nu}z + \frac{(1-e^2)^3}{n^2(1+e\cos\nu)^4}u_z
\end{aligned} \tag{5.2}$$

Equation (5.2) is considered as the dynamic constraint in the trajectory optimization problem.

5.3.2 Problem Formulation

The objective of an optimal control problem is to determine the control inputs minimizing the performance index while satisfying various constraints. Let us consider the following cost function J_1 for minimum energy and J_2 for minimum fuel.

$$J_1 = \int_{\nu_1}^{\nu_2} \boldsymbol{U}^T \Xi \boldsymbol{U} d\nu \tag{5.3}$$

$$J_2 = \int_{\nu_1}^{\nu_2} \sum_{i=1}^{3} |u_i| d\nu \tag{5.4}$$

where $\boldsymbol{U} = [u_x,\ u_y,\ u_z]^T \in \Re^3$ is a control input vector, and $\Xi \in \Re^{3\times 3}$ is a weighting matrix. The control input vector has specified limits as boundary condition as follows:

$$|\boldsymbol{U}| \leq U_B \tag{5.5}$$

Equation (5.2) is the dynamic constraint, and the boundary conditions at ν_1 and ν_2 should be determined considering the situation that (i) the follower spacecraft moves in the LVLH frame with respect to the leader spacecraft, and (ii) transfers from formation radius r_1 to r_2. The initial position and velocity are selected according to the desired formation type with r_1 as described in Chapter 4.

$$x(\nu_1) = x_0, \qquad y(\nu_1) = y_0, \qquad z(\nu_1) = z_0 \tag{5.6}$$

$$x'(\nu_1) = x'_0, \qquad y'(\nu_1) = y'_0, \qquad z'(\nu_1) = z'_0 \tag{5.7}$$

The final position and velocity are chosen according to the desired formation type with r_2.

$$x(\nu_2) = x_f, \qquad y(\nu_2) = y_f, \qquad z(\nu_2) = z_f \tag{5.8}$$

$$x'(\nu_2) = x'_f, \qquad y'(\nu_2) = y'_f, \qquad z'(\nu_2) = z'_f \tag{5.9}$$

The relative motion is expressed in the true anomaly domain, and the transfer angle can be defined as $\Delta\nu = \nu_2 - \nu_1$.

5.3.3 Gauss Pseudospectral Method

In the direct method solving the trajectory optimization problem, the state and control variables are parametrized. Gauss pseudospectral method uses global interpolating polynomials to approximate the state and control parameters on the time interval $\tau \in [-1\ 1]$ [94]. In the Gauss pseudospectral method, the dynamics are collocated at the N Legendre-Gauss points τ_k $(k = 1, \cdots, N)$, and the state and control parameters are approximated using Lagrange interpolating polynomials as the basis functions. The state is approximated using a basis of $N + 1$ Lagrange interpolating polynomials L, and the control is approximated using a basis of N Lagrange interpolating polynomials L' as

$$\boldsymbol{X}(\tau) = \sum_{i=0}^{N} \boldsymbol{X}(\tau_i) L_i(\tau) \tag{5.10}$$

$$\boldsymbol{U}(\tau) = \sum_{i=1}^{N} \boldsymbol{U}(\tau_i) L'_i(\tau) \tag{5.11}$$

where

$$L_i(\tau) = \prod_{j=0, j\neq i}^{N} \frac{\tau - \tau_j}{\tau_i - \tau_j}, \qquad L'_i(\tau) = \prod_{j=1, j\neq i}^{N} \frac{\tau - \tau_j}{\tau_i - \tau_j} \tag{5.12}$$

Now, the variables used in Gauss pseudospectral method are

$$\begin{aligned} &\text{NLP variables corresponding to state:} \quad (\boldsymbol{X}_0, \boldsymbol{X}_1, \cdots, \boldsymbol{X}_N) \\ &\text{NLP variables corresponding to control:} \quad (\boldsymbol{U}_1, \cdots, \boldsymbol{U}_N) \end{aligned} \tag{5.13}$$

Differentiating Eq. (5.10) yields

$$\dot{\boldsymbol{X}}(\tau) = \sum_{i=0}^{N} \boldsymbol{X}(\tau_i) \dot{L}_i(\tau) \tag{5.14}$$

where

$$\dot{L}_i(\tau_k) = \begin{cases} \frac{(1+\tau_k)\dot{P}_K(\tau_k) + P_K(\tau_k)}{(\tau_k - \tau_i)[(1+\tau_i)\dot{P}_K(\tau_i) + P_K(\tau_i)]} & i \neq k \\ \frac{(1+\tau_i)\ddot{P}_K(\tau_i) + 2\dot{P}_K(\tau_i)}{2[(1+\tau_i)\dot{P}_K(\tau_i) + P_K(\tau_i)]} & i = k \end{cases} \tag{5.15}$$

where $k = 1, 2, \cdots, N$, and $i = 0, 1, \cdots, N$. The dynamic equations at the collocation points are obtained as

$$\sum_{i=0}^{K} \dot{L}_i(\tau_k)\boldsymbol{X}(\tau_i) - \frac{t_f - t_0}{2} f(\boldsymbol{X}(\tau_k), \boldsymbol{U}(\tau_k), \tau_k) = 0, \quad k = 1, 2, \cdots, N \quad (5.16)$$

The boundary conditions can also be discretized at the Legendre-Gauss points.

5.4 Impulsive Control Input

5.4.1 Lambert's Problem

Lambert's theorem states that the flight time from one point to another depends on the semi-major axis of transfer orbit, the distance of the initial and final points of the arc from the center of force, and the length of the chord joining the points. The chord length, c, between two position vectors $\vec{r}_1$ and $\vec{r}_2$, as shown in Fig. 5.2, is defined by the cosine law as follows:

$$c = \sqrt{r_1^2 + r_2^2 - 2r_1 r_2 \cos(\theta_T)} \quad (5.17)$$

In Fig. 5.2, F is the primary focus which is the location of the Earth, $\vec{r}_1$ and $\vec{r}_2$ are the position vectors at the initial time t_1 and the final time t_2, and θ_T is the transfer angle between two position vectors defined by

$$\cos(\theta_T) = \frac{\vec{r}_1 \cdot \vec{r}_2}{r_1 r_2} \quad (5.18)$$

The direction of flight can be defined by the transfer angle; the spacecraft moves along the short way when $\theta_T \leq \pi$, and it moves along the long way when $\theta_T > \pi$.

To determine the transfer orbit between two position vectors, two foci and semi-major axis should be found. From the definition of the ellipse, the location of the vacant focus and semi-major axis a of the transfer orbit can be determined. As shown in Fig. 5.2, two circles can be drawn having $2a - r_1$

and $2a - r_2$ as radii and points P_1 and P_2 as centers, respectively, since the sum of the distance from the foci to any point on the ellipse equals twice the semi-major axis as $2a = r_1 + (2a - r_1) = r_2 + (2a - r_2)$. As a result, two intersected points, F' and F'', are determined as shown in Fig. 5.2, which are the candidate locations of other focus of the transfer orbit. Using two vacant foci, two elliptic orbits can be obtained as shown in Fig. 5.3. Note from Fig. 5.3 that two ellipses have different eccentricities; the ellipse with vacant focus F' has the smaller eccentricity, and the ellipse with F'' has the larger eccentricity. The location of vacant focus depends on the semi-major axis of the transfer orbit, and therefore the semi-major axis should be determined carefully through iterative calculation for the minimum energy.

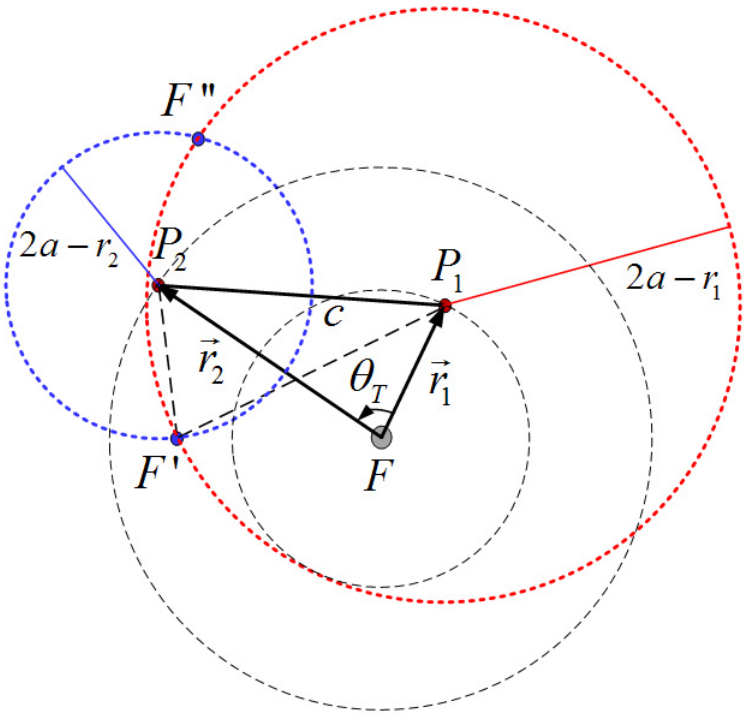

Figure 5.2: Geometry for the Lambert's problem

When the transfer orbit is determined, the velocity vectors of the transfer orbit at the initial and final time, $\vec{v}_{t,1}$ and $\vec{v}_{t,2}$, as shown in Fig. 5.4, can be calculated by the Kepler's equation. Consequently, the velocity changes Δv_1 and Δv_2 at t_1 and t_2 can be obtained as

$$\Delta v_1 = \vec{v}_{t,1} - \vec{v}_1 \tag{5.19}$$

$$\Delta v_2 = \vec{v}_2 - \vec{v}_{t,2} \tag{5.20}$$

where $\vec{v}_1$ and $\vec{v}_2$ are velocity vectors of the spacecraft around a planet at the initial and final time. Figure 5.4 shows the velocity changes using two impulse inputs. The total velocity change can defined as follows:

$$\Delta v = |\Delta v_1| + |\Delta v_2| \tag{5.21}$$

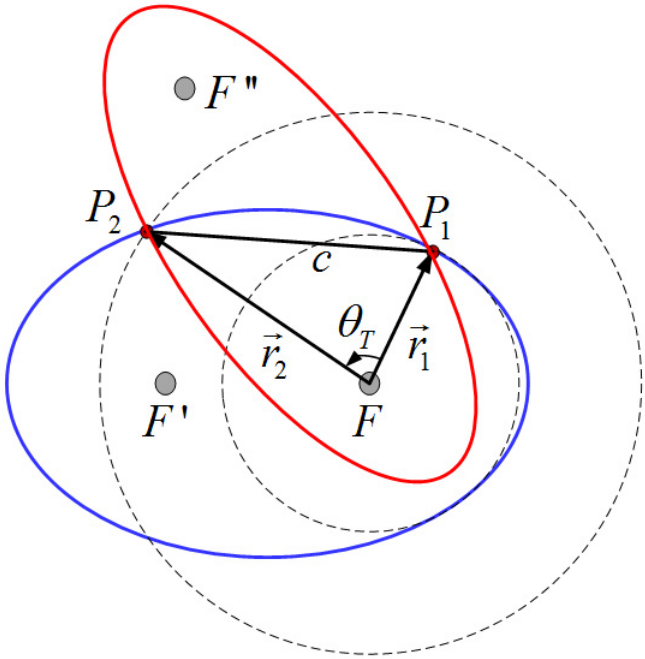

Figure 5.3: Geometry of transfer orbit for the Lambert's problem

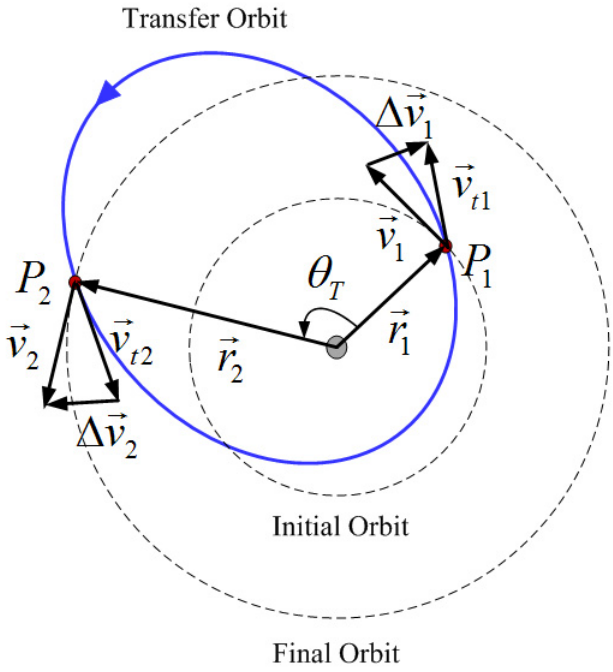

Figure 5.4: Orbit transfer using two impulsive inputs

5.4.2 Lambert's Problem for Follower Spacecraft

The transfer orbit for the follower spacecraft connecting two relative position vectors can be solved using the Lambert's problem, when the orbital elements of the leader spacecraft and the flight time are known. The geometry of the transfer orbit for the follower spacecraft is illustrated in Fig. 5.5.

The relative position vectors of the follower spacecraft with respect to the leader spacecraft, $\vec{\rho}_1 \in \Re^3$ and $\vec{\rho}_2 \in \Re^3$ at the initial time t_1 and the final time t_2 in the LVLH frame, respectively, can be expressed as follows:

$$\begin{aligned} \vec{\rho}_1 &= [x_1, \quad y_1, \quad z_1]^T \\ \vec{\rho}_2 &= [x_2, \quad y_2, \quad z_2]^T \end{aligned} \tag{5.22}$$

The position vectors of the follower spacecraft with respect to the Earth at t_1

and t_2 in the ECI frame can be written as

$$\begin{aligned} \vec{R}_1 &= \vec{r}_1 + \vec{\rho}_1 \\ \vec{R}_2 &= \vec{r}_2 + \vec{\rho}_2 \end{aligned} \tag{5.23}$$

where $\vec{r}_1 \in \Re^3$ and $\vec{r}_2 \in \Re^3$ are the position vectors of the leader spacecraft in the ECI frame at t_1 and t_2, respectively.

Let us define the velocity vectors of the follower spacecraft at t_1 and t_2 in the ECI frame as $\vec{V}_1 \in \Re^3$ and $\vec{V}_2 \in \Re^3$, respectively. Given two position vectors, $\vec{R}_1$ and $\vec{R}_2$, the transfer orbit for the follower spacecraft can be determined through the Lambert's problem as explained in the previous section. The transfer angle can be defined by

$$\cos(\theta_T) = \frac{\vec{R}_1 \cdot \vec{R}_2}{R_1 R_2} \tag{5.24}$$

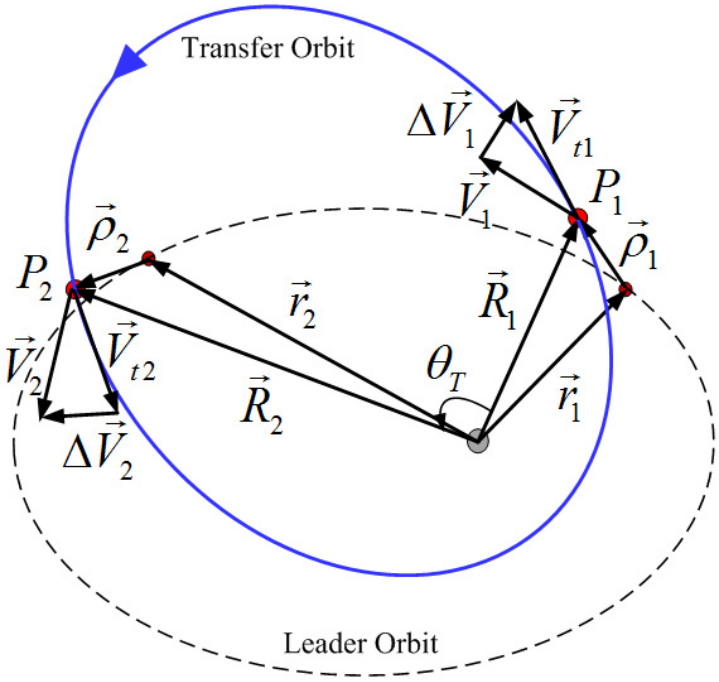

Figure 5.5: Orbit transfer for follower spacecraft

The chord length is determined as

$$c = \sqrt{R_1^2 + R_2^2 - 2R_1 R_2 \cos(\theta_T)} \tag{5.25}$$

Using θ_T and c, the Lambert's problem can provide the velocities of the transfer orbit, $\vec{V}_{t,1} \in \Re^3$ and $\vec{V}_{t,2} \in \Re^3$, as shown in Fig. 5.5. The transfer time for the elliptic orbit is defined from the Kepler's equation as follows [23, 31]:

$$\Delta t = \sqrt{\frac{a^3}{\mu}} \left[2\pi k + (E_2 - e\sin E_2) - (E_1 - e\sin E_1)\right] \tag{5.26}$$

where $\Delta t = t_2 - t_1$, and E_1 and E_2 are eccentric anomalies at t_1 and t_2. In this study, multiple revolutions are not considered, and then $2\pi k$ term in Eq. (5.26) can be ignored. Equation (5.26) can be rewritten as

$$\sqrt{\mu}\Delta t = \sqrt{a^3}\left[\Delta E + e(\sin E_1 - \sin E_2)\right] \tag{5.27}$$

where $\Delta E = E_2 - E_1$. To solve the Kepler's equation, the universal variable, χ, is adopted in this study, which relates energy and angular momentum [31]. The universal variable, χ is defined as follows:

$$\chi = \sqrt{a}\Delta E \tag{5.28}$$

In addition, parameters s_2 and s_3 are defined as

$$s_2 = \frac{1 - \cos\Delta E}{\Delta E^2}, \qquad s_3 = \frac{\Delta E - \sin\Delta E}{\Delta E^3} \tag{5.29}$$

Using Eqs. (5.28) and (5.29), Eq. (5.27) can be expressed as

$$\sqrt{\mu}\Delta t = \chi^3 s_3 + \sqrt{a^3}\,\sin\Delta E + \sqrt{a^3}\,e\,(\sin E_1 - \sin E_2) \tag{5.30}$$

With trigonometric identity, $\sin(a_1 - a_2) = \sin a_1 \cos a_2 - \cos a_1 \sin a_2$, Eq. (5.30) can be rewritten as

$$\sqrt{\mu}\Delta t = \chi^3 s_3 + \sqrt{a^3}\left\{\sin E_1(e - \cos E_2) - \sin E_2(e - \cos E_1)\right\} \tag{5.31}$$

The relation between eccentric anomaly E and true anomaly ν is defined by [23, 31]

$$\cos\nu = \frac{e - \cos E}{e\cos E - 1} \tag{5.32}$$

After some manipulation with Eq. (5.32), Eq. (5.31) can be expressed as follows:

$$\sqrt{\mu}\Delta t = \chi^3 s_3 + \sqrt{a^3}\left(\sin\nu_2\cos\nu_1 - \sin\nu_1\cos\nu_2\right)\left[\frac{(1 - e\cos E_1)(1 - e\cos E_2)}{\sqrt{1 - e^2}}\right] \tag{5.33}$$

With the trigonometric identity, Eq. (5.33) is presented as

$$\sqrt{\mu}\Delta t = \chi^3 s_3 + \sqrt{a^3}\sin\theta_T \frac{(1 - e\cos E_1)(1 - e\cos E_2)}{\sqrt{1 - e^2}} \tag{5.34}$$

The radius is defined as $r = a(1 - e\cos E)$ in the orbital mechanics, and then Eq. (5.34) can be rewritten as

$$\sqrt{\mu}\Delta t = \chi^3 s_3 + A\sqrt{Y} \tag{5.35}$$

where

$$A = \frac{\sqrt{R_1 R_2}\sin\theta_T}{\sqrt{1 - \cos\theta_T}}, \qquad Y = \frac{\sqrt{R_1 R_2(1 - \cos\theta_T)}}{\sqrt{a(1 - e^2)}} \tag{5.36}$$

The resulting A and Y give the velocity vectors of the transfer orbit at t_1 and t_2 as follows:

$$\vec{V}_{t,1} = \frac{\vec{R}_2 - f\vec{R}_1}{g} \tag{5.37}$$

$$\vec{V}_{t,2} = \frac{\dot{g}\vec{R}_2 - \vec{R}_1}{g} \tag{5.38}$$

where

$$f = 1 - \frac{Y}{R_1} \tag{5.39}$$

$$g = A\sqrt{\frac{Y}{\mu}}, \qquad \dot{g} = 1 - \frac{Y}{R_2} \tag{5.40}$$

Finally, the velocity changes ΔV_1 and ΔV_2 for the follower spacecraft at t_1 and t_2 can be obtained as follows:

$$\Delta V_1 = \vec{V}_{t,1} - \vec{V}_1 \tag{5.41}$$

$$\Delta V_2 = \vec{V}_2 - \vec{V}_{t,2} \tag{5.42}$$

Consequently, the total velocity change can be calculated as

$$\Delta V = |\Delta V_1| + |\Delta V_2| \tag{5.43}$$

Note that $\vec{V}_{t,1}$ and $\vec{V}_{t,2}$ are velocities with respect to the Earth and expressed in the ECI frame. Thus, the relative velocity vectors of the follower spacecraft with respect to the leader spacecraft can be expressed as follows:

$$\begin{aligned} \dot{\vec{\rho}}_1 &= \vec{V}_{t,1} - \vec{v}_1 - \omega \times \vec{\rho}_1 \\ \dot{\vec{\rho}}_2 &= \vec{V}_{t,2} - \vec{v}_2 - \omega \times \vec{\rho}_2 \end{aligned} \tag{5.44}$$

where $\vec{v}_1 \in \Re^3$ and $\vec{v}_2 \in \Re^3$ are velocity vectors of the leader spacecraft at t_1 and t_2, respectively, and ω is the angular velocity vector of the leader spacecraft as defined by

$$\omega = \dot{\nu}\vec{k}, \qquad \vec{k} = \frac{r_1 \times r_2}{||r_1 \times r_2||} \tag{5.45}$$

Finally, the relative velocity vectors in the LVLH frame and the orbital elements of the transfer orbit can be found.

5.5 Concluding Remarks

In this chapter, the maneuver problem for the formation reconfiguration is developed. To transfer between two position vectors, two control input types are considered: continuous control input and impulsive control input. For the continuous control input, the optimal control problem is presented for the formation reconfiguration, and the Gauss pseudospectral method is described specifically, in Section 5.3. On the other hand, for the impulsive control input, the Lambert's problem is presented in Section 5.4. Furthermore, to deal with the relative motion of multiple spacecraft, the classical Lambert's problem is modified to solve the maneuver problem for the follower spacecraft with respect to the leader spacecraft. Therefore, the transfer trajectory of the follower spacecraft can be determined according to the thrust system.

Chapter 6

Numerical Simulation: Formation Reconfiguration

6.1 Introduction

In this chapter, numerical simulations are performed for the maneuver problem of the formation reconfiguration. Using two control input types, i.e., continuous control input type and impulsive control input type, three maneuvering cases are considered to verify the formation reconfiguration in the relative motion: (i) change of the formation radius in the radial/along-track plane formation, (ii) change of the formation radius in the along-track/cross-track plane formation, and (iii) change of the formation geometry from the radial/along-track plane to the along-track/cross-track plane formations.

In Section 6.2, the simulation configuration is described for the formation reconfiguration. In Section 6.3, the numerical simulation results for changing the formation radius are illustrated in the radial/along-track plane formation using two control input types. The results of the formation reconfiguration in the along-track/cross-track plane formation are shown in Section 6.4. In Section 6.5, the results for changing the formation geometry from the

radial/along-track plane to the along-track/cross-track plane formations are described.

6.2 Simulation Configuration

The configuration of the numerical simulation is described in Fig. 6.1. First, the objective of the maneuver for the formation reconfiguration is defined according to the formation type considering the formation pattern analysis presented in Chapter 4. Moreover, the control input type is considered according to the spacecraft thrust system. After the consideration of the formation reconfiguration, the relative position vectors and velocity vectors at the initial and final time are obtained through the periodic relative motion as discussed in Chapters 3 and 4. Then, the optimal trajectories are provided by solving the Gauss pseudospectral method of the optimal control problem for the continuous control input (Section 5.3), and by solving the modified Lambert's problem for the impulsive control input (Section 5.4).

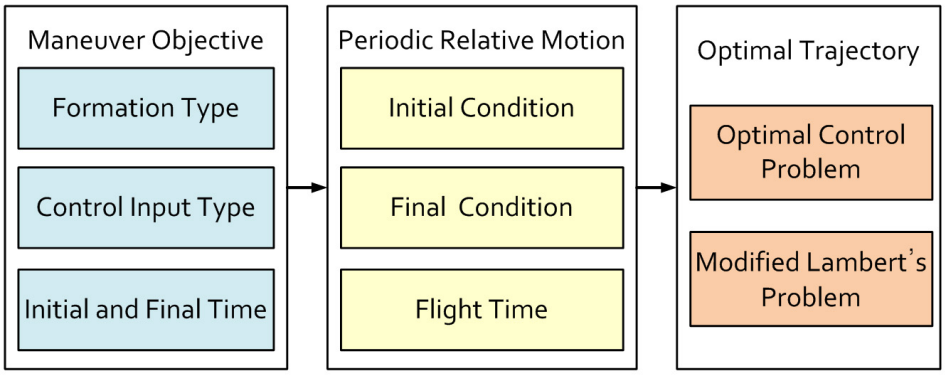

Figure 6.1: Configuration of numerical simulation

6.3 Radial/Along-Track Plane Formation

In this section, the maneuver for the formation reconfiguration in the radial/along-track plane formation (RAPF) is performed using two control input types: continuous and impulsive control inputs. The orbital elements of the leader spacecraft are summarized in Table 3.1. To change the formation radius in the radial/along-track plane formation, we consider a situation that the follower spacecraft moves from the initial formation radius of 500 m to the final formation radius of 1,000 m. The initial and final conditions are given by the formation geometry as described in Chapter 4.

In Section 6.3.1, the optimal trajectory using the continuous control input is illustrated using the Gauss pseudospectral method with the relative position and velocity vectors at the initial and final configuration, which method is described in Section 5.3. In Section 6.3.2, the transfer orbit trajectory using the impulsive control input is shown based on the modified Lambert's problem presented in Section 5.4, where the initial and final position vectors and the flight time are specified. In Section 6.3.3, moreover, the global minimum velocity is described and corresponding transfer orbit is presented to minimize the control effort for the impulsive control input. The simulation results for resizing the formation radius in the radial/along-track plane formation are analyzed in Section 6.3.4.

6.3.1 Continuous Control Input

The initial and final conditions of the follower spacecraft in the LVLH frame are summarized in Table 6.1. For the continuous control input type, two cost functions, J_1 and J_2, are considered as described in Eqs. (5.3) and (5.4).

Figures 6.2–6.4 show the simulation results with the cost function J_1 for minimum energy. Figure 6.2 shows the transfer trajectory of the follower spacecraft with respect to the leader spacecraft in the LVLH frame; the solid line denotes the trajectory of the follower spacecraft with different formation radii, $r_d = 500\,m$ and $r_d = 1,000\,m$, respectively, and the line with square shows the transfer trajectory of the follower spacecraft between two orbits. Figure 6.3 shows the velocity history of the follower spacecraft in the true anomaly domain during the maneuver. In Fig. 6.3, the triangle denotes specified relative velocities at the initial and final time in the LVLH frame, as presented in Table 6.1. Figure 6.4 shows the control input history of the follower spacecraft in the true anomaly domain during the maneuver. As shown in Fig. 6.2, the transfer trajectory is placed on the $x-y$ plane where satisfying the conditions for the initial and final relative positions. In addition, the boundary conditions of the initial and final relative velocities are also satisfied as shown in Fig. 6.3 by the continuous control input presented in Fig. 6.4.

Table 6.1: Initial and final conditions: RAPF

	Initial condition	Final condition
$r_d\ (m)$	500	1,000
$\nu\ (deg)$	98	262
Position (m)	[250.3559, -73.4146, 0]	[-518.7118, -146.8293, 0]
Velocity	[-36.4501, 0, 0]	[-72.9002, 0, 0]

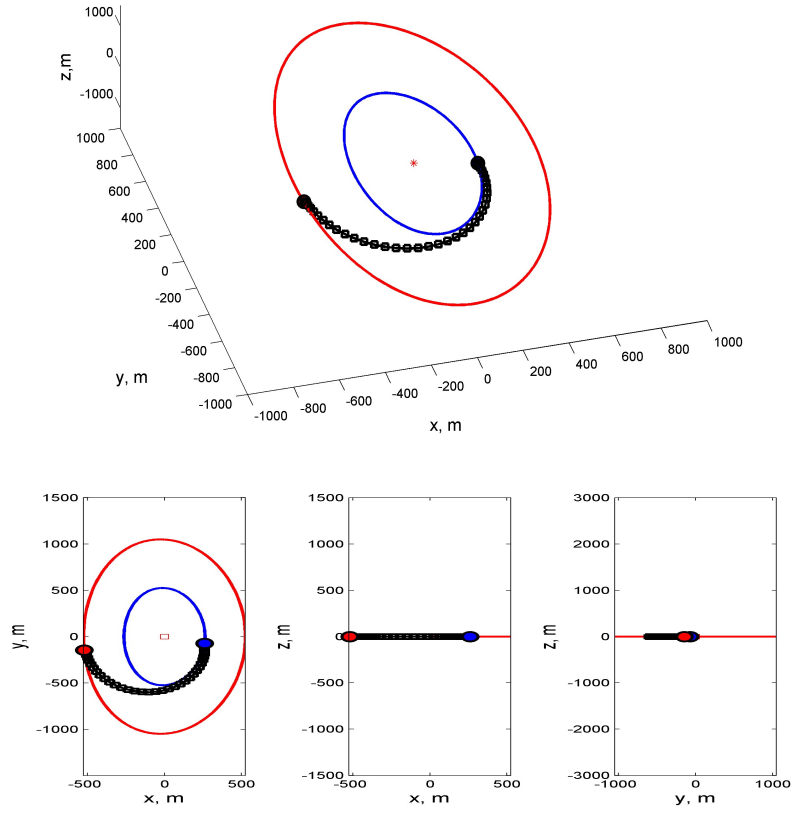

Figure 6.2: Trajectory of follower spacecraft in LVLH frame (J_1): RAPF

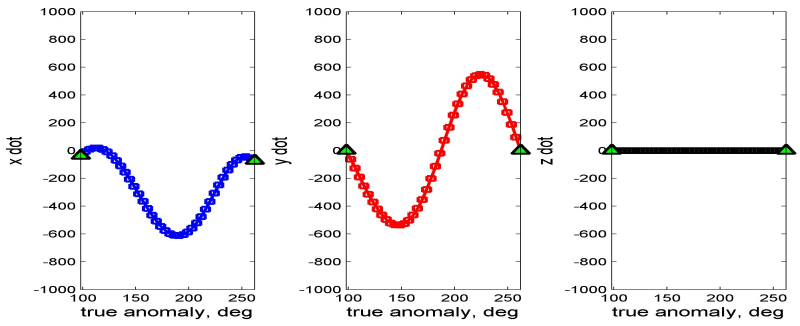

Figure 6.3: Relative velocity history of follower spacecraft (J_1): RAPF

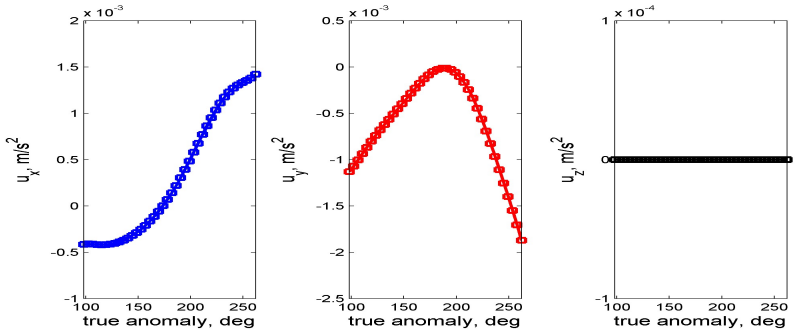

Figure 6.4: Control input history of follower spacecraft (J_1): RAPF

Figures 6.5–6.7 show the simulation results with the cost function J_2 for minimum fuel. Figure 6.5 shows the transfer trajectory of the follower spacecraft with respect to the leader spacecraft in the LVLH frame; the solid line denotes the trajectory of the follower spacecraft with different formation radii, $r_d = 500\,m$ and $r_d = 1,000\,m$, respectively, and the line with square shows the transfer trajectory of the follower spacecraft between two orbits. Figure 6.6 shows the velocity history of the follower spacecraft in the true anomaly domain during the maneuver. In Fig. 6.6, the triangle denotes specified relative velocities at the initial and final time in the LVLH frame, as presented in Table 6.1. Figure 6.7 shows the control input history of the follower spacecraft in the true anomaly domain. The transfer trajectory is placed on the $x - y$ plane as shown in Fig. 6.5, where satisfying the conditions for the initial and final relative positions given in Table 6.1. Moreover, the boundary conditions of the initial and final relative velocities are also satisfied as shown in Fig. 6.6. These results in Figs. 6.5 and 6.6 are similar to Figs. 6.2 and 6.3; however the control input history is different according to the cost function.

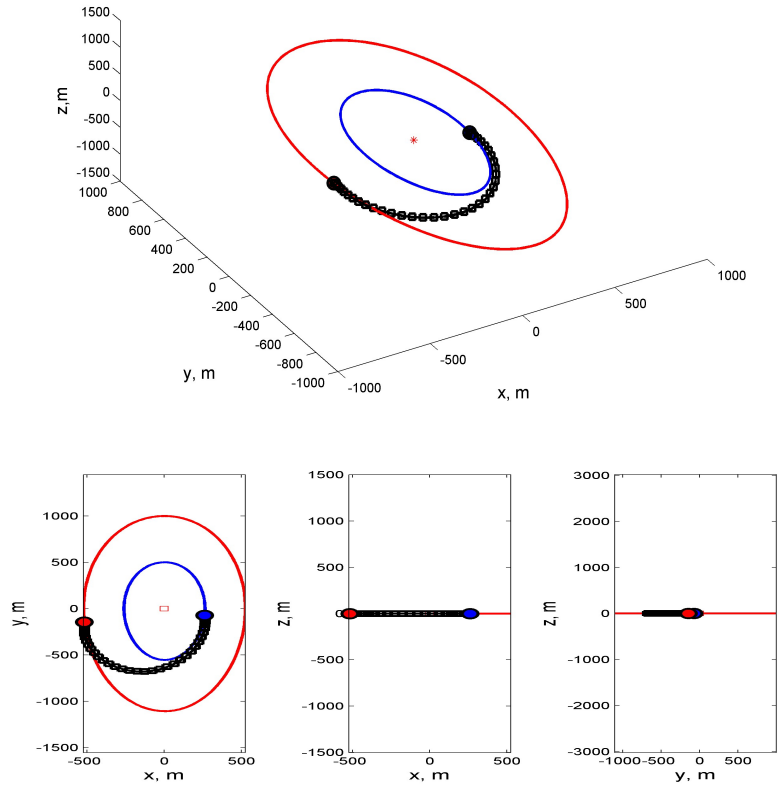

Figure 6.5: Trajectory of follower spacecraft in LVLH frame (J_2): RAPF

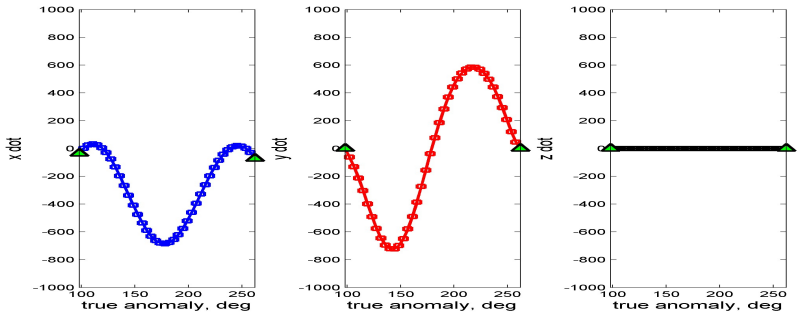

Figure 6.6: Relative velocity history of follower spacecraft (J_2): RAPF

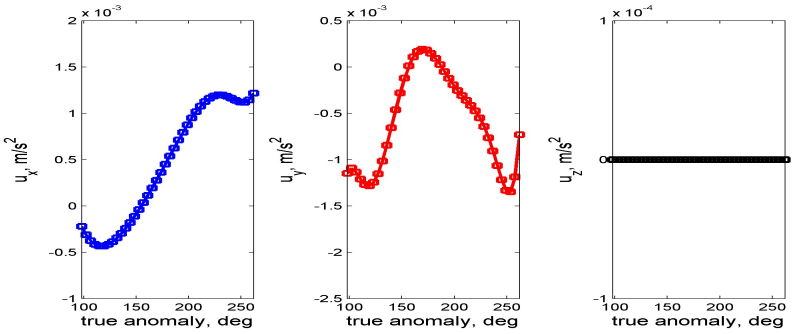

Figure 6.7: Control input history of follower spacecraft (J_2): RAPF

6.3.2 Impulsive Control Input

For the numerical simulation using the impulsive control input in the radial/along-track plane formation, the simulation conditions are same as in Section 6.3.1. Figures 6.8–6.10 show the simulation results for maneuvering in the radial/along-track plane formation. Figure 6.8 shows the trajectories of the leader and follower spacecraft in the ECI frame; the normal line denotes the trajectory of the leader spacecraft and the thick line shows the transfer trajectory of the follower spacecraft. As shown in Fig. 6.8, it is difficult to understand the relative motion of the follower spacecraft with respect to the leader spacecraft in the ECI frame. Instead, Fig. 6.9 shows the transfer trajectory of the follower spacecraft in the LVLH frame. As shown in Fig. 6.9, the follower spacecraft moves from the initial position to the final position on the $x-y$ plane in the LVLH frame. Figure 6.10 describes the relative velocity history of the follower spacecraft during the maneuver. In Fig. 6.10, the triangle denotes specified relative velocities at the initial and final time in the LVLH frame given in Table 6.1. As a result, the difference between the resulting velocity from the modified Lambert's problem and the specified velocity is equal to the required velocity change for the orbit transfer. Table 6.2 summarizes

the relative velocities of the follower spacecraft and the velocity change, ΔV, for the reconfiguration maneuver in the radial/along-track plane formation.

Compared with the results in Section 6.3.1, the obtained transfer trajectory using the two impulse control inputs is similar to the transfer trajectory using the continuous control input; however, the velocity history is different according to the control input type. In the continuous control input case, the resulting velocities at the initial and final time are same as the specified velocities as shown in Table 6.1. On the other hand, in the impulsive control input case, the velocity obtained from the modified Lambert's problem is different from the velocity determined by the periodicity condition. These differences at the initial and final time are compensated using the impulse input.

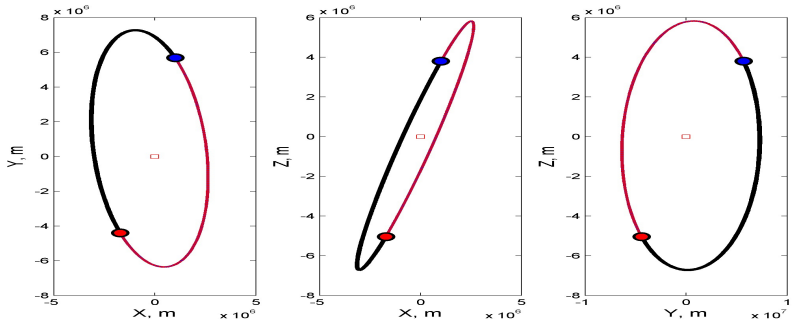

Figure 6.8: Trajectory of two spacecraft in ECI frame: RAPF

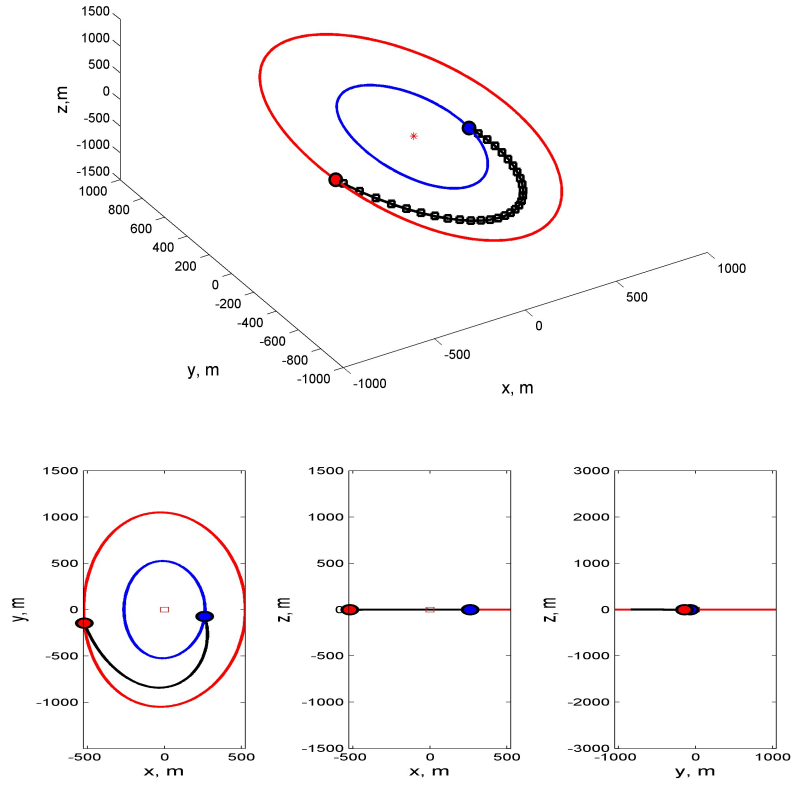

Figure 6.9: Trajectory of follower spacecraft in LVLH frame: RAPF

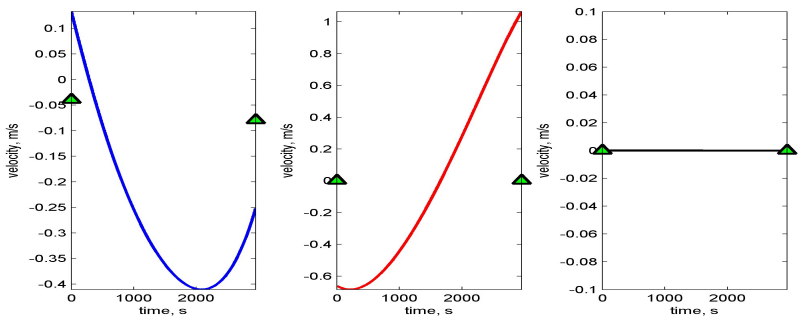

Figure 6.10: Velocity history of follower spacecraft: RAPF

Table 6.2: Solution of Lambert's problem: RAPF

	Initial value	Final value
Velocity (m/s)	[-0.0398, 0, 0]	[-0.0797, 0, 0]
V_t (m/s)	[0.1328, -0.6606, 0]	[-0.2523, 1.0638, 0]
ΔV	[0.1726, -0.6606, 0]	[0.1726, -1.0638, 0]
Total ΔV	[0.3453, 1.7244, 0]	norm: 1.7587

6.3.3 Global Minimum Velocity: Impulsive Control Input

To reduce the control effort for the impulsive control input type, it is necessary to find the transfer orbit minimizing the velocity change at the initial and final time. A set of the initial and final position vectors having minimum ΔV in the relative motion is studied to investigate the reduced energy input of the formation reconfiguration. The initial and final positions can be obtained for the global minimum velocity (GMV) in the radial/along-track plane formation through the grid search.

To search the global minimum velocity, the orbital elements of the leader spacecraft summarized in Table 3.1 are used. Figure 6.11 shows the results of the minimum velocity change with respect to the initial and final position vectors in the LVLH frame; the solid square denotes a set of initial and final positions having the minimum velocity at a given initial true anomaly. Figure 6.12 shows the location of the global minimum velocity; Fig. 6.12 (a) shows the final true anomaly which has the minimum velocity change according to the initial true anomaly, and Fig. 6.12 (b) shows the norm of minimum velocity, $||\Delta V||$, with respect to the initial true anomaly. The points containing global minimum velocity change can be found by the grid search described in Figs. 6.11 and 6.12. Table 6.3 summarizes the initial and final conditions with global minimum change in velocity.

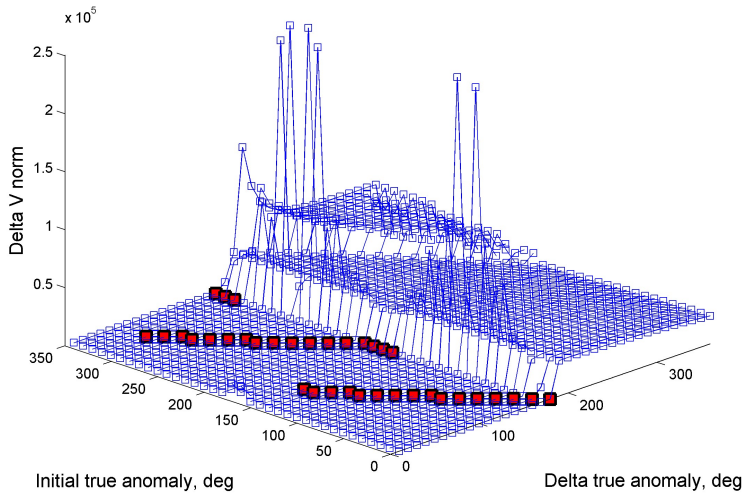

Figure 6.11: Velocity change according to initial and final positions: RAPF

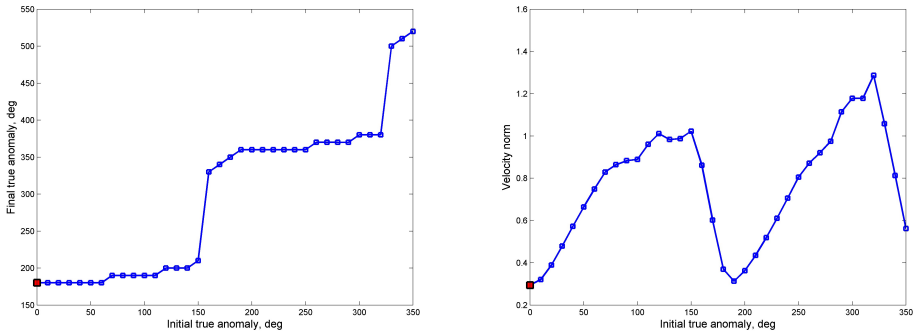

(a) (b)

Figure 6.12: Location of global minimum velocity: RAPF

Table 6.3: Initial and final conditions: RAPF-GMV

	Initial condition	Final condition
r_d (m)	500	1000
ν (deg)	0	180
Position (m)	[0, -500, 0]	[0, -1105.8, 0]

Figures 6.13 and 6.14 show the simulation results for maneuvering in the radial/along-track plane formation using the initial and final conditions given in Table 6.3. Figure 6.13 shows the transfer trajectory of the follower spacecraft with respect to the leader spacecraft in the LVLH frame. As shown in Fig. 6.13, the follower spacecraft moves on the $x - y$ plane for resizing the formation. Figure 6.14 shows the velocity history of the follower spacecraft during the maneuver. In Fig. 6.14, the triangle denotes specified velocities at the initial and final time in the LVLH frame, which are obtained from the periodicity condition in Chapter 4. As a result, the desired velocity change can be achieved by the impulse control input to compensate the difference between the resulting velocity from the modified Lambert's problem and the specified velocity. Table 6.4 summarizes the velocities of the follower spacecraft and ΔV for the maneuver in the radial/along-track plane formation, and Table 6.5 summarizes the orbital elements of the transfer orbit between two orbits. As shown in Tables 6.2 and 6.4, the total velocity change is reduced from 1.7587 to 0.2943 for resizing the formation radius in the radial/along-track plane formation by the global minimum velocity approach.

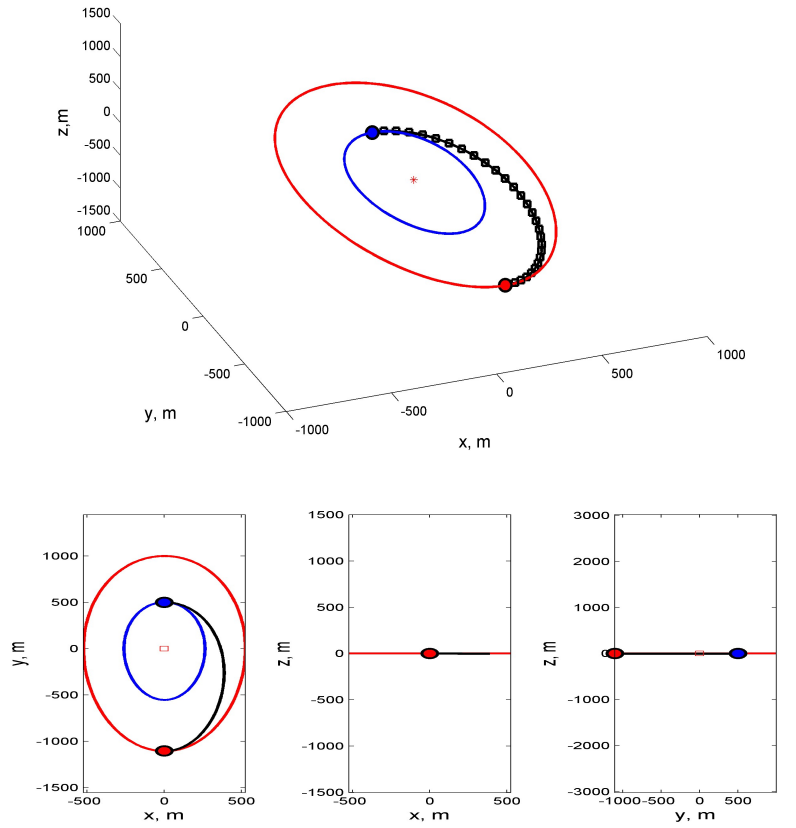

Figure 6.13: Trajectory of follower spacecraft in LVLH frame: RAPF-GMV

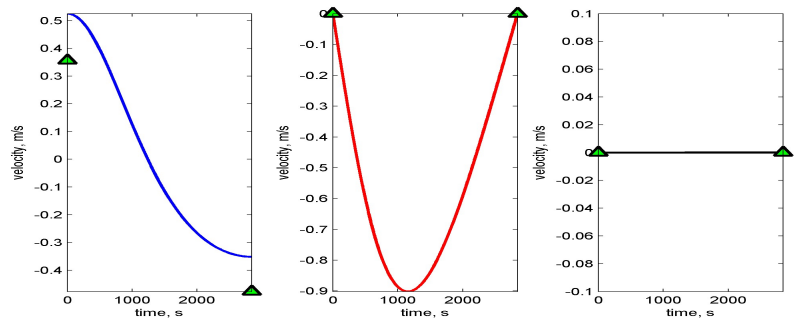

Figure 6.14: Velocity history of follower spacecraft: RAPF-GMV

Table 6.4: Solution of Lambert's problem: RAPF-GMV

	Initial value	Final value
Velocity (m/s)	[0.3561, 0, 0]	[-0.4768, 0, 0]
V_t (m/s)	[0.5252, 0, 0]	[-0.3516, -0.0001, 0]
ΔV	[0.1691, 0, 0]	[-0.1252, 0.0001, 0]
Total ΔV	[0.2943, 0.0001, 0]	norm: 0.2943

Table 6.5: Orbital elements of transfer orbit: RAPF-GMV

Parameter	Value
a (m)	6.8781×10^6
e	0.1
i (deg)	66.0100
Ω (deg)	277
ω (deg)	44.9653

6.3.4 Analysis of Numerical Simulation Results

In this section, the simulation results to change the formation radius in the radial/along-track plane formation are analyzed with respect to the control input type. The simulation results are investigated in terms of (i) velocity change, ΔV, and mass change, Δm according to the control input type, (ii) difference of the orbital elements between the transfer orbit and the reference orbit, and (iii) the global minimum velocity change with respect to the eccentricity of the reference orbit.

First, let us compare the simulation results in terms of ΔV and Δm of two control input types presented in Sections 6.3.1 and 6.3.2. In the numerical simulation, the specific impulse, I_{sp}, is considered according to the control input type: for the continuous control input, $I_{sp} = 3,000\,(s)$, and for the impulsive control input, $I_{sp} = 300\,(s)$ [115, 116, 117, 118]. Table 6.6 summarizes ΔV and Δm with respect to the control input type for changing the formation radius in the radial/along-track plane formation. As shown in Table 6.6, ΔV

Table 6.6: ΔV and Δm for formation reconfiguration: RAPF

	$\Delta V\ (m/s)$	$\Delta m\ (kg)$
Continuous control (J_1)	3.5828	0.0061
Continuous control (J_2)	3.9901	0.0068
Impulsive control	1.7587	0.0299

Table 6.7: ΔV and Δm for formation reconfiguration: RAPF-GMV

	$\Delta V\ (m/s)$	$\Delta m\ (kg)$
Continuous control (J_1)	0.3723	0.0006
Continuous control (J_2)	0.4022	0.0007
Impulsive control	0.2943	0.0050

of the impulsive control input is smaller than that of the continuous control input for changing the formation radius; however, the continuous control input consumes less fuel than the impulsive control input.

Table 6.7 summarizes ΔV and Δm according to control input type with the initial and final conditions given in Table 6.3, which has minimum velocity change for changing the formation radius using the impulsive control input. As shown in Table 6.7, ΔV of the continuous control input as well as the impulsive control input is much smaller compared with ΔV given in Table 6.6. Moreover, the continuous control input has less fuel consumption, Δm, than the impulsive control input, while the impulsive control input has less ΔV compared with the result of the continuous control input.

Next, let us compare the results of the impulsive control input presented in Sections 6.3.2 and 6.3.3; the transfer orbit is generated where the initial and final positions are arbitrarily chosen in Section 6.3.2, and the transfer orbit is designed with a set of the initial and final positions having the global minimum velocity in Section 6.3.3. By comparing with the orbital elements of the leader spacecraft in Table 3.1, it is seen that the transfer orbits of two approaches have almost same orbital elements; however, some orbital elements are different. Table 6.8 summarizes the the differences of the orbital elements:

Table 6.8: Difference of orbital elements: RAPF

Parameter	RAPF	RAPF-GMV
$\Delta a \quad (m)$	122.6358	-0.0163
Δe	-2.4367×10^{-5}	-1.8473×10^{-8}
$\Delta i \quad (deg)$	0	0
$\Delta\Omega \quad (deg)$	0	0
$\Delta\omega \quad (deg)$	0.0330	0.0347

(i) between the reference orbit and the transfer orbit of the radial/along-track plane formation as described in Sections 6.3.2, and (ii) between the reference orbit and the transfer orbit with global minimum velocity of the radial/along-track plane formation in Section 6.3.3. These results show the characteristic of the maneuver problem of the relative motion in the radial/along-tack plane formation. As shown in Table 6.8, the transfer between two orbits in the radial/along-track plane formation produces the difference in the orbital elements including a semi-major a, an eccentricity e, and an augment of perigee ω, which means that the orbit transfer in the radial/along-track plane formation belongs to the coplanar maneuver.

On the other hand, as shown in Table 6.8, the orbital transfer with the initial and final positions containing global minimum velocity has smaller difference in the orbital elements than one with arbitrary initial and final positions; specifically, the semi-major axis is a critical factor that relates to the orbital energy. Compared with the results of Section 6.3.2, Δa reduces from 122.6358 to 0.0163 m, when the initial and final positions are selected to have the global minimum velocity. This leads to the reduction of the total velocity change for the formation reconfiguration in the radial/along-track plane formation. In addition, the difference of the eccentricity in the global minimum velocity case is smaller than that in arbitrary case. Therefore, it can be stated that the smaller difference of the orbital elements between the reference orbit and transfer orbit generates the minimum velocity change for the formation reconfiguration.

Figure 6.15 shows the minimum velocity change according to the initial and final points with respect to the eccentricity of reference orbit; the solid square denotes a set of initial and final positions having the global minimum velocity change. As shown in Fig. 6.15, when the transfer angle is less than 180°, the follower spacecraft requires less ΔV; however, the velocity change for resizing

the formation radius is significantly increased when the transfer angle is larger than 180°. Therefore, the follower spacecraft should have the transfer angle less than 180° to save the fuel consumption for the formation reconfiguration in the radial/along-track plane formation. Table 6.9 summarize two sets of the initial and final true anomalies having the minimum velocity change according to the eccentricity of the reference orbit. As show in Table 6.9, the minimum ΔV is increased from 0.2769 to 0.5112 as the eccentricity becomes from 0.001 to 0.5. It means that the follower spacecraft spends more fuel for changing the formation radius in the radial/along-track plane formation as the eccentricity of the reference orbit is increased. Moreover, it is observed that the initial and final true anomalies having the global minimum velocity change are identical, $\nu_0 = 0°$ (perigee) and $\nu_f = 180°$ (apogee), regardless of the eccentricity of the reference orbit. In addition, the initial and final true anomalies are $\nu_0 = 190°$ and $\nu_f = 360°$ which have the second smallest velocity change with respect to the eccentricity. These results show that the maneuver, which begins near perigee or apogee and has the transfer angle of $170 \sim 180°$, can reduce the velocity change in elliptic orbits for changing the formation radius in the radial/along-track plane formation.

Table 6.9: Initial and final points having minimum velocity change: RAPF

	e	0.001	0.01	0.1	0.3	0.5
Set 1	ν_0 (deg)	0	0	0	0	0
	ν_f (deg)	180	180	180	180	180
	ΔV (m/s)	0.2769	0.2781	0.2943	0.3603	0.5112
Set 2	ν_0 (deg)	190	190	190	190	190
	ν_f (deg)	360	360	360	360	360
	ΔV (m/s)	0.2978	0.2988	0.3127	0.3756	0.5262

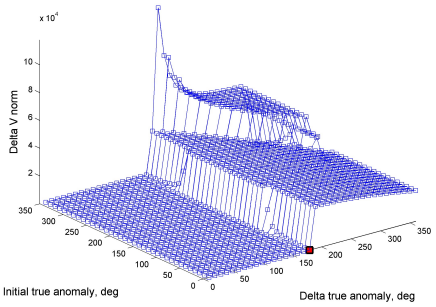

(a) $e = 0.001$

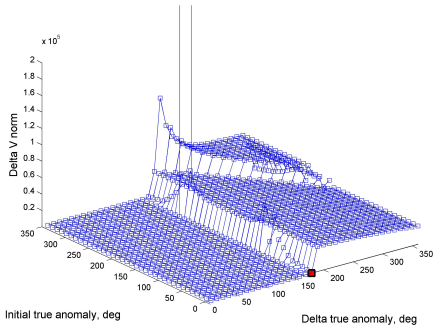

(b) $e = 0.01$

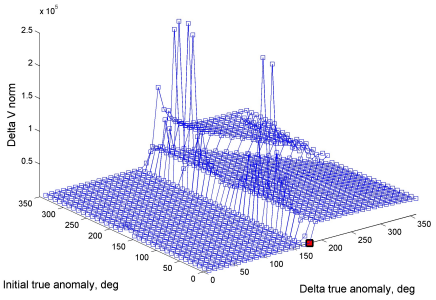

(c) $e = 0.1$

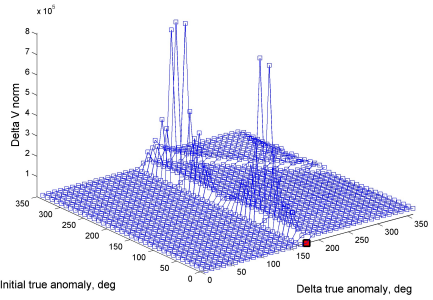

(d) $e = 0.3$

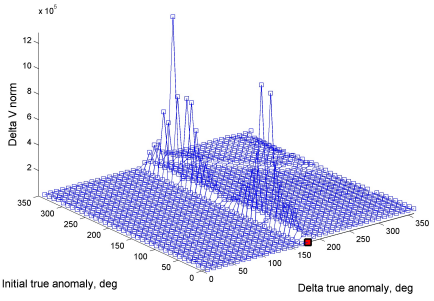

(e) $e = 0.5$

Figure 6.15: Velocity change with respect to eccentricity: RAPF

6.4 Along-Track/Cross-Track Plane Formation

In this section, the maneuver for the formation reconfiguration in the along-track/cross-track plane formation (ACPF) is performed using two control input types: continuous and impulsive control inputs. The considered orbital elements of the leader spacecraft are summarized in Table 6.10. Similar to the simulation in Section 6.3, the follower spacecraft changes the formation radius from 500 m to 1,000 m in the along-track/cross-track plane formation. The initial and final conditions are given by the formation geometry as described in Chapter 4.

In Section 6.4.1, the optimal trajectory using the continuous control input is illustrated using the Gauss pseudospectral method with the relative position and velocity vectors at the initial and final configuration, which method is described in Section 5.3. In Section 6.4.2, the transfer orbit trajectory using the impulsive control input is shown based on the modified Lambert's problem presented in Section 5.4, where the initial and final position vectors and the flight time are specified. In addition, in Section 6.4.3, a set of initial and final positions is described, which contains the global minimum velocity change for the impulsive control input in the along-track/cross-track plane formation. The simulation results are analyzed in Section 6.4.4.

Table 6.10: Orbital elements of leader spacecraft: ACPF

Parameter	Value
$a \quad (m)$	6.8781×10^6
e	0.01
$i \quad (deg)$	66.01
$\Omega \quad (deg)$	277
$\omega \quad (deg)$	45

6.4.1 Continuous Control Input

The initial and final conditions of the follower spacecraft in the LVLH frame are summarized in Table 6.11. For the continuous control input type, two cost functions as J_1 and J_2 in Eqs. (5.3) and (5.4) are considered.

Figures 6.16–6.18 show the simulation results with the cost function J_1 for minimum energy. Figure 6.16 shows the transfer trajectory of the follower spacecraft with respect to the leader spacecraft in the LVLH frame; the solid line denotes the trajectory of the follower spacecraft with different formation radii, $r_d = 500\,m$ and $r_d = 1,000\,m$, and the line with square shows the transfer trajectory of the follower spacecraft between two orbits. Figure 6.17 shows the velocity history of the follower spacecraft during the maneuver. In Fig. 6.17, the triangle denotes specified relative velocities at the initial and final time in the LVLH frame, as presented in Table 6.11. Figure 6.18 shows the control input history of the follower spacecraft in the true anomaly domain during the maneuver. As shown in Figs. 6.16 and 6.17, the boundary conditions at the initial and final time are satisfied, and the transfer trajectory is placed near the $y - z$ plane by the continuous control input presented in Fig. 6.18.

Table 6.11: Initial and final conditions: ACPF

	Initial condition	Final condition
$r_d\ (m)$	500	1,000
$\nu\ (deg)$	95	265
Position (m)	[250.2877,-43.8138,501.0121]	[-500.5754, -87.6276, -1002.0]
Velocity	[-21.8973, 0, -38.8375]	[-43.7947, 0, -77.6749]

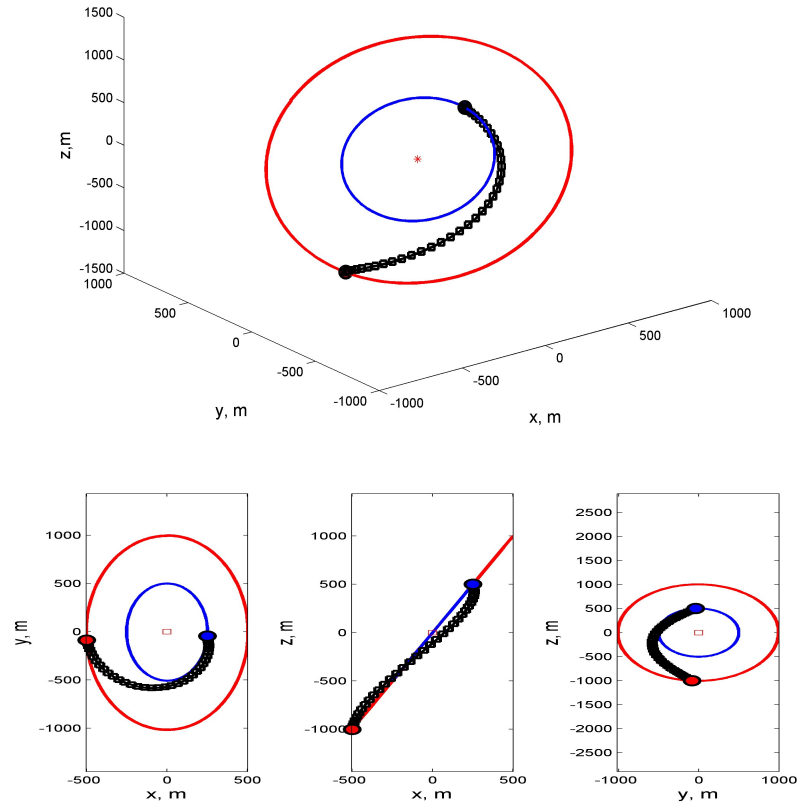

Figure 6.16: Trajectory of follower spacecraft in LVLH frame (J_1): ACPF

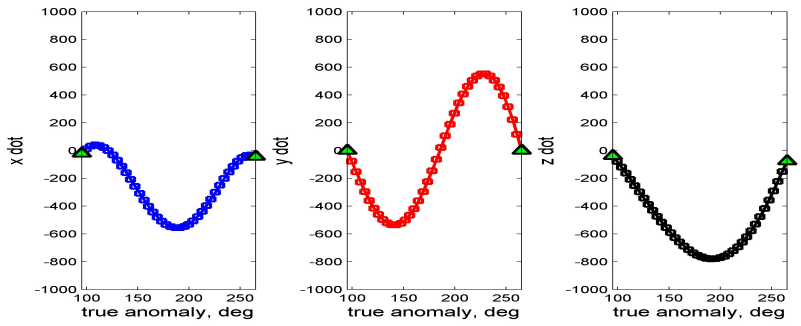

Figure 6.17: Relative velocity history of follower spacecraft (J_1): ACPF

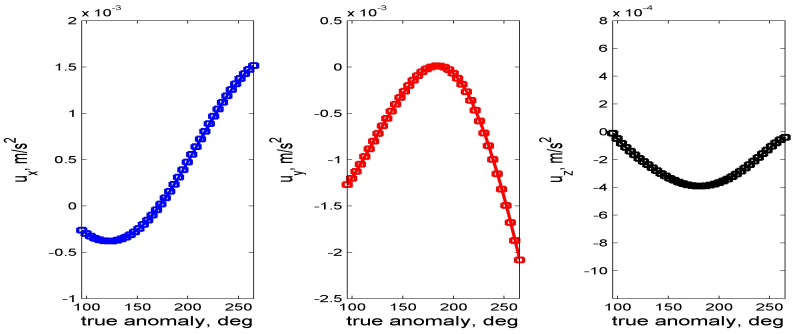

Figure 6.18: Control input history of follower spacecraft (J_1): ACPF

Figures 6.19–6.21 show the simulation results with the cost function J_2 for minimum fuel. Figure 6.19 shows the transfer trajectory of the follower spacecraft with respect to the leader spacecraft in the LVLH frame; the solid line denotes the trajectory of the follower spacecraft with different formation radii, $r_d = 500\,m$ and $r_d = 1,000\,m$, and the line with square shows the transfer trajectory of the follower spacecraft between two orbits. Figure 6.20 shows the velocity history of the follower spacecraft during the maneuver. In Fig. 6.20, the triangle denotes specified relative velocities at the initial and final time in the LVLH frame, as presented in Table 6.11. Figure 6.21 shows the control input history of the follower spacecraft in the true anomaly domain during the maneuver. The boundary conditions of the positions and relative velocities are satisfied at initial and final time, as shown in Figs. 6.19, and 6.20. Moreover, it can be observed in Figs. 6.16 and 6.19 that the transfer trajectory of J_1 is similar with the result of J_2; however, the control input history is different according to the cost function.

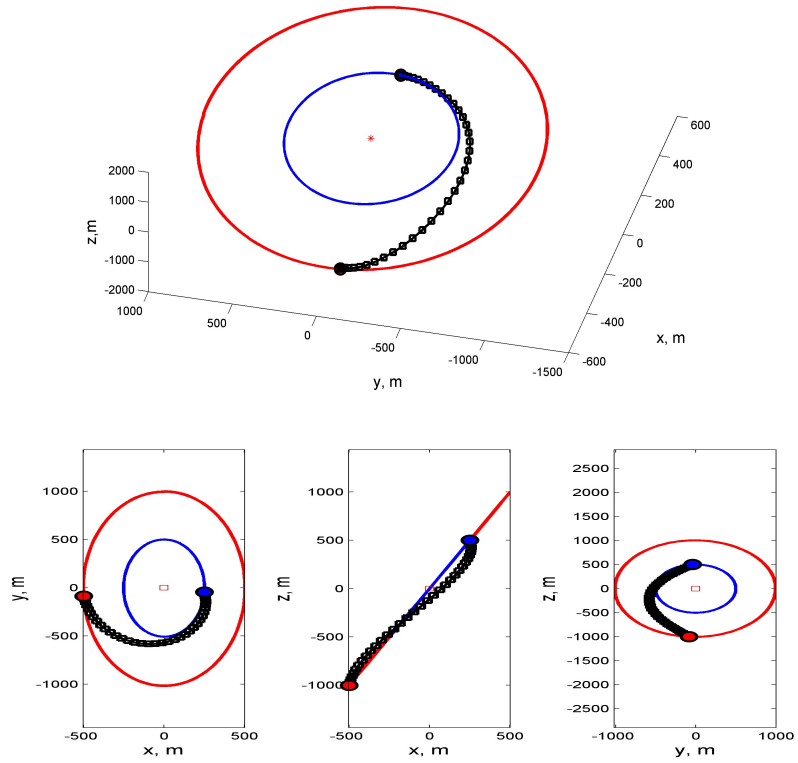

Figure 6.19: Trajectory of follower spacecraft in LVLH frame (J_2): ACPF

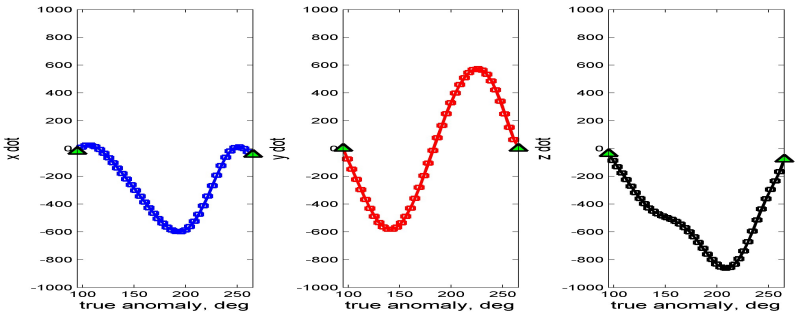

Figure 6.20: Relative velocity history of follower spacecraft (J_2): ACPF

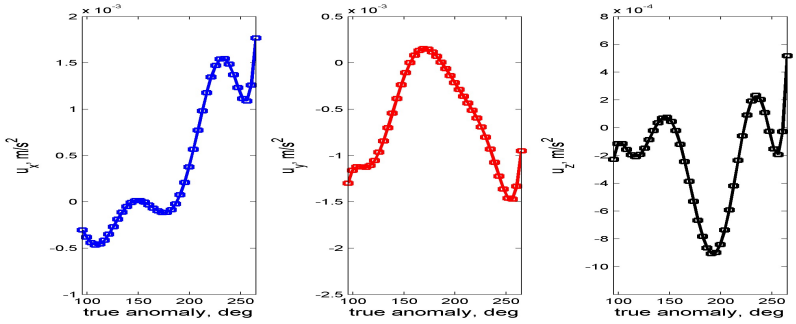

Figure 6.21: Control input history of follower spacecraft (J_2): ACPF

6.4.2 Impulsive Control Input

For the formation reconfiguration in the along-track/cross-track plane formation using the impulsive control input, the simulation conditions are same as in Section 6.4.1. Figures 6.22–6.24 show the simulation results for formation reconfiguration using the impulsive control input in the along-track/cross-track plane formation. Figure 6.22 shows trajectories of the leader and follower spacecraft in the ECI frame; the normal line denotes the trajectory of the leader spacecraft and the thick line shows the transfer trajectory of the follower spacecraft. Figure 6.23 shows the transfer trajectory of the follower spacecraft with respect to the leader spacecraft in the LVLH frame. Figure 6.24 shows the velocity history of the follower spacecraft during the maneuver. In Fig. 6.24, the triangle denotes specified velocities at the initial and final time in the LVLH frame given in Table 6.11. Therefore, the required velocity change can be obtained by computing the difference between the resulting velocity from the modified Lambert's problem and the specified velocity. Table 6.12 summarizes the velocities of the follower spacecraft and ΔV for the maneuver in the along-track/cross-track plane formation.

Compared with the results in Section 6.4.1, the obtained transfer trajectory in Fig. 6.23 strays away from the formation plane, while the trajectories in Figs. 6.16 and 6.19 almost place on near formation plane. Moreover, the resulting velocities at the initial and final time as shown in Figs. 6.17 and 6.20 are same as the specified velocities as shown in Table 6.11; however, the velocity obtained from the modified Lambert's problem as shown in Fig. 6.24 is different from the velocity determined by the periodicity condition. Therefore, these differences are compensated using the impulse input at the initial and final time.

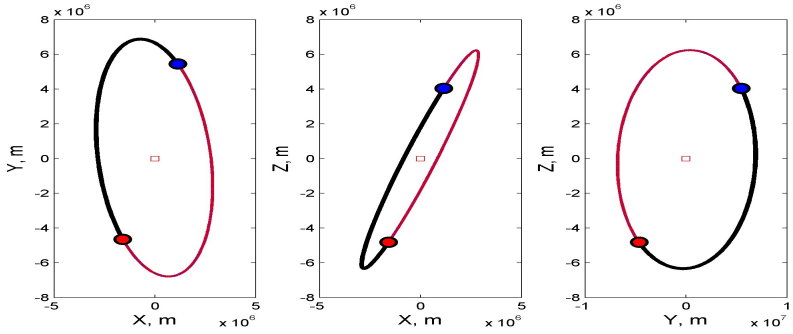

Figure 6.22: Trajectory of two spacecraft in ECI frame: ACPF

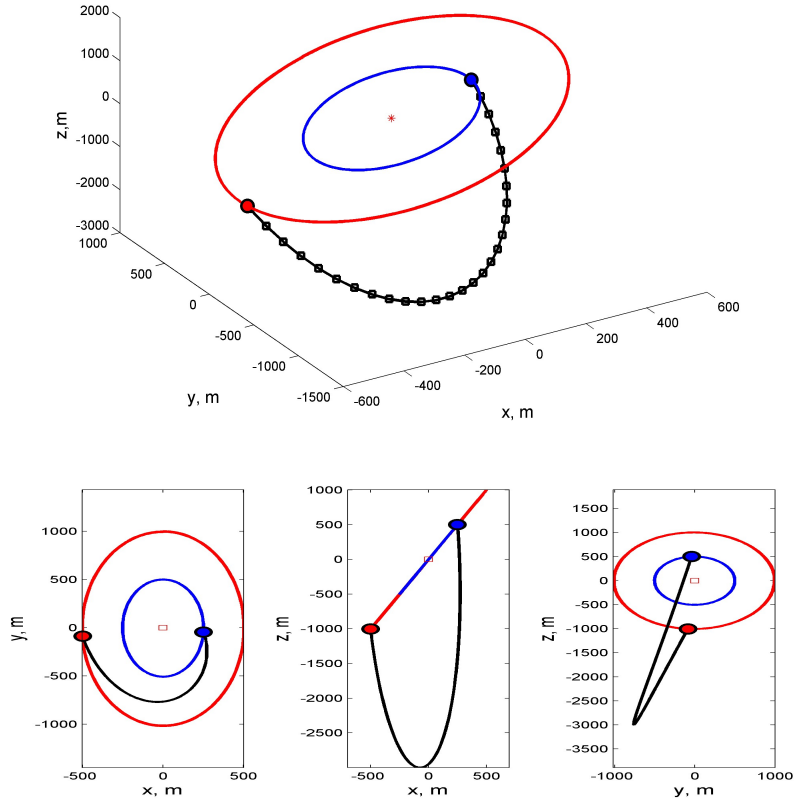

Figure 6.23: Trajectory of follower spacecraft in LVLH frame: ACPF

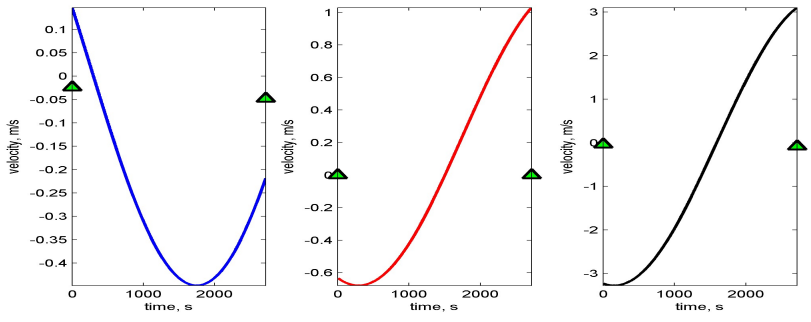

Figure 6.24: Velocity history of follower spacecraft: ACPF

Table 6.12: Solution of Lambert's problem: ACPF

	Initial value	Final value
Velocity (m/s)	[-0.0242, 0, -0.0429]	[-0.0484, 0, -0.0858]
V_t (m/s)	[0.1468, -0.6316, -3.2316]	[-0.2187, 1.0294, 3.1032]
ΔV	[0.1710, -0.6316, -3.1887]	[0.1703, -1.0294, -3.1891]
Total ΔV	[0.3412, 1.6610, 6.3778]	norm: 6.5994

6.4.3 Global Minimum Velocity: Impulsive Control Input

To reduce the control effort for the impulsive control input, it is necessary to find the transfer orbit minimizing the velocity changes at the initial and final time. A set of initial and final position vectors having minimum ΔV for transfer in the relative motion is studied to investigate the reduced energy input for the formation reconfiguration. The initial and final positions can be obtained through the grid search, which have the global minimum velocity in the along-track/cross plane formation.

The orbital elements of the leader spacecraft described in Table. 6.10 are used, and the follower spacecraft moves from 500 m radius to 1,000 m radius in the along-track/cross-track plane formation. Figure 6.25 shows the results of the minimum velocity change with respect to the initial and final position vectors in the LVLH frame; the solid square denotes the final true anomaly having the minimum velocity at a given initial true anomaly. Figure 6.26 shows the location of global minimum velocity; Fig. 6.26 (a) shows the final true anomaly which has minimum change in velocity according to the initial true anomaly, and Fig. 6.26 (b) shows the norm of minimum velocity, $||\Delta V||$, with respect to the initial true anomaly. Table 6.13 summarizes the initial and final conditions with global minimum change in velocity for maneuvering in the along-track/cross-track plane formation.

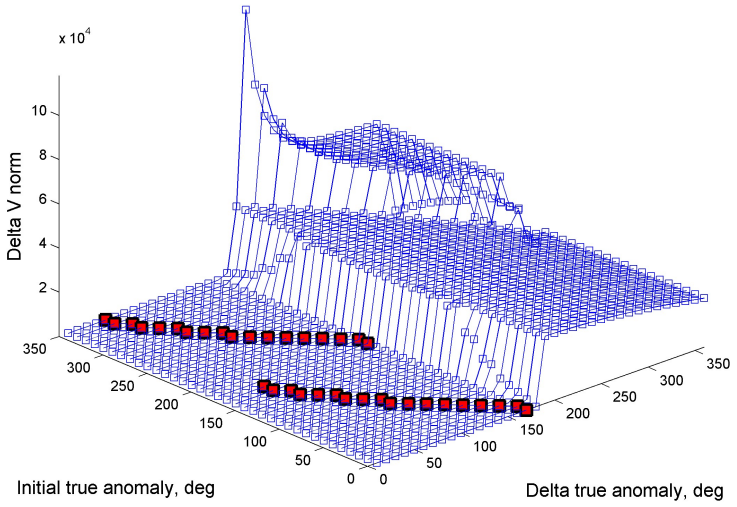

Figure 6.25: Velocity change according to initial and final positions: ACPF

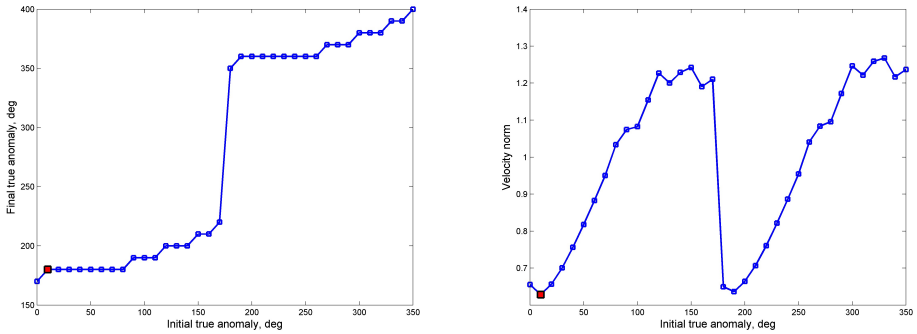

(a) (b)

Figure 6.26: Location of global minimum velocity: ACPF

Table 6.13: Initial and final conditions: ACPF-GMV

	Initial condition	Final condition
r_d (m)	500	1000
ν (deg)	10	180
Position (m)	[43.6280, 492.4407, 86.4051]	[0, -1010.1, 0]

Figures 6.27 and 6.28 show the simulation results for maneuvering in the along-track/cross-track plane formation using the initial and final conditions given in Table 6.13. Figure 6.27 shows the transfer trajectory of the follower spacecraft with respect to the leader spacecraft in the LVLH frame. As shown in Fig. 6.27, the follower spacecraft moves on near formation plane for resizing the formation, while the transfer trajectory deviates from the formation plane as shown in Fig. 6.23. Figure 6.28 shows the velocity history of the follower spacecraft during the maneuver. In Fig. 6.28, the triangle denotes specified velocities at the initial and final time in the LVLH frame, which are obtained from the periodicity condition in Chapter 4. Therefore, the difference between resulting velocity from the modified Lambert's problem and the specified velocity is equal to the required velocity change. Table 6.14 summarizes the velocities of the follower spacecraft and ΔV for the maneuver in the along-track/cross-track plane formation, and Table 6.15 summarizes the orbital elements of the transfer orbit between two orbits in the relative motion. As shown in Tables 6.12 and 6.14, the total velocity change is reduced from 6.5994 to 0.6281 for resizing the formation radius in the along-track/cross-track plane formation by the global minimum velocity approach.

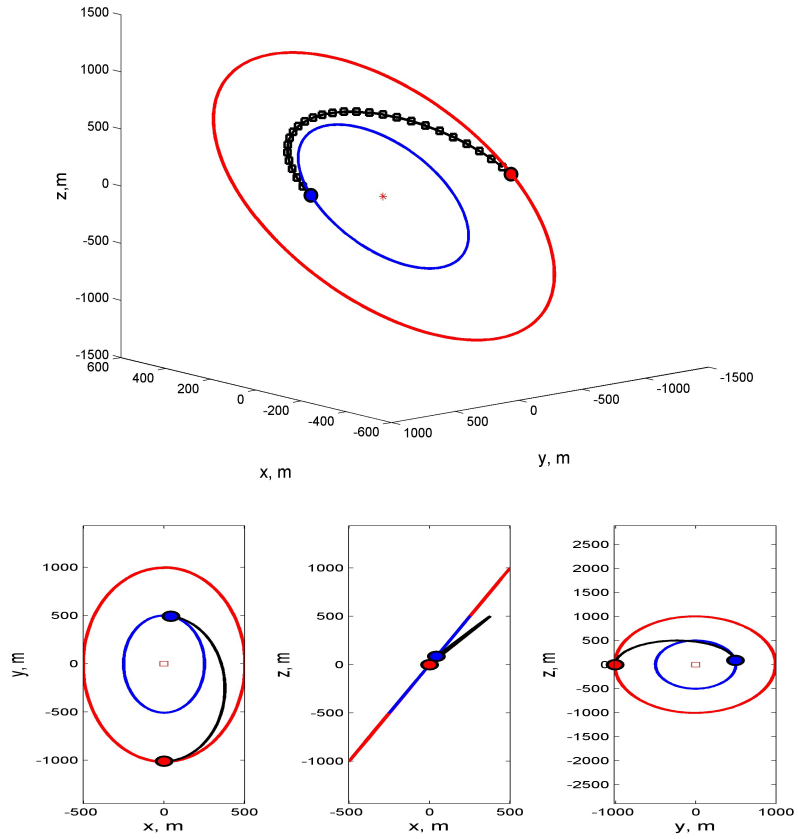

Figure 6.27: Trajectory of follower spacecraft in LVLH frame: ACPF-GMV

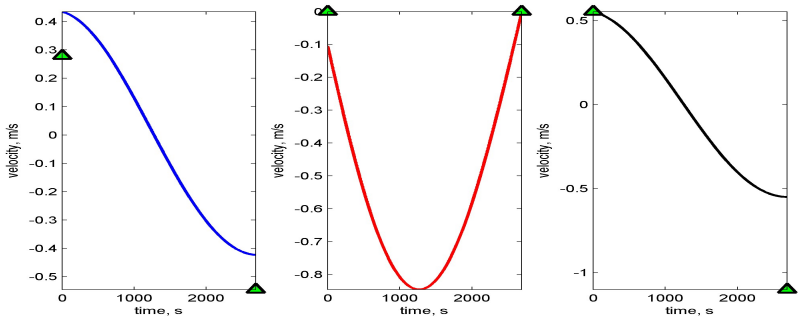

Figure 6.28: Velocity history of follower spacecraft: ACPF-GMV

Table 6.14: Solution of Lambert's problem: ACPF-GMV

	Initial value	Final value
Velocity (m/s)	[0.2793, 0, 0.5534]	[-0.5452, 0, -1.1014]
V_t (m/s)	[0.4353, -0.1045, 0.5527]	[-0.4231, -0.0069, -0.5500]
ΔV	[0.1560, -0.1045, -0.0007]	[-0.1221, 0.0069, -0.5514]
Total ΔV	[0.2781, 0.1113, 0.5521]	norm: 0.6281

Table 6.15: Orbital elements of transfer orbit: ACPF-GMV

Parameter	Value
$a \quad (m)$	6.8781×10^6
e	0.01
$i \quad (deg)$	66.0130
$\Omega \quad (deg)$	277.0032
$\omega \quad (deg)$	44.6720

6.4.4 Analysis of Numerical Simulation Results

In this section, the simulation results for the formation reconfiguration in the along-track/cross-track plane formation are analyzed. The simulation results are investigated in terms of (i) velocity change, ΔV, and mass change, Δm according to the control input type, (ii) difference of the orbital elements between the transfer orbit and the reference orbit, and (iii) the global minimum velocity change with respect to the eccentricity of the reference orbit.

At first, let us compare the simulation results in terms of ΔV and Δm of two control input types presented in Sections 6.4.1 and 6.4.2. Table 6.16 summarizes ΔV and Δm according to control input type. As shown in Table 6.16, for changing the formation radius in the along-track/cross-track plane formation, ΔV of the continuous control input is smaller than that of the impulsive control input. Also, the continuous control input consumes less fuel than the impulsive control input.

Table 6.16: ΔV and Δm for formation reconfiguration: ACPF

	ΔV (m/s)	Δm (kg)
Continuous control (J_1)	4.5366	0.0077
Continuous control (J_2)	4.8624	0.0083
Impulsive control	6.5994	0.1122

Table 6.17: ΔV and Δm for formation reconfiguration: ACPF-GMV

	ΔV (m/s)	Δm (kg)
Continuous control (J_1)	0.8595	0.0015
Continuous control (J_2)	1.1043	0.0019
Impulsive control	0.6281	0.0107

Table 6.17 summarizes ΔV and Δm according to control input type with the initial and final conditions given in Table 6.13, which has the minimum velocity change for changing the formation radius using the impulsive control input. As shown in Table 6.17, ΔV of the continuous control input as well as the impulsive control input is much smaller compared with ΔV given in Table 6.16. In addition, the impulsive control input has less ΔV compared with the result of the continuous control input; however, the continuous control input has less fuel consumption, Δm, than the impulsive control input.

Next, let us compare the results of the impulsive control input presented in Sections 6.4.2 and 6.4.3; the transfer orbit is generated where the initial and final positions are arbitrarily chosen in Section 6.4.2, and the transfer orbit is designed with a set of the initial and final positions having the global minimum velocity in Section 6.4.3. By comparing with the orbital elements of the leader spacecraft in Table 6.10, the transfer orbits of two approaches have almost same orbital elements; however, some orbital elements are different. Table 6.18 summarizes the difference of the orbital elements: (i) between the reference orbit and the transfer orbit of the along-track/cross-track plane formation as described in Section 6.4.2, and (ii) between the reference orbit and the transfer orbit with global minimum velocity of the along-track/cross-

Table 6.18: Difference of orbital elements: ACPF

Parameter	ACPF	ACPF: GMV
$\Delta a \quad (m)$	136.3179	12.0619
Δe	-2.4157×10^{-5}	-1.9394×10^{-6}
$\Delta i \quad (deg)$	-0.0214	-0.0030
$\Delta\Omega \quad (deg)$	0.0137	-0.0032
$\Delta\omega \quad (deg)$	0.3076	0.3280

track plane formation in Section 6.4.3. These results show the characteristic of the maneuver problem of the relative motion in the along-track/cross-track plane formation. As shown in Table 6.18, in the along-track/cross-track plane formation, not only a, e, and ω, but also inclination i and longitude of the ascending node Ω are changed during the maneuver. Note that only a, e, and ω are changed in the radial/along-track plane formation. It means that the orbit transfer in the along-track/cross-track plane formation is related to the combined maneuver of coplanar and non-coplanar maneuver.

On the other hand, as shown in Table 6.18, the orbital transfer with the initial and final positions containing global minimum velocity has smaller difference in the orbital elements than one with arbitrary initial and final positions; specifically, the semi-major axis is a critical factor that relates to the orbital energy. Compared with the results of Section 6.4.2, Δa reduces from 136.3179 to 12.0619 m, when the initial and final positions are chosen to have the global minimum velocity. This result produces the reduction of the total velocity change for the formation reconfiguration in the along-track/cross-track plane formation. Moreover, the difference of the eccentricity in the global minimum velocity case is smaller than that in arbitrary case, and Δi and $\Delta\Omega$ decrease from 0.0214° to 0.0030°, and from 0.0137° to 0.0032°, respectively. Therefore, it can be stated that the results of global minimum velocity by the grid search provide the small difference of the orbital elements, and it reduces the control effort during the maneuver in the along-track/cross-track plane formation.

Figure 6.29 shows the minimum velocity change according to the initial and final points with respect to the eccentricity of the reference orbit; the solid square denotes a set of initial and final positions having the global minimum velocity change. Similar to the radial/along-track plane formation, the follower spacecraft requires less ΔV when the transfer angle is less than 180°, as shown in Fig. 6.29; the velocity change for resizing the formation radius

is significantly increased when the transfer angle is larger than 180°. Therefore, the follower spacecraft should have the transfer angle less than 180° to reduce the fuel consumption for the formation reconfiguration in the along-track/cross-track plane formation. Table 6.19 summarize two sets of the initial and final true anomalies having the minimum velocity change according to the eccentricity of the reference orbit. As show in Table 6.19, the minimum ΔV is increased as the eccentricity become large to 0.5. It means that the follower spacecraft consumes more fuel for changing the formation radius in the along-track/cross-track plane formation as the eccentricity of the reference orbit is increased. Moreover, it is observed that the initial and final true anomalies having the global minimum velocity change are equal to $\nu_0 = 10°$ and $\nu_f = 180°$, and the initial true anomaly is near apogee and the final true anomaly is near perigee in the set having the second smallest velocity change, when the eccentricity is larger than 0.001. Therefore, when the follower spacecraft starts near perigee or apogee and has the transfer angle of 170°, the velocity change can be reduced for changing the formation radius in the along-track/cross-track plane formation.

Table 6.19: Initial and final points having minimum velocity change: ACPF

	e	0.001	0.01	0.1	0.3	0.5
Set 1	ν_0 (deg)	190	10	10	10	10
	ν_f (deg)	360	180	180	180	180
	ΔV (m/s)	0.6292	0.6281	0.6207	0.6501	0.7935
Set 2	ν_0 (deg)	10	190	180	180	180
	ν_f (deg)	180	360	350	350	350
	ΔV (m/s)	0.6294	0.6363	0.6485	0.7044	0.9148

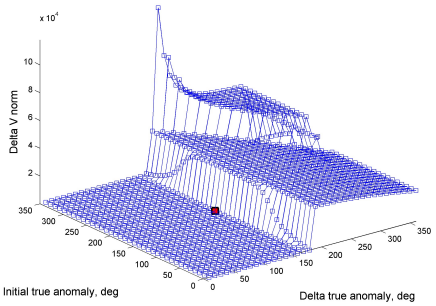

(a) $e = 0.001$

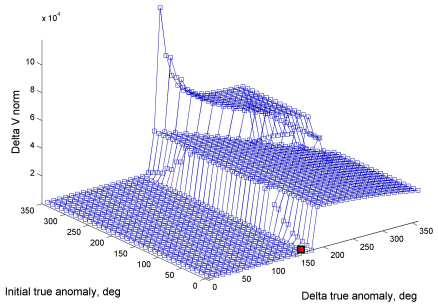

(b) $e = 0.01$

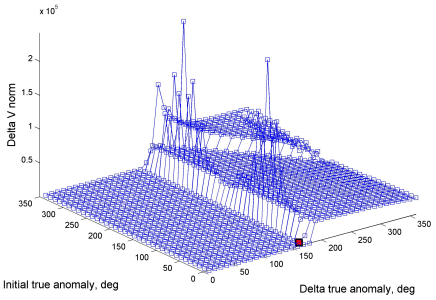

(c) $e = 0.1$

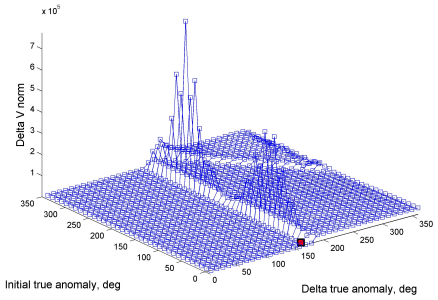

(d) $e = 0.3$

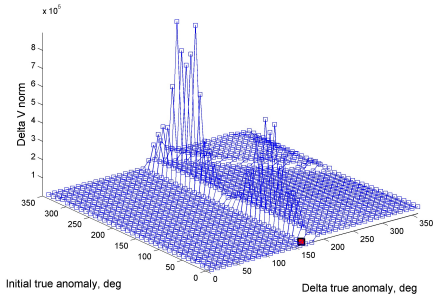

(e) $e = 0.5$

Figure 6.29: Velocity change with respect to eccentricity: ACPF

6.5 Radial/Along-Track Plane to Along-Track/Cross-Track Plane Formation

In this section, the maneuver problem is considered for changing the formation geometry from the radial/along-track plane to the along-track/cross-track plane. The orbital elements of the leader spacecraft are summarized in Table 3.1. The follower spacecraft flying in the radial/along-track plane formation with the formation radius of 500 m is considered to change its formation geometry to the along-track/cross-track plane formation with the same formation radius.

In Section 6.5.1, the optimal trajectory using the continuous control input is shown using the Gauss pseudospectral method with the relative position and velocity vectors at the initial and final configuration, which method is presented in Section 5.3. In Section 6.5.2, the transfer orbit trajectory using the impulsive control input is shown based on the modified Lambert's problem described in Section 5.4, where the initial and final position vectors and flight time are specified. The simulation results are analyzed in Section 6.5.3.

6.5.1 Continuous Control Input

For the maneuver problem using the continuous control input, the initial and final conditions of the follower spacecraft in the LVLH frame are summarized in Table 6.20. Two cost functions, J_1 and J_2 as presented in Eqs. (5.3) and (5.4), are considered for the optimal control problem.

Figures 6.30–6.32 show the simulation results with the cost function J_1 for minimum energy. Figure 6.30 shows the transfer trajectory of the follower spacecraft with respect to the leader spacecraft in the LVLH frame; the solid line denotes the trajectory of the follower spacecraft with different formation types, and the line with square shows the transfer trajectory of the follower

spacecraft between two orbits. Figure 6.31 shows the velocity history of the follower spacecraft during the formation reconfiguration. In Fig. 6.31, the triangle denotes specified relative velocities at the initial and final time in the LVLH frame, as presented in Table 6.20. Figure 6.32 shows the control input history of the follower spacecraft in the true anomaly domain during the maneuver. The boundary conditions of the relative positions at the initial and final time are satisfied as shown in Fig. 6.30. Also, the relative velocities are equal to the boundary condition at the initial and final time as described in Table 6.20 using the continuous control input presented in Fig. 6.32.

Table 6.20: Initial and final conditions: RAPF to ACPF

	Initial condition	Final condition
r_d (m)	500	500
ν (deg)	0	270
Position (m)	[0, 500, 0]	[-261.9048, 0, -523.8095]
Velocity	[261.9048, 0, 0]	[0, 0, 52.3810]

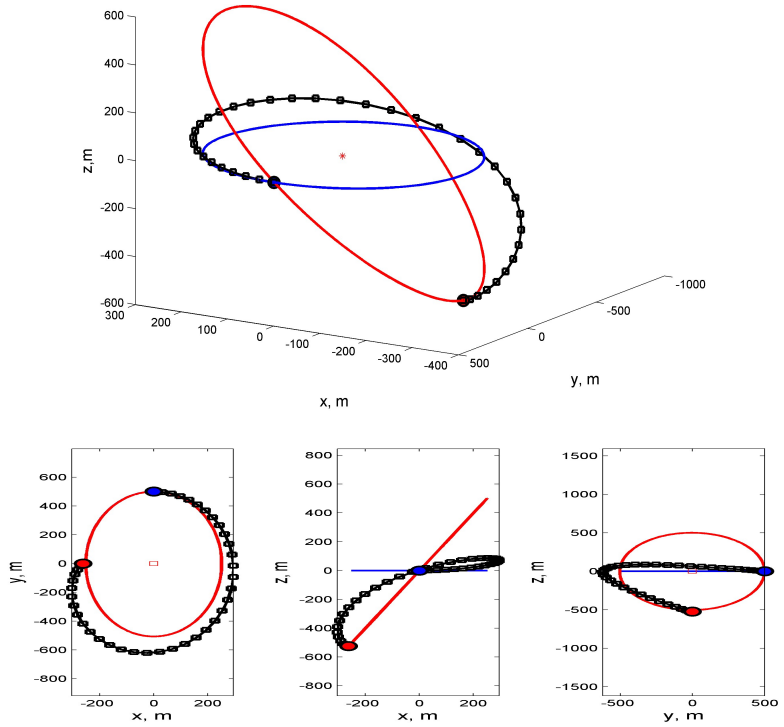

Figure 6.30: Trajectory of follower spacecraft in LVLH frame (J_1): RAPF to ACPF

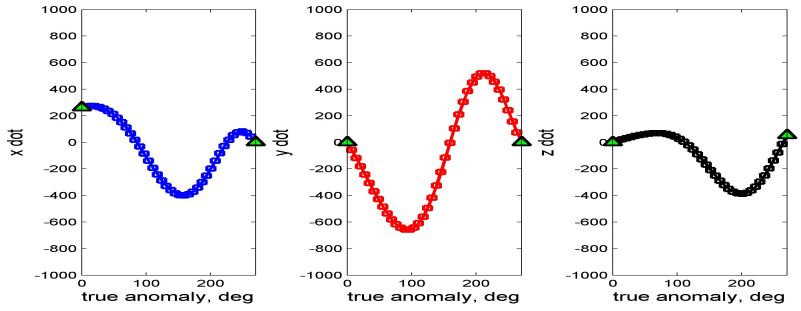

Figure 6.31: Relative velocity history of follower spacecraft (J_1): RAPF to ACPF

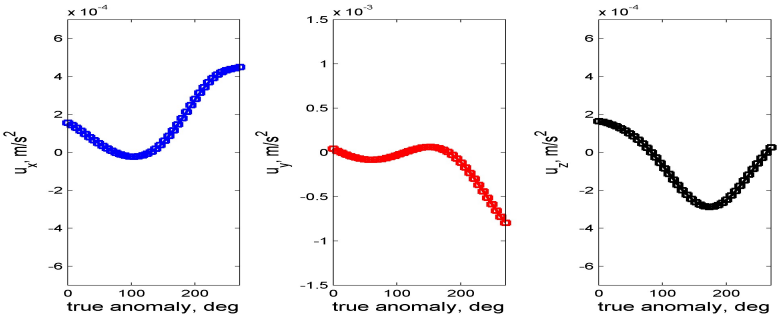

Figure 6.32: Control input history of follower spacecraft (J_1): RAPF to ACPF

Figures 6.33–6.35 show the simulation results with the cost function J_2 for minimum fuel. Figure 6.33 shows the transfer trajectory of the follower spacecraft with respect to the leader spacecraft in the LVLH frame; the solid line denotes the trajectory of the follower spacecraft with different formation types, and the line with square shows the transfer trajectory of the follower spacecraft between two orbits. Figure 6.34 shows the velocity history of the follower spacecraft during the formation reconfiguration. In Fig. 6.34, the triangle denotes specified relative velocities at the initial and final time in the LVLH frame, as presented in Table 6.20. Figure 6.35 shows the control input history of the follower spacecraft in the true anomaly domain during the maneuver. As shown in Figs. 6.33 and 6.34, the boundary conditions of the position and velocity are satisfied at the initial and final time by the continuous control input presented in Fig. 6.35. Compared with the results with J_1, the transfer trajectory in Fig. 6.33 is different from the trajectory in Fig. 6.30, since the different cost function is used for the optimal control problem.

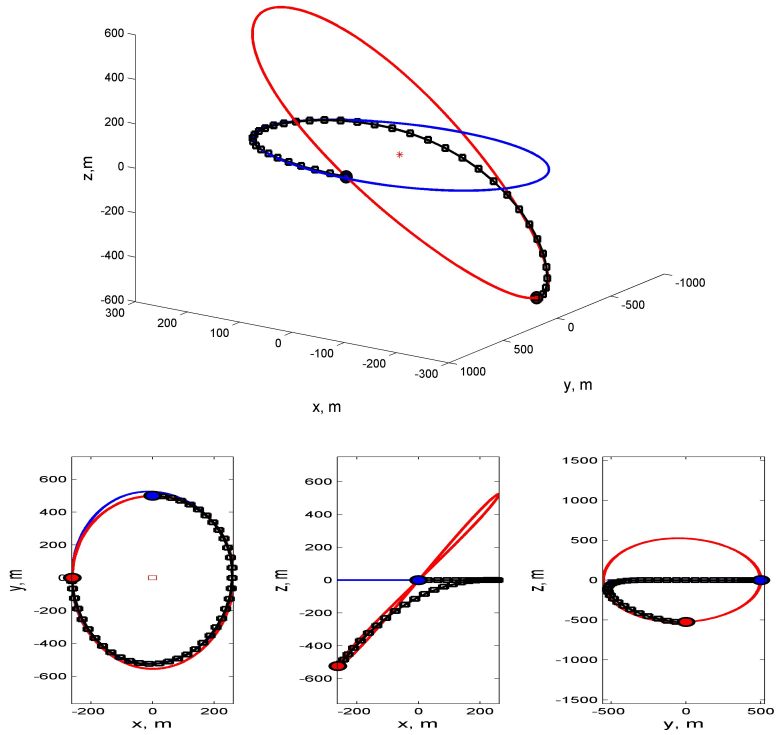

Figure 6.33: Trajectory of follower spacecraft in LVLH frame (J_2): RAPF to ACPF

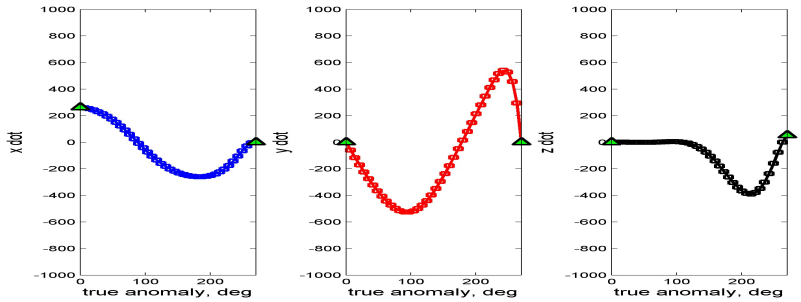

Figure 6.34: Relative velocity history of follower spacecraft (J_2): RAPF to ACPF

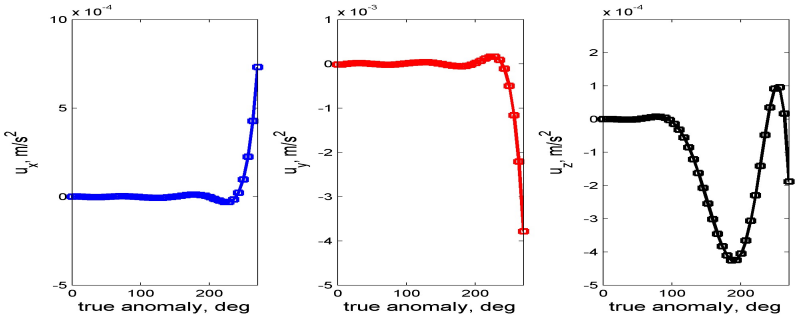

Figure 6.35: Control input history of follower spacecraft (J_2): RAPF to ACPF

6.5.2 Impulsive Control Input

For the maneuver to change the formation geometry using the impulsive control input, the simulation conditions are same as in Section 6.5.1. Figure 6.36 shows the transfer trajectory of the follower spacecraft with respect to the leader spacecraft in the LVLH frame. Figure 6.37 shows the relative velocity history of the follower spacecraft during the maneuver. In Fig. 6.37, the triangle denotes specified velocities at the initial and final time in the LVLH frame as described in Table 6.20. The difference between the resulting velocity from the modified Lambert's problem and specified velocity is equal to ΔV for the orbital transfer. Table 6.21 summarizes the velocities of the follower spacecraft and ΔV for the maneuver to move from the radial/along-track plane to the along-track/cross-track plane formations.

Compared with results in Section 6.5.1, the trajectory of the follower spacecraft using the impulsive control input in Fig. 6.36 is entirely different from the trajectory using the continuous control input illustrated in Figs. 6.30 and 6.33. In the continuous control input case, the optimal control problem is solved to satisfy the boundary conditions including the relative velocity vectors as well as the relative position vectors at the initial and final time, as

shown in Figs. 6.30, 6.31, 6.33, and 6.34. However, in the impulsive control input case, the relative positions are only considered to transfer the orbit. Therefore, the velocity at the initial time is adjusted to transfer the orbit by the impulsive control input, and then the follower spacecraft moves to the final position. When the follower spacecraft arrives at the final position, the velocity is changed to satisfy the periodicity condition by the impulse control. Therefore, the velocity obtained from the modified Lambert's problem presented in Fig. 6.37 is different from the velocity determined by the periodicity condition in Table 6.20. Consequently, these results provide different trajectories.

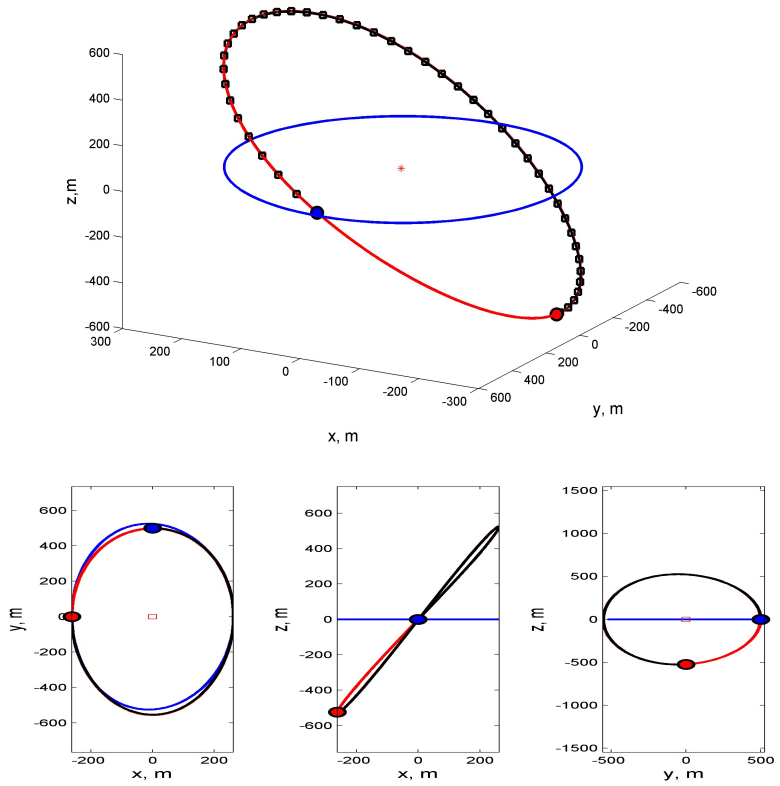

Figure 6.36: Trajectory of follower spacecraft in LVLH frame: RAAC to ACPF

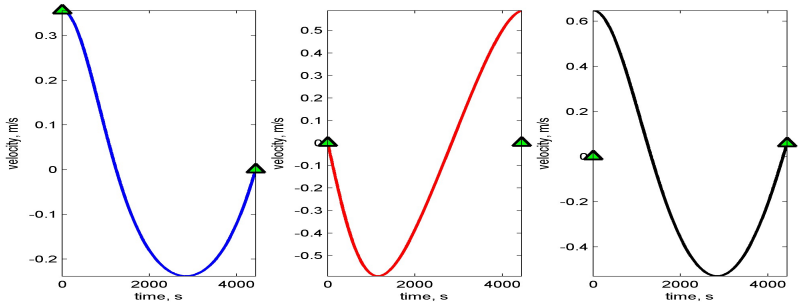

Figure 6.37: Velocity history of follower spacecraft: RAPF to ACPF

Table 6.21: Solution of Lambert's problem: RAPF to ACPF

	Initial value	Final value
Velocity (m/s)	[0.3561, 0, 0]	[0, 0, 0.0589]
V_t (m/s)	[0.3561, -0.001, 0.6475]	[0, 0.5886, 0.0588]
ΔV	[0, -0.0001, 0.6475]	[0, -0.5886, 0]
Total ΔV	[0, 0.5886, 0.6475]	norm: 0.8751

6.5.3 Analysis of Numerical Simulation Results

In this section, the simulation results for changing the formation geometry are analyzed. Let us compare the simulation results in terms of velocity change, ΔV, and mass change, Δm, of two control input types presented in Sections 6.5.1 and 6.5.2. Table 6.22 summarizes ΔV and Δm according to the control input type. As shown in Table 6.22, for changing the formation geometry, ΔV of the continuous control input is smaller than that of the impulsive control input. Furthermore, the continuous control input spends less fuel consumption than the impulsive control input.

Table 6.22: ΔV and Δm for formation reconfiguration: RAPF to ACPF

	ΔV (m/s)	Δm (kg)
Continuous control (J_1)	0.9732	0.0017
Continuous control (J_2)	0.7150	0.0012
Impulsive control	0.8751	0.0149

6.6 Concluding Remarks

In this chapter, numerical simulations are performed to solve the maneuver problem for the formation reconfiguration using two control input types: continuous control input and impulsive control input. The numerical simulation results of changing the formation radius in the radial/along-track plane formation are shown in Section 6.3; the results using the continuous control input are illustrated in Section 6.3.1, and the results using the impulsive control input are described in Section 6.3.2. In Section 6.4, the numerical simulation results of changing the formation radius in the along-track/cross-track plane formation are illustrated via two control input types; the results using the continuous control input are shown in Section 6.4.1, and the results using the impulsive control input are presented in Section 6.4.2. In Section 6.5, to change the formation geometry from the radial/along-track plane formation to the along-track/cross-track plane formation, the numerical simulation is performed and results are shown; the results using the continuous control input are illustrated in Section 6.5.1, and the results using the impulsive control input are described in Section 6.5.2. These results show the maneuver characteristics of the transfer orbit trajectories with respect to the control input type.

In the impulsive control input case, a set of the initial and final positions having minimum ΔV is obtained for the formation reconfiguration by the grid search in Sections 6.3.3 and 6.4.3. The difference between the orbital elements of the leader spacecraft and those of the transfer orbit is analyzed. Through these results, it can be concluded that the transfer orbit with the global minimum velocity change provides smaller changes in orbital elements, which reduces the control effort during the maneuver. Furthermore, a set of the initial and final true anomalies having minimum ΔV is obtained with respect to the eccentricity of the reference orbit. From this result, it is noted

that the minimum ΔV is increased as the eccentricity becomes large, and the follower spacecraft can reduce the fuel consumption by the first burn at perigee or apogee and the second burn with the transfer angle of $170 \sim 180°$.

Chapter 7

Conclusions

7.1 Summary

In this dissertation, the periodic relative motion and the maneuver problem were treated for the spacecraft formation flying in an elliptical orbit. The general periodicity condition stems from the state transition matrix and the energy matching condition using the analytic solution of the relative motion dynamics in the elliptic reference orbit. Two kinds of formation geometry were designed and analyzed: radial/along-track plane formation and along-track/cross-track plane formation. Furthermore, the maneuver problem for the formation reconfiguration was solved using two control input types: continuous control input and impulsive control input. The followings summarize the problem and solutions proposed in this dissertation.

General periodicity condition was presented through not only the state transition matrix approach, but also the energy matching condition approach. The general periodicity condition guarantees the natural periodic relative motion in the elliptic reference orbit as well as in the circular reference orbit. In addition, this periodic condition can express the bounded relative motion at an arbitrary position including specific positions, perigee and apogee, in

the elliptic reference orbit. To construct a bounded formation with the leader spacecraft as a center in the relative motion, the zero offset condition in the along-track direction was investigated. As a result, the periodic relative motion based on the general periodic condition and the zero offset condition was derived. This periodic relative motion has an advantage that an additional method such as the perturbation method or optimization method is not required to determine the initial condition with respect to the position of the follower spacecraft.

Using the obtained periodic relative motion, two formation types were designed. One formation type is the radial/along-track plane formation, and another one is the along-track/cross-track plane formation which becomes the projected circular formation when the leader spacecraft is in a circular reference orbit. The formation pattern of each formation type was analyzed with respect to the eccentricity and the true anomaly of the reference orbit. Numerical simulations were performed to investigate the formation geometries and analyze the formation pattern. Both the variation of eccentricity of the follower spacecraft in the relative motion and the change of the formation radius increase, as the eccentricity of the leader spacecraft is increased in all designed formation geometries. These results provide the constraint and guideline to design the spacecraft formation in the elliptic reference orbit.

The maneuver problem was also presented for the formation reconfiguration. To operate the multiple spacecraft system, it is required to change the formation radius or the formation geometry according to the mission. For this reason, the maneuver problem was solved for the formation reconfiguration based on the periodic relative motion and designed formation geometry. Two control input types were considered depending on the thrust system. For the continuous control input type, Gauss pseudospectral method was used to solve the optimal control problem, where two cost functions were defined

to minimize the energy and fuel, respectively, and dynamic constraints and boundary conditions were specified through the formation design procedure. For the impulsive control input type, the classical Lambert's problem was modified to find a transfer trajectory between two orbits in the local frame, where two position vectors at the initial and final time and the flight time are specified. Numerical simulations were performed to demonstrate the transfer orbit trajectory for the formation reconfiguration according to the control input type. From the numerical simulation, the reconfiguration of the formation radius and geometry with respect to the leader spacecraft was illustrated in the radial/along-track plane formation and the along-track/cross-track plane formation. Furthermore, the solution of the minimum velocity change was obtained by the grid search for the impulsive control input type. The obtained set of the initial and final positions provided the transfer orbit, and the orbital elements of the resulting transfer orbit were similar to those of the reference orbit. This small difference of the orbital elements leads to the reduced ΔV for the impulsive control input. Moreover, it is noted that the transfer orbit in the radial/along-track plane formation belongs to the coplanar maneuver, and that in the along-track/cross-track plane formation relates to the combined maneuver of coplanar and non-coplanar maneuver.

7.2 Directions for Future Research

There are several challenges related to the design and control of the spacecraft formation that are not addressed in this dissertation. As an extension of the research reported herein, some ongoing and prospective subjects are described below.

In the analysis of the relative motion, it is necessary to account for the perturbations of the spacecraft. The largest effect on the spacecraft is a perturbation due to the Earth's oblateness, which is required to model the long-term

dynamics as well as the short-term dynamics of the spacecraft in the formation to maintain the relative motion. Recently, J_2 perturbation has been studied for the spacecraft formation flying. However, not only J_2 perturbation but also J_3 and high-order terms of geopotential perturbation have effects on the dynamics of the relative motion. Furthermore, the perturbation due to atmospheric drag and N-body including sun and moon has influence on the spacecraft in the low Earth orbit, specifically. The relative dynamics including the perturbations has to be developed to precisely describe the relative motion, and then the resulting dynamics will lead to the reduction of fuel consumption to adjust the orbit trajectory during the operation.

Nonlinearity in the relative motion should be considered in the relative dynamics of spacecraft. The HCW equation and TH equation are assumed that the relative distance between two spacecraft is much smaller than the distance between the spacecraft and the center of the Earth, $||\rho|| \ll ||R||$. The dynamic equation under this assumption could not exactly describe the relative motion between two spacecraft, when the relative distance becomes large according to the space mission. To deal with this problem, the relative dynamics has to be analyzed considering the effects of the nonlinearity in the relative motion between two spacecraft.

The optimal control problem has to be developed to maintain the angle difference between follower spacecraft for the formation flying in elliptic orbits. In this dissertation, the angle difference was analyzed with respect to the eccentricity of the reference orbit, and it was shown that the the follower spacecraft cannot maintain a constant angle difference due to the eccentricity without the control input. In order to consider the various missions including mapping the target, the angle difference must be controlled by the external control input, while minimizing the fuel consumption. Thus, the optimal control is required to keep an angle difference and to reduce the control input for

the spacecraft formation flying.

It is also necessary to consider the collision avoidance in the optimal control problem for the operational spacecraft in the formation. Recently, the growth in space debris around the Earth has become a concern, which consists of discarded rocket stages, defunct satellites, and erosion, explosion and collision fragments. These objects are potential collision risks to the spacecraft, and therefore the collision avoidance maneuver should be developed for the reliable spacecraft system. To deal with the space debris, the optimal control problem can be solved to transfer the spacecraft in formation from the current orbit to safe orbit, while minimizing the control input. In addition, the formation reconfiguration should be designed to avoid the collision as well as to change the formation radius or geometry considering the minimum fuel consumption during the maneuver.

Bibliography

[1] Schiff, C., and Bristow, J., "Formation Flying in Elliptical Orbits," *IEEE Aerospace Conference*, Big Sky, MT, March 2000.

[2] Beard, R. W., Lawton, J. R., and Hadaegh, F. Y., "A Coordination Architecture for Spacecraft Formation Control," *IEEE Transactions on Control System Technology*, Vol. 9, No. 6, 2001, pp. 777-790.

[3] Scharf, D. P., Hadaegh, F. Y., and Ploen, S. R., "A Survey of Spacecraft Formation Flying Guidance and Control (Part 1): Guidance," *American Control Conference*, Piscataway, NJ, June 2003.

[4] Scharf, D. P., Hadaegh, F. Y., and Ploen, S. R., "A Survey of Spacecraft Formation Flying Guidance and Control (Part 2): Control," *American Control Conference*, Piscataway, NJ, June 2003.

[5] Bauer, F., Bristow, J., Folta, D., Hartman, K., Quinn, D., and How, J. P., "Satellite Formation Flying using an Innovative Autonomous Control System (AUTOCON) Environment," *AIAA Guidance, Navigation, and Control Conference*, New Orleans, LA, Aug. 1997.

[6] Folta, D., and Hawkins, A., "Results of NASA's First Autonomous Formation Flying Experiment: Earth Observing-1 (EO-1)," *AIAA/AAS Astrodynamics Specialist Conference*, Monterey, CA, Aug. 2002.

[7] Beichman, C. A., Woolf, N. J., and Lindensmith, C. A., *The Terrestrial Planet Finder (TPF): A NASA Origins Program to Search for Habitable Planets*, JPL Publication, Pasadena, CA, 1999.

[8] Folta, D., Hartman, K., Howell, K., and Marchand, B., "Formation Control of the MAXIM L2 Libration Orbit Mission," *AIAA/AAS Astrodynamics Specialist Conference*, Providence, RI, Aug. 2004.

[9] Curtis, S., "The Magnetospheric Multiscale Mission Resolving Fundamental Processes in Space Plasmas," NASA/TM2000-209883, NASA GSFC, Greenbelt, MD, Dec. 1999.

[10] Das, A., Cobb, R., and Stallard, M., "TechSat 21: A Revolutionary Concept in Distributed Space Based Sensing," *AIAA Defense and Civil Space Programs Conference*, Huntsvill, AL, Oct. 1998.

[11] Burns, R., McLaughlin, C. A., Leitner, J., and Martin, M., "TechSat 21: Formation Design, Control, and Simulation," *IEEE Aerospace Conference*, Big Sky, MT, March 2000.

[12] Hocken, D., and Schoenmaekers, J., "Optimization of Cluster Constellation Maneuvers," *16th International Symposium on Space Flight Dynamics*, Pasadena, CA, Dec. 2001.

[13] Dow, J., Matussi, S., Dow, R. M., Schmidt, M., and Warhaut, M., "The Implementation of the Cluster II Constellation," *Acta Astronautica*, Vol. 54, No. 9, 2004, pp. 657-669.

[14] Fridlund, C. V. M., "Darwin-The Infrared Space Interferometry Mission," *ESA Bulletin*, Vol. 103, 2000, pp. 20-25.

[15] Chabot, T., and Udrea, B., "XEUS Mission Guidance Navigation and Control," *AIAA Guidance, Navigation, and Control Conference*, Keystone, CO, Aug. 2006.

[16] Ferrier, C., Boschetti, M., Fourcade, J., and Gamet, P., "Exit the A-Train Constellation: PARASOL and CALIPSO Different Responses," *SpaceOps Conference*, Huntsville, AL, April 2010.

[17] Folkner, W. M., Hellings, R. W., Maleki, L., Bender, P., Faller, J., Stebbins, R., Danzmann, K., Cornelisse, J. W., Jafry, Y., Reinhard, R., Brillet, A., Barillet, R., Ciufolini, I., Hough, J., Robertson, D., Ward, H., Lobo, A., Sandford, M., Gray, P., Schutz, B., Touboul, P., Cavaliere, A., Sumner, T. J., Polnarev, A., Barlier, F., Rudiger, A., Schilling, R., Winkler, W., and Tunnermann, A., "LISA: Laser Interferometer Space Antenna For Gravitational Wave Measurements," *33rd Aerospace Science Meeting*, Reno, NV, Jan. 1995.

[18] Borde, J., Teston, F., Santandrea, S., and Boulade, S., "Feasibility of the PROBA 3 Formation Flying Demonstration Mission as a Pair of Microsats in GTO," *55th International Astronautical Congress*, Vancouver, Canada, Oct. 2004.

[19] D'Amico, S., Ardaens, J.-S., and Larsson, R., "Spaceborne Autonomous Formation-Flying Experiment on the PRISMA Mission," *Journal of Guidance, Control, and Dynamics*, Vol. 35, No. 2, 2012, pp. 834-850.

[20] Hill, G. W., "Researches in Lunar Theory," *American Journal of Mathematics*, Vol. 1, No. 1, 1878, pp. 5-26.

[21] Clohessy, W. H., and Wiltshire, R. S., "Terminal Guidance System for Satellite Rendezvous," *Journal of the Aerospace Sciences*, Vol. 27, No. 9, 1960, pp. 653-658.

[22] Tschauner, J., and Hempel, P., "Rendezvous zu einem in elliptischer Bahn umlaufenden Ziel," *Acta Astronautica*, Vol. 11, 1965, pp. 104-109.

[23] Sidi, M. J., *Spacecraft Dynamics and Control: A Practical Engineering Approach*, Cambridge University Press, New York, NY, 1997.

[24] Schaub, H., "Relative Orbit Geometry Through Classical Orbit Element Differences," *Journal of Guidance, Control, and Dynamics*, Vol. 27, No. 5, 2004, pp. 839-848.

[25] Gurfil, P., "Generalized Solutions for Relative Spacecraft Orbits under Arbitrary Perturbations," *Acta Astronautica*, Vol. 60, No. 2, 2007, pp. 61-78.

[26] Jiang, F., Li, J., Baoyin, H., and Gao, Y., "Study on Relative Orbit Geometry of Spacecraft Formations in Elliptical Reference Orbits," *Journal of Guidance, Control, and Dynamics*, Vol. 31, No. 1, 2008, pp. 123-134.

[27] Wiesel, W. E., *Spaceflight Dynamics*, McGraw-Hill, New York, NY, 1989.

[28] Vaddi, S. S., Vadali, S. R., and Alfriend, K. T., "Formation Flying: Accommodating Nonlinear and Eccentricity Perturbations," *Journal of Guidance, Control, and Dynamics*, Vol. 26, No. 2, 2003, pp. 214-223.

[29] Inalhan, G., Tillerson, M., and How, H. P., "Relative Dynamics and Control of Spacecraft Formations in Eccentric Orbits," *Journal of Guidance, Control, and Dynamics*, Vol. 25, No. 1, 2002, pp. 48-59.

[30] Sabol, C., Burns, R., and McLaughlin, C. A., "Satellite Formation Flying Design and Evolution," *Journal of Spacecraft and Rockets*, Vol. 38, No. 2, 2001, pp. 270-278.

[31] Vallado, D. A., and McClain, W. D., *Fundamentals of Astrodynamics and Applications*, Space Technology Library, Microcosm Press, El Seguendo, CA, and Kluwer Academic Publishers, Dordrecht, Netherlands, 2001.

[32] Vassar, R. H., and Sherwood, R. B., "Formationkeeping for a Pair of Satellite in a Circular Orbit," *Journal of Guidance, Control, and Dynamics*, Vol. 8, No. 2, 1985, pp. 235-242.

[33] Karlgaard, C. D., and Lutze, F. H., "Second-Order Relative Motion Equations," *Journal of Guidance, Control, and Dynamics*, Vol. 26, No. 1, 2003, pp. 41-49.

[34] Gurfil, P., and Kasdin, N. J., "Nonlinear Modeling of Spacecraft Relative Motion in the Configuration Space," *Journal of Guidance, Control, and Dynamics*, Vol. 27, No. 1, 2004, pp. 154-157.

[35] Richardson, D. L., and Mitchell, J. W., "A Third-Order Analytical Solutions for Relative Motions with a Circular Reference Orbit," *Journal of the Astronautical Sciences*, Vol. 51, No.1, 2003, pp. 1-12.

[36] Gomez, G., and Marcote, M., "High-order Analytical Solutions of Hill's Equations," *Celestial Mechanics and Dynamical Astronomy*, Vol. 94, No. 2, 2006, pp. 197-211.

[37] Carter, T. E., "New Form for the Optimal Rendezvous Equations Near a Keplerian Orbit," *Journal of Guidance, Control, and Dynamics*, Vol. 13, No. 1, 1990, pp. 183-186.

[38] Carter, T. E., and Humi, M., "Fuel-Optimal Rendezvous near a Point in General Keplerian Orbit," *Journal of Guidance, Control, and Dynamics*, Vol. 10, No. 6, 1987, pp. 567-573.

[39] Carter, T. E., "Optimal Impulsive Space Trajectories Based on Linear Equations," *Journal of Optimization Theory and Applications*, Vol. 70, No. 2, 1991, pp. 277-297.

[40] Carter, T. E., and Brient, J., "Fuel-Optimal Rendezvous for Linearized Equations of Motion," *Journal of Guidance, Control, and Dynamics*, Vol. 15, No. 6, 1992, pp. 1411-1416.

[41] Carter, T. E., "Optimal Power-Limited Rendezvous for Linearized Equations of Motion," *Journal of Guidance, Control, and Dynamics*, Vol. 17, No. 5, 1994, pp. 1082-1086.

[42] Carter, T. E., "State Transition Matrices for Terminal Rendezvous Studies: Brief Survey and New Examples," *Journal of Guidance, Control, and Dynamics*, Vol. 21, No. 1, 1998, pp. 148-155.

[43] Melton, R. G., "Time-Explicit Representation of Relative Motion Between Elliptical Orbits," *Journal of Guidance, Control, and Dynamics*, Vol. 23, No. 4, 2000, pp. 604-610.

[44] Broucke, R. A., "Solution of the Elliptic Rendezvous Problem with the Time as Independent Variable," *Journal of Guidance, Control, and Dynamics*, Vol. 26, No. 4, 2003, pp. 615-621.

[45] Broucke, R. A., and Cefola, P. J., "On the Equinoctial Orbit Elements," *Celestial Mechanics and Dynamical Astronomy*, Vol. 5, 1972, pp. 303-310.

[46] Baoyin, H., Junfeng, L., and Yunfeng, G., "Dynamical Behaviors and Relative Trajectories of the Spacecraft Formation Flying," *Aerospace Science and Technology*, Vol. 6, 2000, pp. 295-301.

[47] Garrison, J. L., Gardner, T. G., and Axelrad, P., "Relative Motion in Highly Elliptical Orbits," *AAS/AIAA Space Flight Mechanics Conference*, Albuquerque, NM, Feb. 1995.

[48] Bond, V. R., "A New Solution for the Rendezvous Problem," *AAS/AIAA Space Flight Mechanics Meeting*, Breckenridge, CO, Feb. 1999.

[49] Vadali, S. R., Schaub, H., and Alfriend, K. T., "Initial Conditions and Fuel-Optimal Control for Formation Flying of Satellites," *AIAA Guidance, Navigation, and Control Conference*, Portland, OR, Aug. 1999.

[50] Schaub, H., and Alfriend, K. T., "J_2 Invariant Relative Orbits for Spacecraft Formations," *Celestial Mechanics and Dynamical Astronomy*, Vol. 79, No. 2, 2001, pp. 77-95.

[51] Yamanaka, K., and Ankerse, F., "New State Transition Matrix for Relative Motion on an Arbitrary Elliptical Orbit," *Journal of Guidance, Control, and Dynamics*, Vol. 25, No. 1, 2002, pp. 60-66.

[52] Gim, D., and Alfriend, K. T., "State Transition Matrix of Relative Motion for the Perturbed Noncircular Reference Orbit," *Journal of Guidance, Control, and Dynamics*, Vol. 26, No. 6, 2003, pp. 956-971.

[53] Gurfil, P., "Relative Motion between Elliptic Orbits: Generalized Bounded Conditions and Optimal Formationkeeping," *Journal of Guidance, Control, and Dynamics*, Vol. 30, No. 4, 2007, pp. 953-964.

[54] Xing, J., Tang, G., Xi, X., and Li, H., "Satellite Formation Design and Optimal Stationkeeping Considering Nonlinearity and Eccentricity," *Journal of Guidance, Control, and Dynamics*, Vol. 30, No. 5, 2007, pp. 1523-1527.

[55] Sengupta, P., Sharma, R., and Vadali, S. R., "Periodic Relative Motion Near a Keplerian Elliptic Orbit with Nonlinear Differential Gravity," *Journal of Guidance, Control, and Dynamics*, Vol. 29, No. 5, 2006, pp. 1110-1121.

[56] Sengupta, P., and Vadali, S. R., "Relative Motion and the Geometry of Formations in Keplerian Elliptic Orbits," *Journal of Guidance, Control, and Dynamics*, Vol. 30, No. 4, 2007, pp. 953-964.

[57] Jiang, F., Li, J., and Baoyin, H., "Approximate Analysis for Relative Motion of Satellite Formation Flying in Elliptical Orbits," *Celestial Mechanics and Dynamical Astronomy*, Vol. 98, No. 1, 2007, pp. 31-66.

[58] Sabatini, M., Izzo, D., and Bevilacqua, R., "Special Inclinations Allowing Minimal Drift Orbits for Formation Flying Satellites," *Journal of Guidance, Control, and Dynamics*, Vol. 31, No. 1, 2008, pp. 94-100.

[59] Bando, M., and Ichikawa, A., "Periodic Orbits of Nonlinear Relative Dynamics and Satellite Formation," *Journal of Guidance, Control, and Dynamics*, Vol. 32, No. 4, 2009, pp. 1200-1208.

[60] Sedwick, R., Hacker, T., and Miller, D., "Optimum Aperture Placement for a Space-Based Radar System Using Separated Spacecraft Interferometry," *AIAA Guidance, Navigation, and Control Conference*, Portland, OR, Aug. 1999.

[61] Carpenter, J. R., Leitner, J. A., Folta, D. C., and Burns, R. D., "Benchmark Problems for Spacecraft Formation Flight Missions," *AIAA Guidance, Navigation, and Control Conference*, Austin, TX, Aug. 2003.

[62] Maihe, L., Schiff, C., and Hughes, S., "Formation Flying in Highly Elliptical Orbits: Initializing the Formation," *International Symposium on Space Dynamics*, Biarritz, France, June 2000.

[63] Guzman, J., and Schiff, C., "A Preliminary Study for a Tetrahedron Formation: Quality Factors and Visualization," *AIAA/AAS Astrodynamics Specialists conference*, Monterey, CA, Aug. 2002.

[64] Zhang, H., and Sun, L., "Spacecraft Formation Flying in Eccentric Orbits," *AIAA Guidance, Navigation, and Control Conference*, Austin, TX, Aug. 2003.

[65] Wang, H., Yang, W., and Li, J., "Solution Set on the Natural Satellite Formation Orbits under First-Order Earth's Non-Spherical Perturbation," *Acta Mechanica Sinica*, Vol. 21, No. 5, 2005, pp. 503-510.

[66] Lane, C., and Axelrad, P., "Formation Design in Eccentric Orbits using Linearized Equations of Relative Motion," *Journal of Guidance, Control, and Dynamics*, Vol. 29, No. 1, 2006, pp. 146-160.

[67] Palmer, P., and Halsall, M., "Designing Natural Formations of Low-Earth-Orbiting Satellites," *Journal of Guidance, Control, and Dynamics*, Vol. 32, No. 3, 2009, pp. 860-868.

[68] Xu, G., Wang, D., Wu, B., and Pho, E. K., "Passive and Periodic Circular-Like Formations at Critical Inclination around an Oblate Earth," *Chinese Control and Decision Conference*, Mianyang, China, May 2011.

[69] Kirk, D. E., *Optimal Control Theory: An Introduction*, Prentice-Hall, Upper Saddle River, NJ, 1970.

[70] Betts, J. T., "Survey of Numerical Methods for Trajectory Optimization," *Journal of Guidance, Control, and Dynamics*, Vol. 21, No. 2, 1998, pp. 193-207.

[71] Lawden, D. F., *Optimal Trajectory for Space Navigation*, Butterworths, London, UK, 1963.

[72] Prussing, J. E., and Chiu, J., "Optimal Multi-Impulse Time-Fixed Rendezvous Between Circular Orbits," *Journal of Guidance, Control, and Dynamics*, Vol. 9, No. 1, 1987, pp. 17-22.

[73] Jezewski, D. J., and Stoolz, J. M., "A Closed-Form Solutions for Minimum-Fuel Constant-Thrust Trajectories," *Journal of AIAA*, Vol. 8, No. 7, 1970, pp. 1229-1234.

[74] Billik, B. H., "Some Optimal Low-Acceleration Rendezvous Maneuvers," *Journal of AIAA*, Vol. 2, No. 3, 1964, pp. 510-516.

[75] Guelman, M., and Aleshin, M., "Optimal Bounded Low-Thrust Rendezvous with Fixed Terminal-Approach Direction," *Journal of Guidance, Control, and Dynamics*, Vol. 24, No. 2, 2001, pp. 378-385.

[76] Edelbaum, T. N., "Optimal Low-Thrust Rendezvous and Stationkeeping," *Journal of AIAA*, Vol. 2, No. 7, 1964, pp. 1196-1201.

[77] Gobertz, F. W., "Linear Theory of Optimal Low-Thrust Rendezvous Trajectories," *Journal of the Astronautical Science*, Vol. 12, No. 3, 1965, pp. 69-76.

[78] Schaub, H., Vadali, S. R., Junkins, J. L., and Alfriend, K. T., "Spacecraft Formation Flying Control using Mean Orbit Elements," *Journal of the Astronautical Sciences*, Vol. 48, No. 1, 2000, pp. 69-87.

[79] Alfriend, K. T., and Kashiwagi, Y., "Minimum Time Orbital Rendezvous Between Neighboring Elliptic Orbits," *Journal of Optimization Theory Applications*, Vol. 4, No. 4, 1969, pp. 260-276.

[80] Euler, E. A., "Optimum Low-Thrust Rendezvous Control," *Journal of AIAA*, Vol. 7, No. 6, 1969, pp. 1140-1144.

[81] Humi, M., "Fuel-Optimal Rendezvous in a General Central Gravity Field," *Journal of Guidance, Control, and Dynamics*, Vol. 16, No. 1, 1993, pp. 215-217.

[82] Epenoy, R., "Fuel Optimization for Continuous-Thrust Orbital Rendezvous with Collision Avoidance Constraint," *Journal of Guidance, Control, and Dynamics*, Vol. 34, No. 2, 2011, 493-503.

[83] Zanon, D. J., and Campbell, M. E., "Optimal Planner for spacecraft formation in Elliptic Orbits," *Journal of Guidance, Control, and Dynamics*, Vol. 29, No. 1, 2006, pp. 161-171.

[84] Palmer, P. L., "Optimal Relocation of Satellites Flying in Near-Circular-Orbit Formations," *Journal of Guidance, Control, and Dynamics*, Vol. 29, No. 3, 2006, pp. 519-526.

[85] Hargraves, C. R., and Paris, S. W., "Direct Trajectory Optimization using Nonlinear Programming and Collocation," *Journal of Guidance, Control, and Dynamics*, Vol. 19, No. 4, 1987, pp. 338-342.

[86] Enright, P. J., and Conway, B. A., "Optimal Finite-Thrust Spacecraft Trajectories using Collocation and Nonlinear Programming," *Journal of Guidance, Control, and Dynamics*, Vol. 14, No. 5, 1991, pp. 981-985.

[87] Tang, S., and Conway, B. A., "Optimization of Low-Thrust Interplanetary Trajectories using Collocation and Nonlinear Programming," *Journal of Guidance, Control, and Dynamics*, Vol. 18, No. 3, 1995, pp. 599-604.

[88] Hull, D. G., "Conversion of Optimal Control Problems into Parameter Optimization Problems," *AIAA Guidance, Navigation, and Control Conference*, San Diego, CA, July 1996.

[89] Herman, A. H., and Conway, B. A., "Direct Optimization using Collocation Based on High-Order Gauss-Lobatto Quadrature Rules," *Journal of Guidance, Control, and Dynamics*, Vol. 19, No. 3, 1996, pp. 592-599.

[90] Conway, B. A., and Larson, K. M., "Collocation Versus Differential Inclusion in Direct Optimization," *Journal of Guidance, Control, and Dynamics*, Vol. 21, No. 5, 1998, pp. 780-785.

[91] Hughes, S. P., "General Method for Optimal Guidance of Spacecraft Formations," *Journal of Guidance, Control, and Dynamics*, Vol. 31, No. 2, 2008, pp. 414-423.

[92] Massari, M., and Bernelli-Zazzera, F., "Optimization of Low-Thrust Reconfiguration Maneuvers for Spacecraft Flying in Formation," *Journal of Guidance, Control, and Dynamics*, Vol. 32, No. 5, 2009, pp. 1629-1638.

[93] Gong, Q., Ross, I. M., and Alfirend, K. T., "Triangle Formation Design in Eccentric Orbits using Pseudospectral Optimal Control," *AIAA Guidance, Navigation, and Control Conference*, Honolulu, HI, Aug. 2008.

[94] Huntington, G. T., and Rao, A. V., "Optimal Reconfiguration of Spacecraft Formations using the Gauss Pseudospectral Method," *Journal of Guidance, Control, and Dynamics*, Vol. 31, No. 3, 2008, pp. 689-698.

[95] Wu, B., Wang, D., Poh, E. K., and Xu, G., "Nonlinear Optimization of Low-Thrust Trajectory for Satellite Formation: Legendre Pseudospectral Approach," *Journal of Guidance, Control, and Dynamics*, Vol. 32, No. 4, 2009, pp. 1371-1381.

[96] Goberta, F. W., and Doll, J. R., "A Survey of Impulsive Trajectories," *AIAA Journal*, Vol. 7, No. 5, 1969, pp. 801-834.

[97] Lancaster, E. R., Blanchard, R. C., and Devaney, R. A., "A Note on Lambert's Theorem," *Journal of Spacecraft and Rockets*, Vol. 3, No. 9, 1966, pp. 1436-1438.

[98] Battin, R. H., and Vaughan, R. H., "An Elegant Lambert Algorithm," *Journal of Guidance, Control, and Dynamics*, Vol. 7, No. 6, 1984, pp. 662-670.

[99] Brusch, R. G., "Constrained Impulsive Trajectory Optimization for Orbit-to-Orbit Transfer," *Journal of Guidance, Control, and Dynamics*, Vol. 2, No. 3, 1979, pp. 204-212.

[100] Won, C-H., "Fuel- or Time-Optimal Transfers between Coplanar, Coaxial Ellipse using Lambert's Problem," *Journal of Guidnace, Control, and Dynamics*, Vol. 22, No. 4, 1999, pp. 536-542.

[101] Prussing, J. E., "A Class of Optimal Two-Impulse Rendezvous using Multiple-Revolution Lambert Solutions," *Journal of the Astronautical Sciences*, Vol. 48, No. 2-3, 2000, pp. 131-148.

[102] Shen, H., and Tsiotras, P., "Optimal Two-Impulse Rendezvous Between Two Circular Orbits using Multiple-Revolution Lambert's Solutions," *AIAA Guidance, Navigation, and Control Conference*, Monterey, CA, Aug. 2002.

[103] Shen, H., and Tsiotras, P., "Optimal Two-Impulse Rendezvous using Multiple-Revolution Lambert's Solutions," *Journal of Guidance, Control, and Dynamics*, Vol. 26, No. 1, 2003, pp. 50-61.

[104] Thomas, S. J., and Surka, D., "Numeric Delta-V Mapping for General Rendezvous Problems," *AIAA Infotech*, Seattle, WA, April 2009.

[105] Jiang, F., Li, J., Baoyin, H., and Gao, Y., "Two-Point Boundary Value Problem Solutions to Spacecraft Formation Flying," *Journal of Guidance, Control, and Dynamics*, Vol. 32, No. 6, 2009, pp. 1827-1837.

[106] Tillerson, M., Inalhan, G., and How, J. P., "Co-ordination and Control of Distributed Spacecraft Systems using Convex Optimization Techniques," *International Journal of Robust and Nonlinear Control*, Vol. 12, 2002, pp. 207-242.

[107] Tillerson, M., Breger, L., and How, J. P., "Distributed Coordination and Control of Formation Flying Spacecraft," *American Control Conference*, Denver, CO, June 2003.

[108] Richards, A., Schouwenaars, T., How, J. P., and Feron, E., "Spacecraft Trajectory Planning with Avoidance Constraints using Mixed-Integer Linear Programming," *Journal of Guidance, Control, and Dynamics*, Vol. 25, No. 4, 2002, pp. 755-764.

[109] Campbell, M. E., "Planning Algorithm for Multiple Satellite Clusters," *Journal of Guidance, Control, and Dynamics*, Vol. 26, No. 5, 2003, pp. 770-780.

[110] Guibou, V., and Scheeres, D., "Solving Relative Two Point Boundary Value Problems: Applications to Spacecraft Formation Flight Transfers," *Journal of Guidance, Control, and Dynamics*, Vol. 27, No. 4, 2004, pp. 693-704.

[111] Vaddi, S., Alfirend, K., Vadali, S., and Sengupta, P., "Formation Establishment and Reconfiguration using Impulsive Control," *Journal of Guidance, Control, and Dynamics*, Vol. 28, No. 2, 2005, pp. 262-268.

[112] Ketema, Y., "Optimal Satellite Transfers using Relative Motion Dynamics," *Journal of Guidance, Control, and Dynamics*, Vol. 32, No. 5, 2009, pp. 1508-1518.

[113] Schaub, H., and Junkins, J. L., *Analytical Mechanics of Space Systems*, AIAA Education Series, American Institute of Aeronautics and Astronautics, Reston, VA, 2003.

[114] Bryson, A., and Ho, Y., *Applied Optimal Control*, Wiley, New York, NY, 1975.

[115] Larsson, W. J., and Wertz, J. R., "Space Mission Analysis and Design," *Space Propulsion Systems*, Microcosm, Inc., Torrance, California and Kluwer Academic Publishers, Dodrecht, Boston, and London, 1995.

[116] Erichsen, P., "Performance Evaluations of Spacecraft Propulsion Systems in Relation to Mission Impulse Requirements," *Proceedings of the Second European Spacecraft Propulsion Conference*, Noordwijk, May 1997.

[117] Goebel, D. M., and Katz, I., *Fundamentals of Electric Propulsion: Ion and Hall Thrusters*, Wiley, John Wiley and Sons, Hoboken, NJ, 2008.

[118] Turner, M. J. L., *Rocket and Spacecraft Propulsion: Principles, Practice and New Developments*, Springer, Praxis Publishing Ltd, Chichester, UK, 2009.

[119] Bock, H., and Plitt, K., "A Multiple Shooting Algorithm for Direct Solution of Optimal Control Processes," *Proceedings of the 9th IFAC World Congress*, Budapest, Hungary, July 1984.

[120] Elnager, J., Kazemi, M. A., and Razzaghi, M., "The pseudospectral Legendre Method for Discretizing Optimal Control Problem," *IEEE Transactions on Automatic Control*, Vol. 40, No. 10, 1995, pp. 1793-1796.

[121] Elnager, J., and Razzaghi, M., "A Collocation-Type Method for Linear Quadratic Optimal Control Problems," *Optimal Control Applications and Methods*, Vol. 18, No. 3, 1977, pp. 227-235.

[122] Fahroo, F., and Ross, I. M., "A Spectral Patching Method for Direct Trajectory Optimization," *Journal of the Astronautical Sciences*, Vol. 48, No. 2-3, 2000, pp. 269-286.

[123] Fahroo, F., and Ross, I. M., "Direct Trajectory Optimization by a Chebyshev Pseudospectral Method," *American Control Conference*, Chicago, IL, June 2000.

[124] Fahroo, F., and Ross, I., "Direct Trajectory Optimization by Chebyshev Pseudospectral Method," *Journal of Guidance, Control, and Dynamics*, Vol. 25, No. 1, 2002, pp. 160-166.

초 록

본 논문에서는 타원 궤도에서의 다수 인공위성의 군집비행을 위한 주기적 상대운동과 군집반경 및 군집형상의 변경을 위한 기동에 대해 다음과 같은 연구를 수행하였다.

타원 기준궤도에서의 주기적 상대운동을 기술하였다. 군집비행을 수행하는 다수 인공위성의 운동은 인공위성 간의 상대운동으로 기술한다. 인공위성 간 상대운동은 원 기준궤도에서는 보편적으로 Hill-Clohessy-Wiltshire (HCW) 방정식으로, 타원 기준궤도에서는 Tschauner-Hempel (TH) 방정식이나 궤도요소로 나타낸다. 다수의 인공위성이 연료소모를 최소화하며 군집형상을 유지하기 위해서는 주기조건이 매우 중요한데, 상대운동 방정식과 그 해석적 해를 통해 구할 수 있다. 원 기준궤도의 경우, HCW 방정식의 해석적 해를 통해 쉽게 주기조건을 구할 수 있다. 그러나 타원 기준궤도의 경우, 상대운동 방정식과 해석적 해의 복잡성으로 인해 주기조건을 구하기 위한 해석적 접근이 필요하다. 본 연구에서는 타원 기준궤도에서의 다수 인공위성 군집비행을 위한 주기조건을 두 가지 해석적 방법인 상태천이 행렬(State Transition Matrix) 기법과 에너지 일치조건(Energy Matching Condition) 기법을 통하여 구하였다. 수치 시뮬레이션을 수행하여 타원 기준궤도에서의 주기조건을 검증하였으며, 기준 인공위성을 군집형상의 중심으로 하기 위한 오프셋 조건(offset condition)을 구하여 타원 기준궤도에서 군집비행을 유지하기 위한 주기적 상대운동을 기술하였다.

주기적 상대운동을 바탕으로 자연적 상대운동을 위한 두 가지 군집형상을 설계하고, 각 군집형상에 따른 인공위성의 상대운동을 분석하였다. 다수 인공위성의 군집비행은 연료소모를 최소화하면서 다양한 임무를 수행하기 위하여 특정 군집형상을 이루어 비행한다. 본 논문에서는 타원 기준궤도에서의 주기적 상대운동 방정식을 바탕으로 두 가지 군집형상을 설계하였다. 첫 번째 군집형상은 국지(LVLH) 좌표계 상의 $x-y$ 평면에서 다수 인공위성이

군집비행을 유지하는 radial/along-track plane formation이고, 두 번째 군집형상은 $y-z$ 평면에서 군집비행을 유지하는 along-track/cross-track plane formation 이다. 설계한 두 군집형상을 위한 초기값을 설정하고 수치 시뮬레이션을 수행하여, 다수 인공위성의 군집비행과 그 형상에 대해 검증하였다. 한편, 원 기준궤도와는 달리 타원 기준궤도에서의 군집비행은 이심률의 영향으로 인해 설계한 군집반경을 일정하게 유지하지 못하는 상대운동을 한다. 설계한 각 군집형상에 따른 인공위성의 상대운동을 분석한 결과, 인공위성의 군집형상은 기준궤도의 이심률에 크게 영향을 받음을 알 수 있었다. 기준궤도의 이심률이 작을 경우에는 설계한 군집형상을 유지하며 군집비행을 하지만, 이심률이 점점 커질수록 두 인공위성 간의 상대거리가 변하게 되어 일정한 군집형상을 이루지 못하고 변화율이 점점 커짐을 확인하였다. 이러한 분석결과는 다수 인공위성의 군집비행 설계 시 구속조건 및 설계지침으로 활용이 가능하다.

군집반경 및 군집형상 변경하기 위한 인공위성의 기동에 대한 연구를 수행하였다. 다수 인공위성이 군집비행을 할 경우, 임무에 따라 군집반경을 크게 늘리거나 줄이는 등의 군집반경 변화나 군집형상 변경이 요구된다. 이러한 군집 재형상의 경우, 인공위성의 수명에 직접적으로 영향을 주는 연료사용을 줄이기 위한 인공위성의 기동이 필요하다. 본 논문에서는 인공위성의 두 가지 제어입력 유형을 고려하여 인공위성 기동에 대한 연구를 수행하였다. 연속적 제어입력의 경우에는 주어진 두 상대위치와 상대속도를 만족하는 최적궤적을 구하기 위해 Gauss pseudospectral method를 이용한 최적제어 문제를 정의하여 해를 도출하였다. 불연속 임펄스 제어입력의 경우에는 지구를 중심으로 한 인공위성의 기동을 다루는 고전 Lambert 문제를 수정하여 인공위성의 상대운동에 대한 속도 변화를 구하고, 이를 통한 LVLH 좌표계 상에서의 기동궤적을 구하였다. 수치 시뮬레이션을 수행하여 두 가지 제어입력 유형에 따른 인공위성의 기동성능을 검증하였다. 수치 시뮬레이션에서는 앞에서 설계한 두 가지 군집형상에서 군집반경을 증가하거나 군집형상을 변경하는 경우를 고려하였으며, 제어입력유형에 따른 인공위성의 기동궤적을 구하고 속도변

화와 질량변화 관점에서 기동을 비교하였다. 이와 더불어 임펄스 제어입력의 경우, 전역에서 초기조건과 말기조건에 따른 기동궤적과 속도 변화를 구하고, 상대속도 차이를 최소화하는 기동을 구하여 천이궤도를 나타내었다. 결과를 분석하기 위해 수치 시뮬레이션 결과인 천이궤도와 인공위성의 기준궤도의 궤도요소 차이를 구하고, 이를 이용하여 각 군집형상에 따른 기동궤적을 분석하였다.

인공위성의 군집비행을 위한 본 연구의 결과는 다양한 임무를 위한 군집비행 설계에 활용될 수 있으며, 항공우주공학 및 로봇공학 분야의 협력제어 및 분산제어 연구에 적용될 수 있을 것이다.

주요어: 인공위성 군집비행, 주기적 상대운동, 군집형상 설계,
군집형상 분석, 군집형상 변경을 위한 기동, 타원 기준궤도
학 번: 2005–23437

감사의 글

반짝이는 별과 무한한 우주에 대한 호기심은 항공우주 공학도의 길로 저를 이끌었고 이제 또 다른 새로운 여정을 맞이하려 합니다. 2005년 무덥던 여름부터 지금까지의 대학원 생활을 돌이켜보니 즐겁고 행복한 기억과 아쉬운 기억이 모두 추억이 되어 되살아납니다. 학위논문을 마무리할 수 있도록 도와주신 모든 분께 감사의 인사를 전하고 싶습니다.

항공우주 공학분야에 첫 발을 내딛고 지금까지 연구에 매진할 수 있도록 이끌어주신 김유단 교수님께 진심으로 감사드립니다. 교수님의 큰 가르침과 따뜻한 격려가 있어 행복한 대학원 생활을 할 수 있었습니다. 앞으로도 교수님의 가르침을 되새기며 씩씩하게 앞으로 나아가는 제자가 되겠습니다. 교수님, 항상 건강하시고 행복하세요.

논문심사뿐만 아니라 더 나은 연구를 위해 아낌없이 조언해 주신 박찬국 교수님, 방효충 교수님, 김현진 교수님, 박찬덕 교수님께 감사드립니다. 대학원 생활 동안 많은 가르침을 주신 탁민제 교수님, 정인석 교수님, 기창돈 교수님, 석진영 교수님, 그리고 제게 우주공학의 길을 열어주시고 지도해주신 박상영 교수님께 감사드립니다.

지금까지 함께한 비행역학 및 제어 연구실의 선배님, 동기님, 후배님, 행정직원님께 감사의 인사를 전하고 싶습니다. 함께한 소중한 시간들 잊지 못할 거예요. 모두에게 좋은 일만 가득하길 기원합니다. 더불어 대학원 동안 인연을 맺은 항공우주 분야의 모든 분들께 감사의 인사를 드립니다.

사랑으로 키워주시고 한결같이 저를 믿고 응원해주신 부모님, 누나가 최고라고 힘을 주는 동생 종호, 어떤 말로 제 마음을 전할 수 있을까요. 진심으로 감사합니다. 옆에서 격려해주시고 보살펴주신 소중한 가족들께 감사드립니다. 그리고 사랑합니다. 자랑스러운 딸, 며느리, 누나, 형수가 되도록 더욱 노력하겠습니다. 지치고 힘들 때마다 응원해준 소중한 친구들에게 고마움을 전합니다. 마지막으로 언제나 행복을 꿈꾸게 하는 든든한 나의 편, 승호오빠에게 감사와 사랑을 전합니다.